Combination treatment to target KIT mutant cells

By

Alison Macleod

A THESIS/DISSERTATION

Presented to the Cell And Developmental Biology Department
and the Oregon Health & Science University
School of Medicine
in partial fulfillment of
the requirements for the degree of

Doctor of Philosophy

December 2013

School of Medicine
Oregon Health & Science University
CERTIFICATE OF APPROVAL

This is to certify that the PhD dissertation of

Alison Macleod has been approved

_____
Mentor/Advisor (Dr. Michael Heinrich)

_____
Member (Dr. Jeffrey Tyner)

_____
Member (Dr. Maureen Hoatlin)

_____
Member (Dr. William Fleming)

_____
Member (Dr. Christopher Corless)

Table of Contents

List of Abbreviations

AML	Acute myeloid leukemia
AP-1	Activator-protein 1 (hetero- homo- dimer)
BCL-2	Gene name for B-cell lymphoma 2
BCR-ABL	Fusion gene on chromosome 22 known as “The Philadelphia Chromosome”
BRAF	Gene name for proto-oncogene rat sarcoma viral oncogene homolog B1
CA	constitutively active
CCND1, CCND2	Cyclin D1, cyclin D2
CDK	Cyclin-dependent kinase
cDNA	Complementary DNA
CI	combination index
CML	Chronic myeloid leukemia
CMV	Cytomegalovirus
CNPI	Calcineurin phosphatase inhibitor
CSA	cyclosporine A
CSF-1R	Colony stimulating factor 1 receptor
CTG	Cell Titer Glow
DMEM	Dulbecco's modified Eagle's medium
EDTA	Ethylenediaminetetraacetic acid, a chelating agent
FBS	Fetal bovine serum
FLT3	FMS-like tyrosine kinase 3
GIST	Gastrointestinal Stromal Tumor
HEPES	(4-(2-hydroxyethyl)-1-piperazineethanesulfonic acid), an organic chemical buffer
IonM	ionomycin, ionophore that enhances Ca2+ signaling
JAK	Janus protein tyrosine kinase family
JM	juxtamembrane
KD	Knockdown
KEGG	Kyoto encyclopedia of genes & genomes
KIT	Gene name for KIT receptor tyrosine kinase (protein aka CD117)
MAPK	Mitogen-activated protein kinase, pathway downstream of KIT signaling
MDR1	Multi-drug resistance protein 1
NFAT	Gene name for nuclear factor of activated T-cells
NFκB	Gene name for nuclear factor-light-chain enhancer of activated B cells
NLS	nuclear localization signal
NRE	NFAT response element
OS	Overall survival
PCR	Polymerase Chain Reaction
PDGFRA	Platelet derived growth factor receptor alpha
PFS	Progression-free survival

PgP	P-glycoprotein
PI3K	Phosphatidylinositide 3-kinase
PPP3CA	protein phosphatase 3, catalytic subunit, alpha isozyme
PPP3CB	protein phosphatase 3, catalytic subunit, beta isozyme
PPP3CC	protein phosphatase 3, catalytic subunit, gamma isozyme
PPP3R1	protein phosphatase 3 regulatory subunit 1
PPP3R2	protein phosphatase 3 regulatory subunit 2
qRT-PCR	Quantitative reverse transcriptase PCR
RAF	Gene name for proto-oncogene rat sarcoma viral oncogene
RIPA	Radioimmunoprecipitation assay buffer, used to lyse cells
RNAi	RNA interference
RNA-SEQ	RNA whole transcriptome sequencing platform
RPKM	Read per thousand million
RQ PCR	Real-time quantitative PCR
RTK	Receptor tyrosine kinase
SCF	Stem cell factor
shCN	shRNA-PPP3R1
shNT	shRNA non-targeting (mammalian)
shRNA	short-hairpin RNA
STAT	Signal transducer and activator of transcription
TaqMAN	Hydrolysis probes used in quantitative PCR
THPB	tributylhexadecylphosphonium bromide
TKI	Tyrosine kinase inhibitor
TPA	12-O-tetradecanoylphorbol-13-acetate, phorbol ester, enhances Ca2+ signaling
WT	Wild-type (lacking KIT or PDGFRA gene mutations)
XTT	Colorimetric assay for cellular proliferation utilizing XTT tetrazolium salt

List of Tables

List of Figures

Acknowledgements

I would like to thank all of my lab mates, my family, my friends, and my mentor for your love and support during my studies. You made this an adventure and not just a degree. I am blessed to have been part of the Heinrich lab and I know I've left it in good hands with the next generation of graduate students. In the words of Michael Jackson, I hope you guys continue to heal the world!

GO COUGS!

Abstract

Potent and specific kinase inhibitors have revolutionized the treatment of kinase-driven cancers by providing targeted inhibition of known cancer driving kinases. However, disease resistance and disease persistence have prevented targeted kinase therapy from being curative. Depending upon the disease state, kinase inhibitors may be effective for many years or only a few months before secondary resistance develops. Even for diseases where treatment is efficacious for many years, patients must be treated continuously, as interruption of the therapy results in disease growth within a few weeks or months. The goal of this thesis work was to address both disease resistance and persistence in KIT-mutant mast cell cancer models through the development of novel combination therapies.

Activating KIT mutations have been found in acute myeloid leukemia (AML), mast cell tumors, melanoma, seminoma, and gastrointestinal stromal tumors (GIST). This thesis focuses on KIT-mutant cell lines derived from mast cell tumors. Mast cell tumors have historically been difficult to treat with targeted kinase inhibitors because 90% of patients have a highly resistant KIT mutation driving their tumors – KIT D816V.

The first portion of this thesis is focused on the investigation of a hypothesis that originated from a chronic mylogenous leukemia (CML) model. In the CML model, imatinib was found to synergize with cyclosporine A (CSA) to inhibit the proliferation and survival of BCR-ABL+ CML cell lines. This synergy required inhibition of calcineurin (CN) enzyme activity and hyperphosphorylation of NFAT species. Given similarities in kinase signaling between CML and mast cells with activating KIT mutant alleles, I hypothesized that combining a KIT inhibitor with a CN phosphatase inhibitor such as CSA would synergistically inhibit the growth and survival of KIT-mutant mast cells. To

characterize the effects of a similar combination on disease resistance in KIT-mutant mast cell lines I measured cell viability, and apoptosis in six distinct KIT-mutant mast cell lines following treatment with a spectrum of KIT and CN inhibitors. I found that combination therapy synergized to reduce cell viability and increase caspase 3/7. To assess the effects of this combination on disease persistence I measured replating efficiency of KIT-mutant P815 cells because of their adherent, colony-forming nature. Here too, after long-term drug exposure, I found that combining CSA with a KIT inhibitor synergized to reduce the replating efficiency of KIT-mutant P815 cells.

Next, I investigated the mechanism underlying the observed synergy. Through the use of NFAT-reporter assays, shRNA knockdown of calcineurin, and NFAT specific pharmacologic inhibitors, I was able to determine that the effects of CSA were exerted through inhibition of calcineurin phosphatase activity, and subsequently inhibition of NFAT activity. Notably, NFAT species were found to be constitutively active in all of the KIT-mutant mast cell lines evaluated to date. This could explain the success of combining an NFAT inhibitor with a KIT inhibitor in KIT-mutant mast cells and may suggest a point of crosstalk or cooperation between KIT and NFAT signaling pathways.

Following up on my observation that the synergistic effects were at least partially mediated by the transcription factor NFAT, I used an RNA-Seq screen to identify novel combination therapies to test against the CSA plus KIT inhibitor combination *in vivo.* It was our goal to identify effective combination therapies that would not rely on an immunosuppressive agent (CSA). This approach revealed that following combination therapy in P815 cells, members of the JAK-STAT and “Cancer” pathways were overrepresented in the list of target genes that were significantly downregulated or upregulated. I followed up on this finding by testing three targets within these pathways: JAK1/2, CCND1/2, and MYC.

Through a sequence of assays (similar to those used to evaluate the CSA plus KIT inhibitor combination) I determined that combination treatments inhibiting both JAK1/2 kinases and KIT kinase with separate inhibitors synergized to the same extent as inhibiting calcineurin plus KIT. Additionally, inhibiting CCND1/2 plus using a CDK4.6 inhibitor synergized with a KIT kinase inhibitor to nearly the same extent, and would also be a good candidate for *in vivo* testing. In contrast, the MYC plus KIT inhibitor combination did not perform as well as the other combinations with respect to cellular viability, caspase activity, or long term replating efficiency. These results were confirmed with caspase 3/7 assays and target knockdown experiments similar to those performed during the calcineurin investigation.

I have concluded that constitutive NFAT signaling may be a characteristic of KIT-mutant mast cells, or perhaps activated mast cells in general, that can be leveraged to selectively sensitize these cells to KIT inhibition. It appears that combining an NFAT inhibitor with a KIT inhibitor synergistically inhibits JAK-STAT signaling leading to cell death and decreased long-term cell viability in KIT-mutant mast cell models. We plan to advance the CSA, JAK, and CCND plus KIT inhibitor combinations to *in vivo* testing in mice with the hopes of moving these combination therapies into clinical trials.

Chapter 1: Introduction

The following introduction to KIT (section 1.1) was adapted from a review on KIT as part of a compilation of cancer targets called *Cancer Therapeutic Targets* for Springer Reference. Dr. Michael Heinrich and I published this review through Springer Reference. It can be found in its entirety at the following link:

http://www.springerreference.com/docs/html/chapterdbid/367588.html

1.1 KIT (formerly c-kit)

KIT is a type III receptor tyrosine kinase encoded by a gene locus on the long arm of chromosome 4. It is closely related to FLT3, platelet-derived growth factor receptor alpha and beta (PDGFRα, PDGFRβ), and colony-stimulating factor 1 receptor (CSF1R). Depending on its degree of glycosylation, the molecular mass of KIT is 140-160kD. KIT is normally expressed on the surface of hematopoietic stem and progenitor cells, mast cells, melanocytes, germ cells, and interstitial cells of Cajal. There are both transmembrane and soluble forms of KIT; however the transmembrane form is believed to be biologically active, while the role of soluble KIT is poorly understood. The ligand for KIT is stem cell factor (SCF), also known as steel factor, or mast cell growth factor. Both soluble and membrane bound forms of SCF exist, resulting from alternative splicing of exon 6 [1-3].

1.1.2 Biology of KIT

KIT is critical for hematopoiesis, the development and migration of melanocytes, the development of the gonads, gut peristalsis, and the survival and function of mast cells. In mice, KIT is the gene product of the white spotting locus (*W*), and SCF is encoded by the steel locus (*Sl*). Loss of function mutations at these two locations result in similar

phenotypes – bone marrow failure/anemia, white spotting of the fur, loss of mast cells, abnormal peristalsis (decrease in the interstitial cells of Cajal) and sterility. Complete or near complete loss of KIT expression is embryonic lethal. These observations prompted studies which suggested that SCF is the cognate ligand of KIT[4].

KIT becomes activated when stem cell factor (SCF), binds to the KIT extracellular domain. SCF is expressed by cells that make up the microenvironment of KIT-expressing cells including epithelial cells, endothelial cells, fibroblasts, Sertoli cells, etc. Binding of SCF leads to receptor dimerization, kinase activation, KIT autophosphorylation and activation of downstream signaling pathways including the PI3-K, MAP kinase, and JAK/STAT pathways. Signaling via KIT promotes cell growth, survival, and proliferation. However, mutations in KIT lead to its constitutive activation in the absence of SCF. These mutations have been linked to acute myeloid leukemia (AML), mast cell tumors, melanoma, seminoma, and gastrointestinal stromal tumors (GIST)[3, 5]. KIT mutations are typically sporadic point mutations, deletions, or insertions in exons 8, 9, 11, 13, or 17; however, there are rare cases of familial GIST and mastocytosis where germline KIT mutations were observed.

Activating KIT mutations can be located in the intracellular or extracellular domains. Extracellular mutations are typically located in exons 8 or 9 (Figure 1). KIT exon 8 mutations are associated with AML, and these mutations are believed to induce hypersensitivity to SCF, rather than constitutive activation in the absence of SCF. Exon 9 mutations are found in approximately 10% of GIST patients. The activation mechanism of these mutations is being investigated, and may be related to KIT dimerization or conformational changes; however these mutations do cause constitutive activation in the absence of SCF. Intracellular mutations are most commonly associated with exons 11 and 17. Mutations in exon 11 are found in two thirds of GIST patients. These mutations

occur in the juxtamembrane domain and prevent this autoinhibitory region from locking the kinase “off” in the absence of SCF. D816V, a mutation in exon 17, is associated with mast cell neoplasms, leukemia, and seminoma. This mutation is located in the activation loop and stabilizes the kinase activation loop in the active conformation, promoting spontaneous kinase activity.

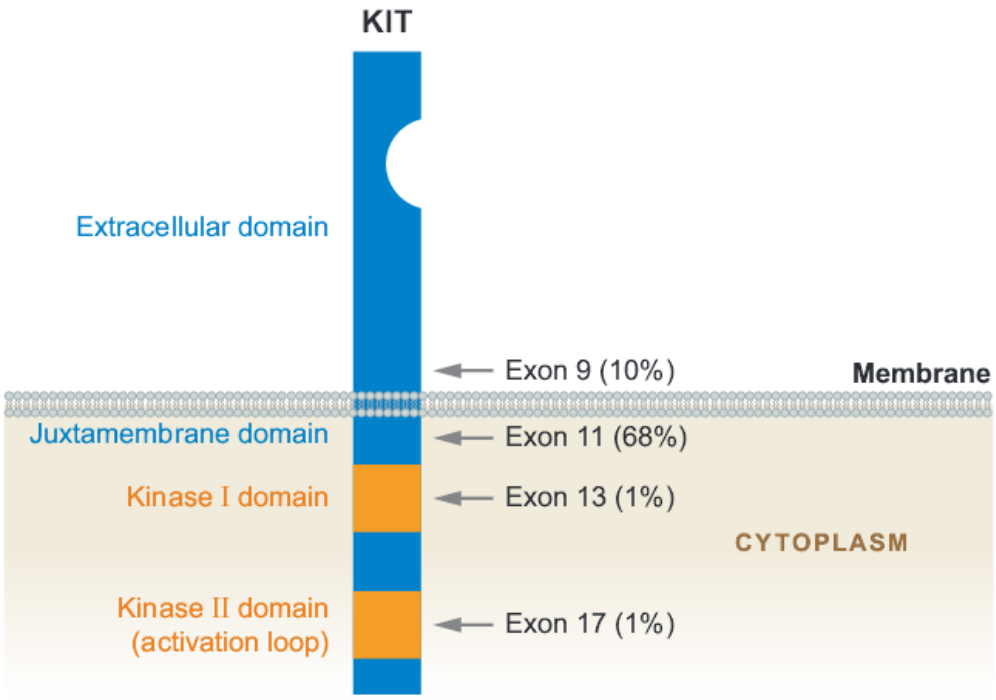

Figure 1 – Distribution of KIT mutations in gastrointestinal stromal tumor patients. Corless CL, Heinrich MC. Annual Reviews of Pathology: Mechanisms of Disease 2008. Reprinted with permission from Annual Reviews.

1.1.3 Clinical Target Assessment

KIT protein expression is readily assessed in fixed tissue using immunohistochemistry (fixed tissue) or flow cytometry (blood, bone marrow) [6-8]. As noted below, measurement of KIT expression has some diagnostic utility. More importantly, detection

of the presence or absence of KIT mutations is predictive of response of GIST, melanoma, and mast cell neoplasms to KIT kinase inhibitors.

1.1.4 High Level Clinical Overview

A number of KIT kinase inhibitors have been approved by the FDA. Three of these inhibitors, imatinib, sunitinib, and regorafenib have specific FDA-approved indications for treatment of GI stromal tumors [9]. In addition, imatinib is FDA approved for treatment of adult patients with aggressive systemic mastocytosis without the D816V KIT mutation or with unknown KIT mutational status [10]. Ongoing clinical trials of KIT inhibitors for treatment of KIT-mutant melanoma (imatinib, nilotinib, sunitinib) and for fourth line treatment of GIST (e.g. ponatinib) may lead to new treatment indications for existing and investigational KIT kinase inhibitors.

A number of these trials are now seeking to combine FDA-approved drugs in combination to increase their effectiveness in patients. Of the approximately 2500 ongoing clinical trials for cancer therapeutics, there are over 350 stage II, III, or IV trials involving a combination approach with at least one kinase inhibitor (cancer.gov). This number is expected to grow as more laboratories test the concept of synthetic lethality as a means to combat disease resistance and disease persistence. Synthetic lethality is the when simultaneously inhibiting two critical pathways synergizes to induce lethality in cells, whereas inhibition of either pathway alone is not lethal to cells. Below is a summary of the ongoing clinical trials for KIT-mutant cancers including several combination therapy studies.

Table 1 - Ongoing clinical trials for KIT-mutant cancers

Compound	Disease	Phase	Target	Study Identifier
Regorafenib	GIST	3	KIT	NCT01646593
Palbociclib	GIST	2	KIT	NCT01907607
Dovitinib	GIST	2	multi-kinase inhibitor	NCT01440959
AUY922	GIST	2	HSP inhibitor	NCT01389583
AT13387+STI	GIST	2	HSP90+KIT	NCT01294202
Ponatinib	GIST	2	KIT	NCT01874665
Cladribine+IFNa2a	SMCD	2/3	KIT	NCT01602939
Midostaurin	SMCD, AML	2	multi-kinase inhibitor	NCT00782067, NCT01830361
Masitinib	SMCD	3	KIT	NCT00814073
Masitinib vs Dacarbazine	Melanoma	3	KIT, PDGFRA	NCT01280565
Nilotinib+Everolimus	AML	1/2	KIT, mTORc1	NCT00762632
Nilotinib+chemotherapy	AML	2	KIT, DNA	NCT01806571

1.1.5 KIT as a diagnostic, prognostic, and predictive tool

Over the past decade, immunohistochemistry for detection of KIT protein (CD117 antigen) has helped standardize the diagnosis of GIST. GIST is the most common spindle cell neoplasm (sarcoma) of the GI tract, but morphologically can be difficult or impossible to distinguish from smooth muscle tumors, schwannomas, desmoids tumors (aggressive fibromatosis), and metastatic melanoma. Indeed, until the application of KIT immunohistochemistry to the pathologic classification of these lesions, GIST was not even recognized as a separate pathologic entity and these tumors were classified as either benign or malignant smooth muscle tumors [7, 8]. As noted below, the use of KIT kinase inhibitors has revolutionized the treatment of GIST—making the accurate diagnosis of GIST even more critical. KIT immunohistochemistry can also be used in the diagnosis of melanoma, AML, mast cell neoplasms, and germ cell tumors.[7] In addition, KIT is a useful marker for flow cytometric identification of bone marrow blast cells and classification of cases of myelodysplastic syndrome and AML [6].

The presence and type of KIT mutation found in primary GIST has been shown to have prognostic value in retrospective population studies [11, 12]. More recently, similar results have been shown in the placebo arm of a double blind, randomized study of placebo vs. one year of adjuvant imatinib following curative intent resection of primary GIST. Notably, the presence of a KIT exon 11 in frame deletion mutation was associated with a much higher risk of recurrence than seen in tumors with other KIT genotypes (HR 3.45, p=0.024 compared with wild-type tumors) [7, 8, 13]. These data are now being incorporated into risk stratification algorithms to help predict the risk of recurrence after surgery and to help guide decision making concerning the use of adjuvant imatinib.

Translational studies utilizing tumor samples from large clinical studies have identified tumor genotype as a strong predictor of clinical benefit for patients with metastatic GIST treated with imatinib. Specifically, patients whose tumor harbors a KIT exon 11 mutation (approximately 70% of GIST), have the highest rates of objective response, PFS and OS compared with patients whose tumors had no kinase mutations (wild-type GIST, approximately 10-15% of GIST) or GIST with somatic KIT exon 9 mutations (~10% of patients). In the SWOG/NCIC study, PFS for these three groups was 24.7 months for KIT exon 11-mutant tumors vs. 16.7 months for wild-type GIST and 12.8 months for patient with KIT exon 9-mutant tumors. In terms of the effect on overall survival, KIT exon 11 mutant-GIST patients had a median OS of 60 months vs. 38.4 months for wild-type GIST patients and 49 months for KIT exon 9-mutant GIST patients [14-17].

The effect of tumor genotype and imatinib dose on clinical outcomes was also analyzed in the MetaGIST study (400 mg vs. 800 mg dosing for metastatic GIST). Within patients with *KIT* exon 9 mutant-GIST, PFS was significantly longer for patients treated with the high-dose arm (*P* =.017). For patients whose tumor had genotypes other than KIT exon 9 mutation, no difference in clinical outcomes was observed between treatment arms. In

terms of OS, there was a trend towards a survival advantage for patients with KIT exon 9-mutant GIST treated with high dose therapy (p=0.15) [18]. These data suggest that routine tumor genotyping may help optimize the target imatinib dose for patients with metastatic GIST. Indeed, this is now recommended in the National Comprehensive Cancer Network (NCCN) guidelines.

1.1.6 Therapeutics for inhibition of KIT

To date, all of the FDA-approved anti-KIT therapeutics are small molecule tyrosine kinase inhibitors. Currently, the following agents with KIT inhibitory activity are FDA-approved for treatment of one or more human malignancies: imatinib, sunitinib, nilotinib, dasatinib, sorafenib, regorafenib, and pazopanib.

1.1.7 Pre-Clinical Summary

A large body of evidence has established KIT as therapeutic target and subsequent research has studied the efficacy of various tyrosine kinase inhibitors in blocking its activity in vivo and in vitro. Research in 2000 by Ma et al. showed efficacy of a small group of indolinones against KIT[19]. They also reinforced a direct link between KIT function and mast cell survival. In the same year, Heinrich et al. and Buchdunger et al. investigated the use of imatinib (formerly STI-571) as a KIT inhibitor. Imatinib was found to selectively inhibit KIT tyrosine kinase activity as well as inhibit the activation of downstream target proteins. They also found that imatinib was more potent against certain KIT mutations than against WT KIT, and concluded that the clinical profile of imatinib should be expanded to include KIT (in addition to its known effects against ABL, BCR-ABL, and PDGFRA and PDGFRB) [20, 21].

In this same time frame, Tuveson et al. developed a GIST tumor cell line – GIST882, harboring an activating mutation in the KIT tyrosine kinase I domain. Incubation of this cell line with imatinib led to decreased proliferation and increased apoptosis supporting a role of KIT in GIST pathology, and the therapeutic potential for imatinib in GIST patients [22]. Later, in 2003, Abrams et al. evaluated the activity of sunitinib (formerly SU11248) against KIT in a small cell lung cancer model [23]. Treatment with sunitinib inhibited KIT tyrosine phosphorylation and cellular proliferation. The results of this study suggested a clinical potential for sunitinib in the treatment of tumors with activating KIT mutations.

KIT mutations are found in the vast majority of human mast cell neoplasms. In particular, the KIT D816V mutation is found in >90% of cases. Pre-clinical studies of mastocytosis cell lines and/or patient samples have shown that KIT inhibition by kinase inhibitors reduces proliferation and induces apoptosis of cells. Unfortunately, the D816V mutation is resistant to most of the available kinase inhibitors. However, these studies do indicate that KIT is a compelling target in mastocytosis and have spurred efforts to develop inhibitors with activity against the D816V mutation [24-26].

More recently, KIT mutations have been found in a subset of human melanoma. In particular, these mutations are more common in acral or mucosal subsets of melanomas. In vitro studies of KIT-mutant melanoma cell lines have demonstrated that KIT inhibitors can exert an antiproliferative and pro-apoptotic effect on these cells [27, 28].

All of these studies and many more have established KIT as a therapeutic target in cancers driven by the hyperactivation of KIT and demonstrated the efficacy of specific tyrosine kinase inhibitors in controlling this hyperactivity.

1.1.8 Clinical Summary

Prior to 2000, there was no active medical treatment for metastatic GIST [29]. However, the introduction of small molecule tyrosine kinase inhibitors (TKIs) for the treatment of GIST has revolutionized the treatment of GIST. Currently, there are three FDA approved treatments for advanced GIST: imatinib for front-line treatment, and sunitinib and regorafenib for treatment of patients who are intolerant of imatinib or whose disease has progressed on imatinib therapy. A number of other TKIs have been tested in phase 2 studies for treatment of GIST in the third-line or later clinical setting. Overall, the use of KIT inhibitors has changed the prognosis for patients with metastatic GIST, with median survival increasing from an estimated 1-1.5 years to the current 4-5 years [9]. Notably, resistance to KIT inhibitors in KIT-mutant GIST is typically associated with the development of secondary KIT mutations that confer drug resistance [30, 31]. Developing new inhibitors to prevent or overcome secondary mutations is a major focus of ongoing GIST research [9].

In addition to GIST, some therapeutic progress has been made in treating mast cell neoplasms with KIT kinase inhibitors. Currently, available KIT kinase inhibitors have reduced potency against the KIT D816V mutation associated with mast cell neoplasms [32, 33]. However, it is anticipated that development of novel KIT inhibitors that are active against the D816V mutation will be clinically effective for treating mast cell neoplasms. It is possible that minor adjustments to existing KIT inhibitors could make them potent against the D816V mutation, or inhibitors with novel mechanisms of KIT inhibition could be effective against the D816V mutation. Currently, imatinib is FDA-approved for treatment of aggressive mastocytosis lacking the D816V mutation or with an unknown KIT genotype.

Clinical studies using KIT inhibitors to treat unselected cases of malignant melanoma have been disappointing [34]. However, a number of case reports have emerged reporting strong activity of KIT kinase inhibitors against KIT mutant melanoma [35, 36]. These reports have resulted in clinical studies of KIT inhibitors for patients with KIT-mutant melanoma.

1.1.9 KIT signaling pathways

First cloned and characterized in 1990, the ligand SCF binds to the extracellular domain of KIT and thereby activates a series of downstream signaling pathways including PI3K-AKT, JAK-STAT, and the MAPK (Figure 2) [37-45]. Collectively signaling through these pathways contributes to normal differentiation and development. However, in the case of constitutive KIT activation, such signaling can lead to uncontrolled cell cycle progression, cellular proliferation, inhibition of apoptosis, and the development of a neoplastic phenotype.

PI3K is a heterodimer, composed of an 85kD regulatory subunit and a 110kD catalytic subunit. The regulatory subunit contains SH2, SH3, and proline-rich motifs for binding to RTKs[45]. The catalytic subunit binds to substrates such as adapter proteins Crkl and Cbl [46]. Upon KIT activation, PI3K interacts with KIT at the phosphorylated residue tyrosine 719 via an SH2 domain[47]. This leads to the recruitment and catalysis of PIP2 into PIP3. PIP3 anchors AKT to the plasma membrane and allows it to be phosphorylated and activated by PDK1. Following activation, AKT activates a number of downstream targets such as Forkhead, BAD, GSK3, and mTOR[48]. This signaling cascade blocks apoptosis, promotes cell cycle progression and cellular proliferation.

Another signaling pathway activated downstream of KIT is MAPK. KIT dimerization leads to autophosphorylation of specific tyrosine residues on KIT. These

phosphorylated tyrosine sites bind and activate the adapter molecule GRB2. GRB2 facilitates the interaction between the guanine nucleotide exchange factor Sos and small GTP binding protein (Ras) [49]. Activation of Ras leads to activation of Raf-1 through phosphorylation at sites Ser338, Tyr340/341, Thr491, and Ser494 [50]. Next, activation of MEK1 and MEK2 occurs through phosphorylation of two serine residues at positions 217 and 221, with partial activation following phosphorylation at either site. Finally, MEK1 and MEK2 phosphorylate ERK1 and ERK2 at Thr202/Tyr204 for human ERK1 and Thr185/Tyr187 for human ERK2. However, unlike MEK, ERK activation requires dual phosphorylation at both sites[51]. Phosphorylated ERK1 and ERK2 translocate to the nucleus where they regulate the expression of target genes [48].

The final, major signaling pathway downstream of KIT is the JAK-STAT pathway. Although initially there was controversy over whether signaling through KIT led to JAK activation [52, 53], there is now ample evidence that this pathway is activated downstream of KIT [28, 44, 54-59]. Activation of KIT leads to the rapid and transient activation of JAK1-3 proteins, which phosphorylate tyrosine residues on KIT, creating interaction sites for proteins with SH2 domains. STAT1, STAT3, and STAT5 proteins contain SH2 domains, and are recruited to these docking sites where they become phosphorylated and activated by JAK proteins [44, 54, 60]. Phosphorylated STAT molecules homo- and hetero-dimerize in order to translocate to the nucleus. A nuclear localization signal (NLS) on STAT1 dimers is recognized by the nuclear import molecule importin-α5 [61], while STAT3 and STAT5 NLS are recognized by importin-α3 [62, 63]. Once in the nucleus STAT proteins bind to the promoter region of target genes in order to activate transcription.

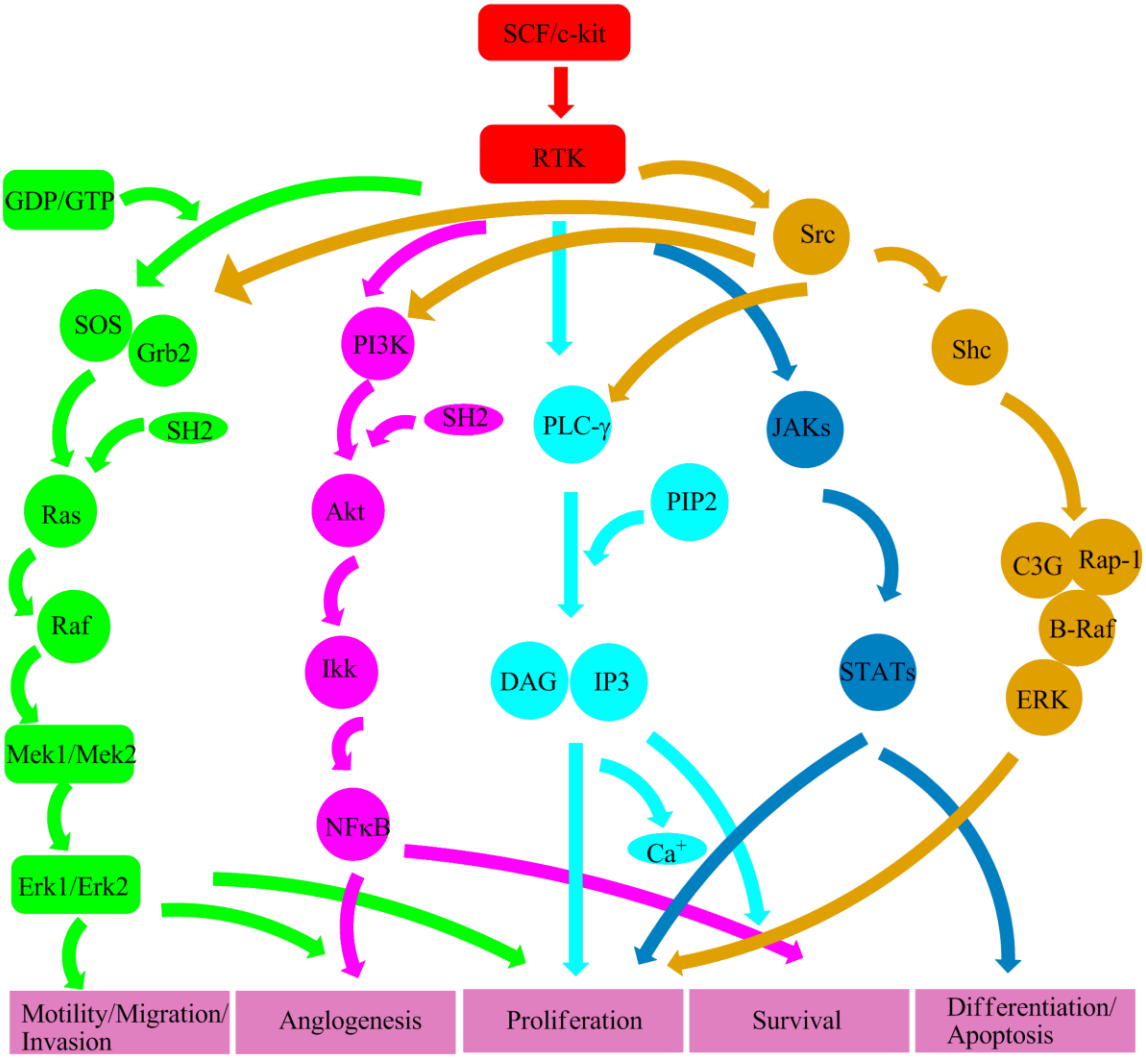

Figure 2 –Signaling pathways downstream of SCF/KIT. Liang et al. IJBS 2013 [64]. Reprinted with permission from IJBS Publishing Team.

1.1.10 KIT in Mastocytosis

First discovered in human mast cell leukemia in 1995, constitutively active KIT mutations, most commonly KIT D816V, are now recognized as a hallmark of human systemic mast cell disease [65-67]. These mutations lead to SCF-independent activation of KIT and its downstream signaling pathways, thus promoting cell survival and proliferation. Systemic mast cell disease is characterized by the accumulation of

mast cells in the bone marrow, liver, spleen, lymph nodes, gastrointestinal tract, and the skin[66]. According to WHO classification, systemic mastocytosis (SM) can be divided into four categories: Indolent mastocytosis (ISM), mastocytosis with an associated hematologic disorder(SM-AHNMD), mast cell leukemia (MCL), and aggressive mastocytosis (ASM)[68].

In addition to activating KIT mutations in human mast cells (HMC1.1, HMC1.2), KIT-mutant mast cell lines have been developed from other species, including mouse, rat, and dog. The murine P815 cell line harbors a KIT D814Y point mutation which is homologous to the mouse equivalent of human KIT D816Y, which is less frequently found in human mast cell disease than the D816V mutation. This mutation causes constitutive activation of KIT as determined via immunoblotting (KIT autophosphorylation) and kinase activity assays, and this activation is ligand independent[69]. The rat RBL2H3 cell line also expresses a constitutively active, ligand-independent KIT isoform, which was determined by Tsujimura et al. to be KIT D817Y. Again, this mutation is in a region conserved within human, mouse, and rat, and corresponds to human D816Y, and mouse D814Y [70]. Finally, the canine mast cell lines BR, and C2 were found to have unique, activating KIT mutations. The BR cell line contains a point mutation, KIT L575P, while the C2 cell line contains a tandem repeat in exon 11 [71]. These cell lines have provided a good model for studying signaling pathways in KIT mutant mast cells. However, findings in these cell lines have not always translated to human studies.

Human studies have confirmed a high incidence of activating KIT mutations in patients with systemic mastocytosis (SM). While 90% of SM patients harbor activating KIT mutations, 95% of these mutations are KIT D816V [72, 73]. Despite promising *in vitro* results using KIT TKIs (dasatinib, nilotinib, midostaurin) to treat KIT D816V-mutant mast

cell lines, monotherapy with a KIT inhibitor has not proven effective in patients harboring the same mutation. For example, the KIT inhibitor PKC412 was tested in a patient with mast cell leukemia. Despite an initial partial response with improved liver function, decreased peripheral blood mast cells, decreased serum histamine and a decrease in KIT phosphorylation, the patient died after 3 months of therapy after their disease advanced to AML [25, 74-76]. However, another case of AML in a patient with KIT D816V showed more promising results. In that case following induction chemotherapy, dasatinib was administered during consolidation treatment, and then alone as a maintenance treatment. The patient experienced hematologic complete remission and the KIT D816V mutation became undetectable [77]. This case study supports the use of combination therapy to treat KIT-mutant cancers.

Activating KIT mutations are also common in canine and feline mast cell disease. Mast cell tumors account for approximately 20% of all canine and feline neoplasms[78, 79]. Activating KIT mutations have been reported in 26% of canine mast cell tumors[78]. Similar to human mast cell tumors, 64% had alterations in exon 11. However contrary to the point mutations found in humans, canine exon 11 mutations are primarily internal tandem duplications (ITD). Exon 8 mutations were identified in 18% of KIT-mutant tumors, with both ITDs and point mutations. Additionally, 16% of KIT-mutant tumors had point mutations in exon 9. A recent study in cats found activating KIT mutations in 56% of mast cell tumors. Of these, 19% contained an exon 8 mutation, 71% contained an exon 9 mutation and 10% contained an exon 11 mutation. Similar to human disease, activating KIT mutations were primarily point mutations[79].

While it is well recognized that constitutive KIT signaling is associated with systemic mastocytosis [66, 67, 80-83] and likely is the causative abnormality, it is also believed that KIT signaling alone is insufficient for disease progression [84] and that additional

mechanisms contribute to therapeutic resistance and eventual disease expansion [72, 76]. The molecular mechanisms leading to disease progression in SM remain unknown. As a result, recent studies have focused on uncovering these additional mechanisms so that more effective therapies can be developed to delay expansion and/or prevent relapse. I explore one possible novel mechanism driving KIT-mutant mast cells in Chapter 1.

In 2013, Schwaab et al. performed in depth next generation sequencing on bone marrow samples obtained from 39 unique patients with SM. Patient diagnoses ranged across all four categories of SM. Sequencing revealed additional genetic mutations in 89% of patients with advanced SM, compared with 25% of patients with ISM. The average number of additional abnormalities in patients with ASM was four. The most commonly mutated genes were TET2, SRSF2, ASXL1, RUNX1 and CBL, and less frequently KRAS, NRAS, JAK2, U2AF1, EZH2 and ETV6. Similar patterns of genetic mutations were observed amongst patients with ASM indicating similar disease progression. Follow-up studies (45 months) found that 6/15 (40%) ASM patients had died, whereas all patients harboring only KIT D816V had survived. This finding, combined with the fact that ASM patients harbor similar mutations, suggest that these additional abnormalities contribute to poor TKI response and clinical phenotype [72].

1.2 Calcineurin: a protein phosphatase

Calcineurin was first independently characterized by the Claude Klee and Philip Cohen laboratories in 1979. At the time of its characterization, calcineurin was thought to be predominantly expressed in brain tissue. In these studies, calcineurin was found to bind to both calcium and calmodulin – thereby, inhibiting calmodulin's ability to activate cyclic nucleotide phosphodiesterase and adenylate cyclase. Based on its presence in

neuronal tissue and its ability to bind calcium, the name calcineurin was coined[85]. However, in the years since its discovery it has been well established that calcineurin is expressed in a wide range of mammalian tissues, and has a number of functions aside from binding calcium and calmodulin – namely its function as a protein phosphatase. Compared to other protein phosphatases calcineurin has narrow substrate specificity. It has been shown to bind DARP32, Inhibitor-1, NFAT, NMDA, and IP_3 receptors [86].

Calcineurin is a heterodimer, comprised of a catalytic subunit, calcineurin A, and a regulatory subunit, calcineurin B. Calcineurin A contains a calcineurin B binding domain, a calmodulin binding domain, and an autoinhibitory domain which binds in the active site cleft in the absence of calcium. Calcineurin B has four calcium binding motifs (Figure 3).

In resting cells, with low calcium concentrations, calcineurin is inactive and cannot bind calmodulin. Following increases in intracellular calcium, calcium binds to calmodulin, leading to a conformational change which allows calmodulin to bind calcineurin A. This binding, along with calcineurin B binding to calcium, activates calcineurin and increases its phosphatase activity[87].

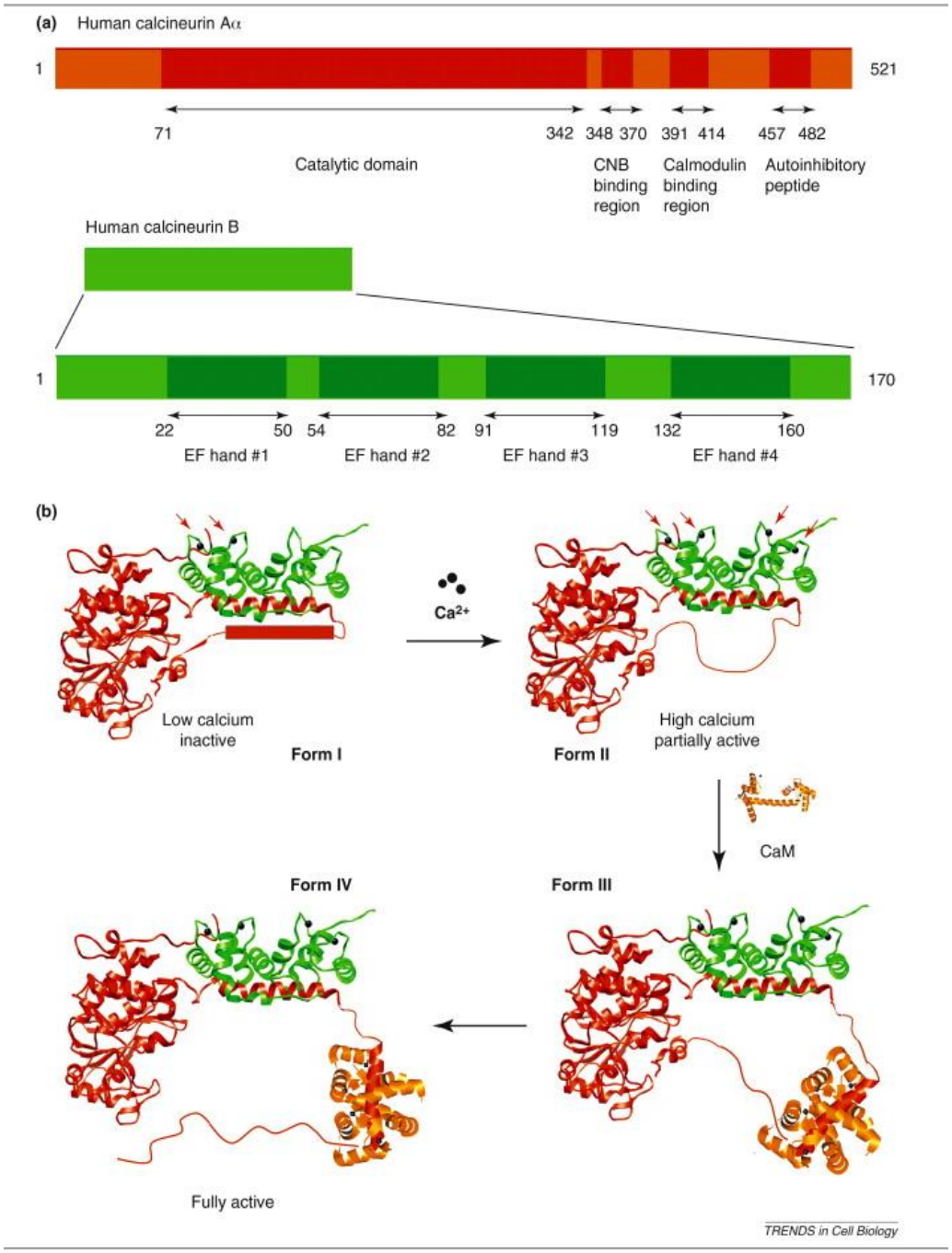

Figure 3 - Calcineurin domain organization and proposed mechanism of activation. (a) Regional organization of calcineurin. **(b)** Proposed mechanism of activation of calcineurin. In this widely accepted model of calcineurin activation, Ca^{2+} occupancy of the low affinity sites on calcineurin B causes dissociation of the calmodulin binding region of calcineurin A from the calcineurin B binding region and causes the transition from form **I** to form **II**, facilitating the subsequent binding of calmodulin (form **III**), which leads to displacement of the autoinhibitory peptide and full calcineurin activation (form **IV**). The structure of the calcineurin A regulatory region between the

calcineurin B binding helix and the autoinhibitory peptide in resting calcineurin (form **I**) remains to be determined. In form **IV**, the portions of calcineurin A between the calcineurin B binding helix and the calmodulin binding site and C-terminal to the calmodulin binding site are depicted as random coil, but might in fact be structured. Li, Rao et al. Trends in Cell Biology 2011[88]. Reprinted with permission from Elsevier.

In 1991, Stuart Schreiber and Irving Weissman discovered that calcineurin was the target of the immunosuppressive agents: cyclosporine A (CSA) and FK506. Although these drugs bind different substrates – CSA binds cyclophilin A and FK506 binds FK-binding protein (FKBP), they both block the ability of calcineurin to interact with its targets[89]. It was subsequently discovered by the laboratories of Crabtree and Rao that the phosphatase activity of calcineurin activates the transcription factor NFAT [90, 91]. These seminal papers linked calcineurin enzymatic activity to transcriptional control via modulation of NFAT activity.

In addition to regulating the activation of NFAT in the cytoplasm, Shibasaki et al. found that calcineurin can translocate with NFAT into the nucleus, where it maintains NFAT in its dephosphorylated state [92]. Aside from regulating gene transcription through NFAT, calcineurin signaling has been shown to contribute to apoptosis. For example in T-cell hybridomas, T-cell mediated apoptosis is mediated by increases in intracellular calcium, and signaling through calcineurin[93]. In a B-cell lymphoma model, CSA and FK506 protects cells from calcium-induced cell death – purportedly through calcineurin inhibition [94]. Along the same lines, another group showed that CSA protects cells from calcium/calcineurin-dependent apoptosis in Burkitt's lymphoma cell lines [95]. The mechanism behind this role in apoptosis is believed to be FasL-dependent. Inducible FasL transcriptional activity was found to be sensitive to FK506 and CSA and induced by a constitutively active form of calcineurin. In addition, the promoter region of FasL contains an NFAT-DNA binding motif [96].

In 2000, it was discovered that the gene *DSCR1 (*Down-syndrome critical region) or *RCAN1* (regulator of calcineurin 1) encodes a protein called MCIP1 (myocyte enriched calcineurin interacting protein). This protein binds to the calcineurin catalytic domain at motifs similar to those used by NFAT. This binding inhibits calcineurin/NFAT interactions – inhibiting activation of NFAT by calcineurin [97]. Following this discovery, it was found that MCIP1 expression was regulated by calcineurin/NFAT activity. Yang et al. found that a constitutively active form of calcineurin led to increased expression of MCIP1 and they subsequently identified an alternative promoter within the MCIP1 gene containing a cluster of 15 NFAT binding sequences. A reporter-construct containing this region of the MCIP1 promoter was shown to be calcium responsive, and serial removal of the NFAT binding motifs led to dose dependent decreases in MCIP1 reporter activity[98]. These papers describe a negative feedback loop for calcineurin regulation, whereby calcineurin signaling activates MCIP1 expression, and MCIP1 binds to and inhibits calcineurin signaling.

1.2.2 Calcineurin Inhibitors

Originally introduced into the clinic in 1983, cyclosporine A (CSA) is now a cornerstone immunosuppressant used in transplant patients to prevent acute organ rejection. Not long after cyclosporine was approved, a second compound, FK506, was approved in 1989 following a large organ transplant study performed at University of Pittsburgh[99]. Initially FK506 was developed for use in transplant patients who failed to respond to CSA [100], but it was soon found that in addition to overcoming CSA resistance, FK506 was more potent than CSA and had less short term toxicities[99]. However, in the long run, FK506 and CSA have similar cumulative side-effects, as described below.

Although CSA and FK506 are distinct compounds, binding different immunophilin proteins, they both inhibit calcineurin phosphatase activity. CSA binds to cyclophilin A, and FK506 binds FK-binding protein (FKBP). By binding these immunophilin proteins, they also inhibit their peptidyl-proline isomerase activity. It is not, however, this inhibition that leads to immunosuppression. Instead the binding of the CSA/cyclophilin A orFK506/FKBP complexes to calcineurin leads to inhibition of calcineurin phosphatase activity that exerts an immunosuppressive effect by inhibition of NFAT-target genes [101].

In addition to use in organ transplant and the subsequent maintenance immunosuppression, CSA and FK506 are being used in a number of other immune-related health issues such as autoimmune disorders, rheumatoid arthritis, psoriasis, and chronic dry eye (for cases with autoimmune damage to tear glands). Unfortunately, chronic systemic use of these compounds is associated with a number of adverse side-effects.

A review of the FK506 clinical trials at University of Pittsburgh broke down the adverse side-effects into four categories: kidney/renal dysfunction, glucose metabolism dysregulation, neurotoxicity, and infection/malignancy [102]. One of the earliest identified side-effects was chronic CSA nephrotoxicity leading to chronic renal dysfunction. This is thought to be due to CSA's ability to cause afferent arteriolar vasoconstriction and decreased glomerular filtration rate leading to increased serum creatinine [103]. Another side-effect of chronic calcineurin phosphatase inhibitor (CNPI) use is altered glucose metabolism, which can lead to diabetogenesis. This is thought to be caused by decreased release of insulin from islets, due to a decreased sensitivity of islet cells to hyperglycemia [102]. Neurotoxicity is experienced by 5% of patients, due to changes in serum electrolytes. This most serious neurotoxicity is encephalopathy;

however this condition resolves when CNPI doses are reduced. Finally, based on these drug's immunosuppressive functions, patients using CNPIs chronically experience increased rates of infection and malignancy. The most common CNPI-induced post-transplant infection is cytomegalovirus (22% of patients). This may be due to either re-activation of previous host infection or acute infection from blood products or the transplanted organ. Finally, unusual forms of lymphoma (post-transplant lymphoproliferative disease) develop in 1.6% of transplant patients. Some of these lymphomas are due to loss of immunity against Epstein-Barr virus. Overall, there is an increased risk of all types of cancer following transplantation and long-term immunosuppression, especially those that are known to be caused by a virus [104, 105].

In the context of organ transplantation, the benefits of immunosuppressant drugs outweigh the side-effects; however, any alternative to long-term use should be explored both in clinic and in the research environment. We explore not only the potential efficacy of calcineurin inhibitors to treat KIT-mutant cancers (chapter 2) but also alternative drug targets that elicit the same beneficial effects (chapter 3).

1.3 Transcription Factors

Transcription factors (TFs) are proteins that function to regulate gene expression at the level of transcription. They are instrumental in orchestrating the transient expression of genes during development, executing specific gene expression profiles in response to environmental and/or intercellular conditions, regulating cell cycle progression, and cancer pathogenesis/cellular transformation. This is accomplished by binding of TFs to specific DNA sequences on target gene promoter regions. This binding leads to the recruitment of RNA polymerase II, which synthesizes precursors of mRNA and miRNA. Transcription factors are known to interact with co-regulators (co-activators or co-

repressors), which can function as chromatin remodelers or adapters. As adapters, co-activators act as a bridge between the DNA-bound TF and the basal transcriptional machinery (ex. TAF proteins). Otherwise, as chromatin remodelers they can remove or alter repressive chromatin structures through histone acetylase activity (ex. SWI/SNF). Conversely, co-repressors have histone deacetylase activity. Both co-activators and co-repressors bind to TFs rather than DNA.

Depending on context, TFs can either promote or inhibit gene expression. A single TF can be a “pure activator” a “pure repressor” or both. This is influenced by transient cellular conditions, distinct DNA-binding sites for the same TF, changes in TF conformation based on interaction with other molecules such as hormones. As a result, TFs stabilize or block the binding of RNA polymerase to DNA.

Based on conserved DNA binding motifs within proteins, it is estimated that approximately 10% of the human exome (around 2600 genes) may act as transcription factors. This represents the largest family of human proteins. Structurally, transcription factors all contain a DNA binding domain, and a trans-activating domain, which binds to transcriptional co-regulators. These co-regulators can be other transcription factors as in the case of NFAT and JUN, or they can be other factors which, themselves, are incapable of binding DNA.

In addition to their intrinsic protein structure, the activity of transcription factors can also be regulated through post-translational modification including protein phosphorylation or glycosylation at specific serine and threonine residues, or acetylation, ubiquitination, or sumoylation at specific lysine residues. Phosphorylation serves to activate or inactivate TFs and leads to changes in subcellular localization and DNA-binding. The role of glycosylation in TF regulation less characterized, but studies have tied O-linked

glycosylation to TF repression [106] while N-linked glycosylation has been implicated in promoting TF stability [107]. Acetylation of TFs leads to changes in protein-protein interactions, protein-DNA interactions, and TF stability. As in other cellular contexts, poly-ubiquitination promotes TF degradation. And sumoylation of a TF affects protein stability and subcellular localization in a TF-specific manner [108].

Some transcription factors exist in inactive pools within the cytoplasm awaiting post-translational modification and protein activation, thereby allowing a rapid response to signaling pathways without the need for new protein synthesis. These signaling pathways can result in phosphorylation or dephosphorylation of relevant transcription factors, allowing them to translocate to the nucleus where they bind DNA and thereby regulate gene expression. Whether a transcription factor requires phosphorylation or dephosphorylation to become active is transcription factor dependent. For example, the transcription factor NFAT requires dephosphorylation by calcineurin in order to expose a nuclear localization signal on its surface and allowing translocation to the nucleus. Conversely, MYC needs to be phosphorylated in order to stabilize the protein and increase transcriptional activity. Notably, MYC dephosphorylation actually plays a role in its degradation [109].

Following activation in the cytoplasm and translocation to the nucleus, constitutively active kinases and phosphatases within the nucleus can inhibit transcription factor activity. Transcription factors subsequently translocate to the cytoplasm where they are degraded or recycled. Some transcription factors participate in autoregulation of their expression, either directly or indirectly. Notably, certain transcription factors bind to their own gene promoter within the nucleus, leading to downregulation of their expression, acting as a negative feedback loop.

1.4 NFAT

Nuclear factor of activated T-cells (NFAT) is a family of transcription factors. Traditionally known for their role in T-cell development, they are also now known to induce genes involved in the development of the heart, the pancreas, skeletal muscle, smooth muscle, blood vessels, neurons, bone, and skin[110]. The NFAT family members include NFAT1-5 and can be divided into two categories. NFAT1-4 are activated by calcium/calcineurin signaling while NFAT5 is activated in response to osmotic stress[110]. NFAT1-4 activity regulates a diverse number of genes controlling the expression of E3 ubiquitin ligases, proteases, tyrosine phosphatases, and transcriptional repressors and activators. These genes are involved in the regulation of cell proliferation, differentiation, survival, and apoptosis [111]. Based on knockout studies in mice and siRNA knockdown studies in cell lines, NFAT1-4 appear to have somewhat overlapping functions; however certain functions appear to be context specific[112]. This review will focus on calcium-responsive NFAT1-4 which we study in relation to signaling pathways in GIST. From here forward, NFAT refers to NFAT1-4.

1.4.2 NFAT Structure

NFAT proteins are related to the Rel-NFKB family of transcription factors[110]. Each NFAT protein has a Rel homology region (RHR) within its DNA binding domain (DBD) composed of an N-terminal specificity domain that makes base-specific contacts with DNA at specific DNA binding elements of the sequence GGAAA[111]. These DNA elements resemble NF-KB binding elements[112]. In addition to the DNA binding domain, each NFAT is composed of an N-terminal transactivation domain, a carboxy-terminal domain, and a regulatory domain (Figure 4).

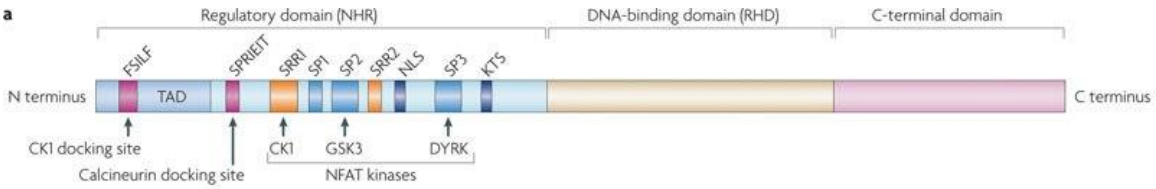

Figure 4 – NFAT structure. Muller et al., 2010, Nature Review – Immunology [113]. Reprinted with permission from Nature Publishing Group.

The regulatory domain contains serine-rich phosphorylation sites that are made up of S-P-X-X repeats. These sites are phosphorylated by kinases including GSK3, CK1, and DYRK (among others) and dephosphorylated by the phosphatase calcineurin[110]. NFAT kinases GSK3, CK1, and DRYK1 are involved in nuclear export of NFAT to the cytoplasm. CK1 and DYRK2 are both involved in the maintenance of NFAT phosphorylation in the cytoplasm – preventing translocation and transcriptional activity during resting conditions[110]. The regulatory domain also contains a calcineurin binding site of the motif: -P-X-I-X-I-T. The variable residues within this motif are always polar in NFAT1-4. Binding of calcineurin leads to dephosphorylation and exposure of the nuclear localization signal (NLS)[114]. The RHR also contains a C-terminal domain involved in dimer formation[112]. NFAT proteins can for homodimers or heterodimers with a number of other transcription binding partners which will be discussed later[110]; however NFAT1-4 are not obligate dimers.

1.4.3 NFAT Activation and Regulation

In resting cells NFAT is localized in the cytoplasm in a highly phosphorylated, inactive state. Increases in intracellular calcium lead to rapid dephosphorylation of NFAT and translocation to the nucleus (<15min) where it can activate the expression of a number of target genes. Extracellular signals lead to the activation of immune-receptors, frizzled receptors, or receptor tyrosine kinases (RTKs) which in turn activate

phospholipase C (PLC). PLC hydrolyzes phosphatidylinositol 4,5-bisphosphate (PIP_2) into second messengers DAG and IP3. DAG goes on to activate the MAPK pathway while IP3 binds to IP3 receptors on the endoplasmic reticulum (ER) causing Ca^{2+} efflux into the cytoplasm. Loss of Ca^{2+} in the ER leads to an influx of extracellular calcium into the cytoplasm through CRAC channels in the plasma membrane. The increased intracellular calcium concentration activates calmodulin, which in turn activates calcineurin. Calcineurin binds to NFAT's regulatory domain and removes five phosphates. This exposes the NLS and allows calcineurin better access to NFAT. Eight additional phosphates are removed by calcineurin leading to a conformational change which masks the nuclear export signal, allowing translocation of NFAT into the nucleus (Figure 5) [110, 112, 114, 115].

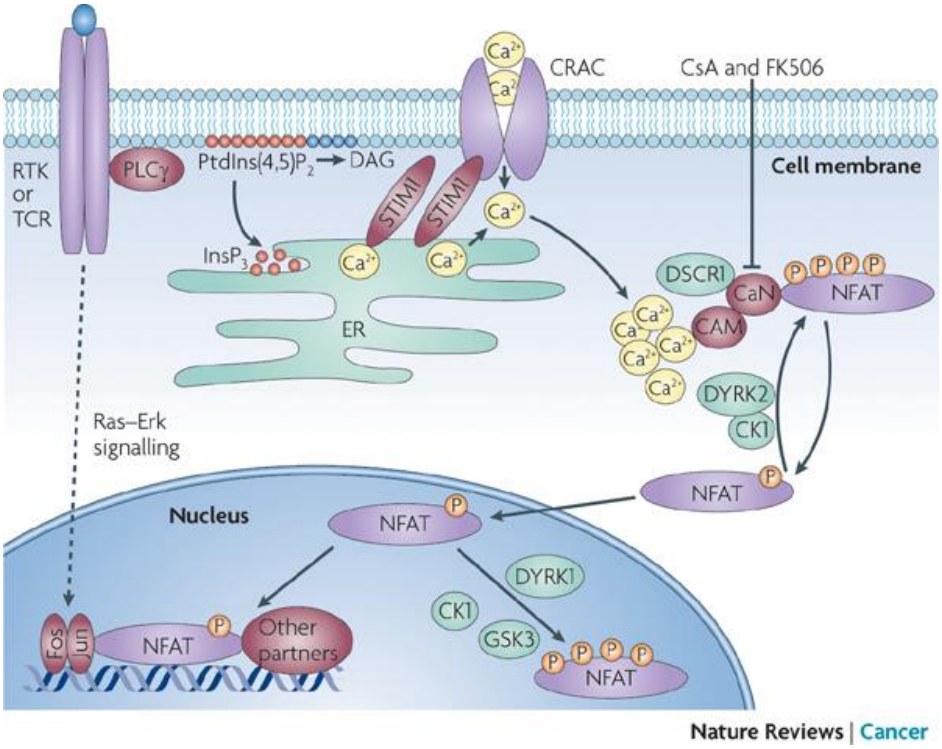

Figure 5 – NFAT signaling pathway. Mancini et al., 2009, Nature Reviews- Cancer. Reprinted with permission from Nature Publishing Group.

Once in the nucleus, active NFAT has a high affinity for DNA and can bind with numerous transcriptional binding partners to drive gene expression[112]. Constitutively active kinases (GSK3, CK1, DRYK1, etc.) within the nucleus rephosphorylate NFAT so it can be translocated back out into the cytoplasm [110, 112, 114].

In addition to kinases there are a number of other mechanisms that regulate NFAT to a lesser degree. HOMER2 and HOMER3 are cytoplasmic scaffold proteins which compete with calcineurin for NFAT binding. This competition prevents activation of NFAT by calcineurin[110]. A non-coding RNA known as NRON and an associated scaffold protein – IQGAP allow kinases to form a complex with NFAT in the cytoplasm and maintain its inactive state [115]. NFAT1 can be post-transcriptionally regulated by caspase-3 cleavage. Within the transactivation domain of NFAT1 there are two caspase 3 cleavage sites which lead to decreased NFAT activity[110] during apoptosis. Sumoylation of NFAT1 was shown to be required for transcriptional activity and nuclear anchorage [116]. DSCR1 is a protein which inhibits calcineurin/NFAT signaling by interacting with calcineurin A – a subunit within calcineurin [117]. DSCR1 expression is upregulated by calcineurin/NFAT signaling, and feedbacks to negatively down-regulate calcineurin activity [112]. And finally, ICER and $p21^{SNFT}$ have been reported to bind NFAT and inhibit its transcriptional activity[112]. ICER and $p21^{SNFT}$ both bind to NFAT:AP-1 composite DNA binding sites, preventing cooperative binding by NFAT and AP-1. In this way, ICER acts as a repressor for IL2 and IL4 transcription and $p21^{SNFT}$ is able to repress IL2 transcription [114].

In addition to endogenous modulators of NFAT there are also pharmacologic modulators of NFAT activity. The most highly utilized small molecules are the immunosuppressant drugs cyclosporine A (CSA) and tacrolimus (FK-506). These molecules bind to the immunophilin proteins cyclophilin A (with CSA) and FKBP12 (with FK506), which bind to

and inhibit calcineurin activity [118]. Due to their immunosuppressive function long term use of these drugs can be undesirable. And sometimes they can cause complications in patients with diabetes and high blood pressure[118]. As a result, small molecule inhibitors that are analogs of CSA and FK506 are being developed (i.e. L-732531 and ISATX47)[118]. Another specific NFAT inhibitor is the synthetic peptide VITIT which interferes with calcineurin-NFAT interaction[118].

1.4.4 NFAT Transcriptional Binding Partners

As mentioned above, NFAT proteins often bind DNA with other transcription factors to regulate specific transcriptional programs. The most well characterized NFAT binding partner is AP-1 [114]. AP-1 is a heterodimeric protein containing members of the Fos, Jun, ATF, and JDP families[114]. Together, NFAT and AP-1 bind composite sites on DNA which are separated by two base pairs, with NFAT binding GGAAA motifs and AP-1 binding to TGTTCA motifs. AP-1 is upregulated and activated by members of the MAPK pathway, not the calcium/calcineurin pathway. Cooperation between NFAT and AP-1 represents a source of signal integration between the Ca^{2+}/calcineurin/NFAT pathway and the MAPK pathway [112, 114]. Complexes formed by NFAT and AP-1 are more stable than when either protein binds alone and these complexes have a positive synergistic effect on gene transcription [114]. The complexes themselves are supported by contact between the amino-terminal domain of the NFAT homology region and the leucine zipper regions of the AP-1 proteins [114]. Determination of which distinct set of genes is transcriptionally activated depends on whether NFAT and/or AP-1 bind to the composite DNA site. A much smaller set of genes is activated when only one transcription factor is present on the composite DNA site[112]. NFAT:AP-1 binding sites have been shown to regulate the expression of IL2, GM-SCF, IL3, IL4, IL5, IL13, IFN-γ, FasL, CD25, and COX2[114] and MYC[119]. Aside from AP-1, NFAT has a number of

other cooperative DNA binding partners including: Maf, ICER, p21^{SNFT}, GATA, EGR, Oct, HNF3, IRF-4, MEF2, p300, and PPAR-γ.

1.4.5 NFAT and Cancer

Our interest in NFAT comes from its recent ties to cancer. Numerous studies have now implicated NFAT in cancer initiation and progression [110, 111, 117-125]. Although mutations in NFAT have not been identified in cancer [110], studies have identified aberrant NFAT expression and signaling in melanoma [123, 125], various lymphomas, CML, breast cancer [118], and pancreatic cancer [120]. The PI3K/AKT signaling pathway is one of the most frequently deregulated pathways in cancer [118]. Constitutive activation of this pathway in cancer turns on AKT which inactivates GSK3 – one of the constitutive kinases responsible for inactivating NFAT, which could account for constitutive NFAT activity in these cancers [118].

Interestingly, adult patients with Down 's syndrome have one-tenth as much risk of getting cancer as a non-Down's syndrome patient [126]. This led to the hypothesis that a gene on chromosome 21 may have tumor suppressor properties. Studies show that Down's syndrome patients have elevated expression of DSCR1 which is a calcineurin and VEGF-A repressor, and DYRK1 (kinase) which is involved in NFAT nuclear export. Cells overexpressing DSCR1 and DYRK1 showed decreased tumor formation in mice as a result of decreased angiogenesis through inhibition of VEGF signaling [127]. These findings support the role of NFAT signaling in cancer progression and provide a mechanism to explain the reduced cancer incidence in Down's syndrome patients [127]. While this study provides evidence for an absence of cancer in the absence of NFAT signaling – other studies have shown the presence of cancer when NFAT signaling is hyperactive.

Table 2 - Summary of NFAT in cancer.

Cancer type	Family Member	Function	Reference
B cell lymphomas	NFAT2	Maintaining lymphoma cell survival and counteracting apoptosis by induction of survival factors such as CD40 ligand and BLYS	[128, 129]
T-ALL	NFAT1-NFAT4	Constitutive activation of calcineurin leads to NFAT activation	[130, 131]
CML	NFAT2	Development of resistance to TKI treatment	[132]
Breast cancer	NFAT1	Control of cancer cell migration and invasion by induction of COX2	[133, 134]
Pancreatic cancer	NFAT2	Induction of MYC expression	[135, 136]
Prostate cancer	ND	Regulation of cancer cell proliferation	[137]
Melanoma	NFAT2 and NFAT4	Induction of COX2	[138]
Endometrial cancer	ND	Regulation of IL11 and CXCL8 expression	[139, 140]

In studies of melanoma, NFAT2 has been shown to regulate quiescence and proliferation of skin stem cells [121]. Additionally, NFAT1 was shown to be constitutively active in many melanoma cell lines, and acted to suppress apoptosis [125]. Inhibition of NFAT1 with calcineurin led to “caspase-dependent melanoma cell death” consistent with the large increase in sub-G1 phase cells [125].

In a study by Flockhart et al. in 2009, NFAT was found to contribute to both the development and progression of melanoma[123]. Activating-BRAF mutations are found in approximately 42% of melanomas [141] and of those 90% are $BRAF^{V600E}$ [123]. It has previously been shown that BRAF can drive NFAT activity [122], and in line with these results, NFAT transcriptional activity was found to be upregulated in $BRAF^{V600E}$-mutated melanoma [123]. Furthermore, NFAT is known to regulate COX-2 expression – elevated

levels of which are correlated with poor prognosis in melanoma [123]. COX-2 activation was shown to be elevated in $BRAF^{V600E}$ melanoma and this overexpression was NFAT dependent. NFAT transcriptional activity was blocked by a MEK inhibitor [123], which confirmed a role for BRAF in the constitutive activation of NFAT in BRAF mutant melanoma cell lines [123].

In pancreatic tumor cells, calcineurin activity drove proliferation and anchorage-independent growth [118]. Signaling through calcineurin led to nuclear localization of NFAT2 and activation of MYC – a well characterized oncogene [118]. Increased expressed of NFATs has also been implicated in aggressive breast cancer [118], due to the upregulation of autotoxin transcription. In another study, many breast cancer patients were found to harbor activating mutations in PI3KCA, which encodes the catalytic subunit of PI3K. Again, activation of PI3K leads to activation of AKT, which decreases nuclear export of NFAT through inhibition of the kinase GSK3.

Recall, that under resting conditions NFAT should be located in the cytoplasm in a highly phosphorylated state. When NFAT is constitutively active, unstimulated cells show nuclear localization and dephosphorylation of NFAT. Constitutively active NFAT has been found in Burkitt's lymphoma, diffuse large B cell lymphoma, T cell lymphoma [118], and CML cell lines [124]. In addition to patient samples and cancer cell lines, constitutively activated NFAT cell lines has been created to help elucidate NFAT's role in cancer. In fibroblasts, constitutively active NFAT2 led to transformation and colony formation [118]. Conversely, constitutively active NFAT1 did not increase transformation or colony formation in these cells [118] demonstrating that specific NFAT involvement in cancer is tissue or context specific. Another study used constitutively active NFATs in NIH 3T3 cells to show that NFAT2activity increased proliferation, and cellular transformation[121]. Despite the identification of constitutively active NFAT in a number

of cancers it is still unknown what genetic and epigenetic factors drive its constitutive activity and nuclear localization [118]. This is an active area of research that we are addressing in a GIST context.

As previously noted, NFAT often acts with other transcription factors. In terms of cancer, NFAT cooperates with a number of transcription factors such as: GATA, EGR, MEF2 and FOXp3, which have all been linked to cancer[118]. Cooperation with AP-1 has been shown to be necessary and sufficient to drive the expression of Src, which leads to lineage commitment in mouse embryonic stem cells. Src signaling in turn mediates the epithelial to mesenchymal transition(EMT) [142]. EMT is characterized by loss of cell adhesion and increased cell mobility and represents the first step in the initiation of metastasis.

1.4.6 NFAT and GIST

Recently, a handful of studies have implicated calcineurin and NFAT signaling in GIST or in closely related cancers. In 2010, Gregory et al. performed a synthetic lethal screen in CML cells with siRNAs. The goal was to identify synthetic lethal drug combinations with imatinib. The group identified a number of family members within the Wnt/Ca2+/NFAT signaling pathway that all led to synergistic cell death when silenced in combination with imatinib therapy. We were interested in this study because CML cells use similar signaling pathways to drive cancer - i.e. PI3K/AKT, and MAPK signaling [124].

Also related to NFAT, a study in 2007 by Guha et al. found that mitochondrial stress activated calcineurin and led to increased resistance to apoptosis and induced invasive behavior in C2C12 myoblasts and in A549 lung cancer cells [143]. Investigators disrupted the mitochondrial membrane potential in these cell lines which initiates stress

signaling. Calcineurin was activated as part of this stress signaling and led to the activation of IGF1R and increased glucose uptake. Silencing of IGF1R mRNA led to an increase in apoptosis, reduced cellular migration through Matrigel membrane, and reduced glucose uptake [143]. Conversely, in control cells, calcineurin was not found to play a role in glucose uptake or the expression of IGF1R. Therefore this mechanism is unique to cells undergoing mitochondrial stress, and may indicate a calcineurin-mediated mechanism of tumor growth [143].

Along this line of research, Chou et al. found that succinate dehydrogenase(SDH)-deficient GISTs are characterized by IGF1R overexpression [144]. This class of GISTs does not display activating KIT or PDGFRA mutations, and is resistant to imatinib therapy. It is unknown what drives cancer in these tumors and characterizing these tumors is an active area of research in our laboratory. IGF1R overexpression was found in 100% of SDH-GIST tumor samples and not in any non-SDH GIST tumors. So, while IGF1R overexpression is associated with SDH-GIST tumors it is not a characteristic of all WT GIST tumors [144].

With NFAT being implicated in numerous cancers, and with the results from the Gregory et al. synthetic lethal screen in CML cells, we would like to investigate whether a similar NFAT signaling phenomenon is at work in KIT mutant cell lines. This investigation would involve identifying upstream activators of NFAT as well as identifying the NFAT target gene responsible for synergistic cell death when NFAT is inhibited in combination with KIT.

1.5 Summary and Hypothesis

We are studying synergistic drug combinations in order to improve patient outcome by decreasing both disease persistence and disease resistance. Based on the

premise of synthetic lethality we are targeting KIT in combination with other vital protein targets which should lead to a synergistic decrease in cell viability and increase in apoptosis. Previous research by Gregory et al. found that combining a BCR-ABL inhibitor with a KIT inhibitor led to synergistic cell death in CML models. Based on similarities between BCR-ABL and KIT signaling pathways we combined a KIT inhibitor and a calcineurin inhibitor in KIT-mutant cancer models and found a synergistic decrease in cell viability. We hypothesized that this synergy was NFAT-dependent. To characterize the observed synergy and to investigate this hypothesis we developed the following aims:

Specific Aim 1: Determine the effects of KIT inhibitors and/or calcineurin inhibitors on cellular proliferation, caspase/apoptosis, and NFAT status in models of KIT mutant cancer. (Chapter 2)

Specific Aim 2: Determine whether the observed synergy requires inhibition of NFAT/calcineurin activity. (Chapter 2)

Specific Aim 3: Determine the downstream targets of combination treatment in P815 cells. (Chapter 3)

Chapter 2: Combination therapy for KIT-mutant mast cells: Targeting constitutive NFAT and KIT activity

Combination therapy for KIT-mutant mast cells: Targeting constitutive NFAT and KIT activity

Alison C Macleod[1,2], Janice Patterson[1,2], Diana Griffith[1,2], Carol Beadling[1,2] , Michael Heinrich[1,2]

[1] Portland VA Medical Center, Portland, OR

[2] OHSU Knight Cancer Institute, Portland, OR

Conflict of interest:

MCH: Consultant: Ariad, Novartis, Pfizer, Molecular MD. Research funding: Novartis, Ariad. Equity Interest: Molecular MD.

ACM: no conflict, JP: no conflict, DG: no conflict, CB: no conflict

Manuscript resubmitted to *Molecular Cancer Therapeutics* on 1/17/14

Abstract:

Purpose: Resistant KIT mutations have hindered the development of KIT kinase inhibitors as treatment for human systemic mast cell disease in patients. The goal of this research was to characterize the synergistic effects of a novel combination therapy involving KIT and calcineurin enzyme inhibition using a panel of KIT-mutant mast cell lines.

Experimental Design: The effects of mono- or combination- therapy on the cellular viability/survival of KIT-mutant mast cells were evaluated. In addition, NFAT-dependent transcriptional activity was monitored in a representative cell line to evaluate the mechanisms responsible for the efficacy of combination therapy. Finally, shRNA was used to stably knockdown calcineurin expression to confirm the role of calcineurin in the observed synergy.

Results: The combination of a KIT and a calcineurin inhibitor synergized to reduce cell viability and induce apoptosis in six distinct KIT-mutant mast cell lines. Both KIT and calcineurin enzyme inhibitors were found to decrease NFAT-dependent transcriptional activity. NFAT specific inhibitors induced similar synergy and apoptosis as calcineurin phosphatase inhibitors when combined with a KIT inhibitor. Notably, NFAT was constitutively active in each KIT-mutant cell line that we tested. Knockdown of calcineurin subunit PPP3R1 sensitized cells to KIT inhibition and increased NFAT phosphorylation and cytoplasmic localization.

Conclusions: These results suggest that constitutive activation of NFAT represents a novel characteristic of KIT-mutant mast cell disease. Our studies suggest that combining a KIT inhibitor and an NFAT inhibitor might represent a novel treatment strategy for mast cell disease.

Introduction:

Activating KIT mutations, most commonly KIT D816V, are a hallmark of human systemic mast cell disease (SMCD) [145, 146]. Related mutations are also found in the mast cell neoplasms of other vertebrates, including mice, rats, and dogs [70, 81, 147-149]. Theoretically, treatment of advanced SMCD with KIT kinase inhibitors should target the neoplastic cells and exert a therapeutic effect. To date, the use of KIT inhibitors against advanced SMCD has had only minor clinical impact. This is due to a variety of reasons. First, current tyrosine kinase inhibitors (TKIs) have limited activity against resistant mutations - such as KIT D816V[150]. Second, patients who do respond to KIT TKI therapy can develop secondary resistance over time due to the emergence of secondary resistance mutations [76]. Third, at least in the case of other KIT-mutant cancers, treatment with KIT inhibitors typically results in a large burden of persistent disease that can quickly progress following discontinuation of KIT TKI therapy [151]. The immediate goal of this research was to investigate a new combination therapy – simultaneous inhibition of KIT and calcineurin – for its effect in KIT-mutant cancer models. In addition, we sought to understand the underlying mechanism behind the efficacy of this combination so that better therapies could be derived from the novel biology. It is our belief that such novel combination therapies will lead to more effective treatment options that overcome both disease resistance and disease persistence in human SMCD, as well as other KIT-mutant cancers.

KIT is a type III receptor tyrosine kinase that is expressed on the surface of mast cells, hematopoietic stem and progenitor cells, melanocytes, interstitial cells of Cajal, and germ cells[152]. KIT is activated by extracellular binding of its ligand, stem cell factor (SCF). Binding of SCF leads to KIT dimerization, tyrosine kinase activation, and subsequent activation of downstream signaling pathways: PI3K-AKT, MAPK, and JAK-

STAT [42, 153]. Signaling through KIT promotes cell growth, survival, and proliferation [154]. Activating KIT mutations, such as D816V, result in ligand-independent kinase activity and activation of KIT-dependent downstream signaling pathways [42, 67]. In addition to SMCD, activating KIT mutations have been identified in gastrointestinal stromal tumors[155], AML[156], melanoma[157], and seminoma[158].

While it is well recognized that constitutive KIT signaling is associated with SMCD [66, 67, 80-83] and likely is the causative abnormality, it is also believed that KIT signaling alone is insufficient for disease progression [84]. The molecular mechanisms leading to disease progression remain unknown. One potential mechanism of progression, which we explore in this paper, is constitutive activation of the NFAT signaling pathway. This pathway was recently identified as being constitutively activated in melanoma, colon cancer, and CML [132, 138, 159-161]. Notably, in melanoma model systems, NFAT family members were not only found to be constitutively active, but also to regulate quiescence and proliferation of skin stem cells [162]. Gregory et al.. found that NFAT inhibition sensitized CML cells to imatinib treatment [132], and similarly, Spreafico et al.. reported the benefits of combining NFAT and MEK inhibition in models of colorectal cancer [159].

Nuclear factor of activated T-cells (NFAT) is a family of transcription factors that are related to the Rel-NFKB family of transcription factors. Each NFAT protein has a Rel-homology region which makes base-specific (GGAAA) contacts with DNA to regulate the transcription of a diverse number of genes involved in the regulation of cellular proliferation, differentiation, survival, and apoptosis [113, 163, 164]. There are four calcium responsive NFAT family members – NFAT1-4. Based on knockout studies in mice and siRNA knockdown studies in cell lines, NFAT1-4 appear to have somewhat overlapping functions; however certain functions appear to be context specific[113, 165].

In resting cells, NFAT is localized in the cytoplasm in a highly phosphorylated, inactive state. Increases in intracellular calcium lead to activation of calcineurin, which binds to NFAT's regulatory domain and dephosphorylates NFAT. Dephosphorylation exposes the nuclear localization signal and leads to rapid translocation into the nucleus (< 15min) where it acts as a transcription factor. NFAT family members bind with numerous other transcription factors to regulate target gene expression [165]. Within the nucleus, constitutively active kinases (i.e. GSK3, CK1, DYRK1) phosphorylate NFAT, resulting in translocation back into the cytoplasm [113, 164, 165].

In this paper we provide evidence that NFAT is constitutively active in KIT-mutant mast cells; and that dual inhibition of KIT and calcineurin enzyme activity leads to synergistic decreases in cell viability as well as increases in apoptosis in KIT-mutant mast cells. We propose that simultaneous inhibition of KIT and calcineurin signaling may improve treatment of KIT-mutant SMCD.

Materials and Methods:

Cell culture:

P815[166], HMC1.1, HMC1.2[167] cells were grown in DMEM (10% FBS, 1% L-glut, 1% pen-strep). RBL2H3s[168] were grown in MEM (15% FBS, 1% L-glut, 1% pen-strep). BR and C2 [169] cells were grown in DMEM (2% calf serum, 0.125g histidine, 12.5mL HEPES per 500mL). All cells were grown at 37°C and 5% CO_2. Each cell line's morphology was monitored, and growth curve analysis and sequencing was performed bi-annually to ensure the identity of each line throughout the course of these studies.
The P815 and RBL2H3 cells were purchased from ATCC. The BR and C2 cells were generously donated by Dr. Bill Raymond. The HMC1.1 and HMC1.2 cells were generously donated by Dr. J.H. Butterfield (Table 3).

Immunoblotting studies:

To prepare nuclear and cytoplasmic protein extracts, we used Thermo-Scientific NE-PER Nuclear Extraction Kit (#78833) and followed the manufacturer's instructions. Lysates were prepared using either the NE-PER kit or routine detergent lysis (RIPA lysis buffer: 50mM Tris-HCl, 1% IGEPAL, .25% deoxycholate, 150mM NaCl, 5mM EDTA). The antibodies used in our immunoblotting experiments are listed in Table 4.

Cell viability and caspase assays:

Cells were plated at 10,000/well at the same time they were treated, in opaque, 96-well plates in a total volume of 50uL per well. Control and treated cells were incubated for 48 hours.

Following incubation, 50uL of Cell Titer Glo substrate (Promega #G7571) was added to each well. Plates were rocked for 15 minutes and then analyzed using the "Cell Titer-

Glo" program on a Microplate luminometer GloMax-96 (Promega). Alternatively, following incubation, 50uL of Caspase 3/7 (Promega #G8091), or Caspase 8/9 reagent (Promega #G8200, G8210) (RBL2H3 cell line only) was added to each well. Plates were rocked for 60 minutes and then read using the "Caspase-Glo" program on a Microplate luminometer GloMax-96 (Promega).

NFAT-P815, shCN-P815 cell lines:

The NFAT-P815 line was created using virions containing the Cignal Lenti NFAT Reporter construct (SABioscience catalog # 336851, CLS-015L). P815 cells were transduced using 78µL DMEM media (+15% FBS, 1% P/S, 1% L-Glut), 6µg/ml polybrene (2µL/well at .3µg/ul), and 20µL Cignal Lenti NFAT reporter. Stably transduced cells were selected for resistance using 1µg/ml of puromycin. Drug resistant cells were tested with the Luciferase Assay System (Promega, #E1501) to quantify firefly luciferase expression.

P815 cells with PPP3R1 knockdown (shCN) or non-targeting knockdown (shNT) were created using pLKO.1 Mission lentiviral transduction particles from Sigma (PPP3R1 shRNA [NM_024459.1-227s1c1], non-targeting shRNA [SHC002V)]). Briefly, P815 cells were transduced overnight with 85.5uL media, 0.006µg polybrene, and 12.5µL of lentiviral particles. Following a 24 hour recovery, stably transduced clones were selected using 1µg/mL of puromycin.

NFAT-dependent transcription assays:

NFAT-P815 cells were plated the same day they were treated. Following incubation, media was aspirated from the wells, and 20uL of Passive Lysis Buffer (Promega) was added to each well. Plates were rocked for 15 minutes and then loaded into the Microplate luminometer GloMax-96. The plates were analyzed with the "Luciferase

Assay System with Injector" program which injects 100uL of firefly luciferase reagent into each well before quantifying luciferase protein present. The luciferase readout was used as an indication of NFAT transcriptional activity and was typically normalized to cell viability (CTG Assay) for drug incubation lasting longer than 3 hours.

RT-PCR:

Total RNA was extracted from P815 cells using a Qiagen RNAeasy Plus Mini Kit combined with the Qiagen RNase-Free DNase Treatment. Single-stranded cDNA was prepared from 1 µg of total RNA in a 50-µL reaction using 60 µmol/L random hexamer primers, 0.5 mmol/L dNTPs, 100 units RNaseOUT, 5 mmol/L DTT (DTT: dithiothreitol), 1× First Strand buffer, and 500 units SuperScript III reverse transcriptase following manufacturer's instructions (Invitrogen by Life Technologies, Grand Island, NY).

Quantitative real-time polymerase chain reaction (qRT-PCR) was carried out in a 20µL reaction using 1ug single stranded cDNA (corresponding to 40 ng initial total RNA) and 19 probes Master MIX (Roche), with a FAM-labeled hydrolysis probe specific to the reference Glyceraldehyde 3-phosphate dehydrogenase (GAPDH). Cycling conditions on a Light-Cycler 480 instrument (Roche) included 10 min at 95^{o}C followed by 40 cycles of 95^{o}C for 10 sec and 60oC for 20 sec. NFAT1, 2, 3, 4, and GAPDH (murine, canine, human, rat) were detected using commercial TaqMan Gene Expression assays (Applied Biosystems by Life Technologies). Murine probes: NFAT2 assay Mm00479445_m1, NFAT1 assay Mm00477776_m1, NFAT4 assay Mm01249200_m1, NFAT3assay Mm00452375_m1, GAPDH assay Mm99999915_g1. Rat probes: NFAT2assay Rn04280453_m1, NFAT1 assay Rn01750325_m1. Canine probes: NFAT2 assay Cf02648711_m1, NFAT4 assay Cf02703251_m1, NFAT3 assay Cf02703250_m1.

Human probes: NFAT2 assay Hs00542678_m01, NFAT1 assay Hs00905451_m01, NFAT4 assay Hs00190046_m01, NFAT3 assay Hs00190037_m01.

Expression results were analyzed using the comparative C_T method (also known as the $2^{-\Delta\Delta CT}$ method) [170].

Results:

Combining a calcineurin inhibitor with a KIT inhibitor leads to synergistic decrease in cell viability and induction of apoptosis

Based on previous studies suggesting that calcineurin phosphatase inhibition synergizes with kinase inhibition to decrease BCR-ABL+ cell viability [132], we evaluated the effects of combining a KIT kinase inhibitor with a calcineurin phosphatase inhibitor in a number of KIT-mutant cell lines. P815 cells (murine KIT D814Y) were treated with a KIT inhibitor (dasatinib 5, 10, or 20nM), 1μM cyclosporine A (CSA), or both for 48 hours before measuring cell viability using a luminometer (Figure 6A, Cell Titer Glo assay, Promega). In this dose range, dasatinib produced a dose-dependent decrease in cell viability. In contrast, single agent CSA at a dose of 1μM had only a minimal effect on cellular viability (< 15% decrease). Notably, there was a significant decrease in cell viability with combination treatment, as compared with either agent alone. The viability data was analyzed using Calcusyn software, which uses the method of Chou and Talalay [171] to quantify synergy through computation of combination index (CI) values. The average CI value was 0.438 for P815 cells when dasatinib was combined with CSA indicating a synergistic effect of combination therapy. This experiment was repeated in five other KIT-mutant mast cell lines (cell line characteristics summarized in Table 5), with six different KIT TKIs and four different CNPIs and we observed similar degrees of synergy (summarized in Table 1). For comparison, we also show cell viability and caspase data for the HMC1.2 cell line (KIT D816V). These cells were also treated for 48 hours with 1μM CSA plus dasatinib (0.5, 1, or 5μM) and cell viability was measured (Figure 6B).

In our cellular proliferation experiments, we noted changes in cell morphology consistent with cellular death. To measure the effects of combination therapy on

induction of apoptosis (as assessed by activation of caspase activity), we performed similar single agent versus combination therapy experiments. We repeated our previous combination experiments treating P815 cells with 5, 10, or 20nM dasatinib alone or in combination with 1μM CSA. After 48 hours, caspase 3/7 activity was quantified as a measure of cellular apoptosis and normalized to cellular viability (Figure 6C). Caspase 3/7 activity was significantly greater in cells treated with combination therapy compared to treatment with dasatinib or CSA alone. We saw similar degrees of caspase induction with each KIT-mutant cell line tested to date with the exception of the RBL2H3 cell line, where caspase 8/9 activity, but not caspase 3 or 7 was induced by combination treatment (data shown for HMC1.2 cell line – Figure 6D).

We expanded these studies to include additional calcineurin phosphatase inhibitors (CNPIs) (FK506, ascomycin, fenvalerate, and pimecrolimus) and KIT inhibitors (imatinib, nilotinib, sunitinib, and ponatinib). Combining each of the KIT TKIs and CNPIs synergistically decreased cell viability and induced apoptosis (data not shown). Notably, calcineurin signaling has not previously been implicated as a critical growth or survival pathway in neoplastic mast cells.

In addition to improving response to therapy in KIT-mutant SM models, we also wanted to test the ability of combination therapy to combat disease persistence. We examined colony forming capacity of cells following extended drug exposure. We treated P815 cells with 1μM CSA, 20nM dasatinib, or CSA + dasatinib for 7 days. At day 7, the cells were washed, drug was removed, and cells were diluted and replated onto 6-well plates. Cells were allowed to recover. Cells treated with 1μM CSA reached confluency at 48 hours post plating and colonies were too numerous to count. Cells treated with dasatinib or combination were allowed to recover in drug

free media for 7 days at which point they were stained with 0.05% crystal violet and colonies were quantified. Colony counts are reported for dasatinib vs. dasatinib plus CSA (Figure 6E). As noted above, CSA alone had no effect on proliferation and replating of CSA-treated cells lead to a confluent lawn of cells after only two days. Dasatinib treatment resulted in an average of 467 colonies while combination therapy further reduced colony count to 82 for an 83% reduction in colony growth. This represents a significant decrease in colony growth over monotherapy with dasatinib ($p=0.049$).

NFAT is constitutively active in KIT-mutant cell lines

Based on the above results, we hypothesized that calcineurin phosphatase inhibitors (CNPIs) reduced the transcriptional activity of members of the NFAT family, and that inhibition of NFAT-induced transcription was required for the observed synergy. It is well known that NFAT is a downstream target of calcineurin; however, treatment with CNPIs has a number of off-target effects that could be responsible for the observed synergy [172-174]. To investigate whether NFAT was mediating the observed synergy between KIT inhibitors and CNPIs, we characterized NFAT expression and activity within KIT- mutant cells.

Given that there are four different calcium/calcineurin responsive NFAT family members, we performed qRT-PCR in human, mouse, canine, and rat KIT-mutant cell lines to determine which, if any, NFAT family member RNA transcripts were expressed. NFAT1, NFAT2, and NFAT4 were expressed in the murine P815 cell line (Table 6) as well as in human mast cell lines HMC1.1 and HMC1.2, and the rat RBL2H3 cell line. In the canine BR and C2 cell lines, NFAT2 and NFAT4 were the only detectable NFAT species. With the exception of the canine BR and C2 cell lines, we confirmed our RNA expression studies using immunoblotting.

To evaluate NFAT phosphorylation and subcellular localization in KIT-mutant mast cell lines, we treated cells for three hours with increasing doses of the calcineurin inhibitor CSA (Figure 7A). Cells were fractionated and probed for NFAT family members. We observed nearly 100% of NFAT species localized in the nucleus of untreated P815 cells, indicating constitutive NFAT activation under resting conditions in these cells. Following treatment with CSA, we saw a shift toward the upper, highly phosphorylated NFAT species and translocation into the cytoplasm. This band shift was observed with each of the three NFAT species expressed in P815 cells (Figure 7B). These experiments not only confirmed our qRT-PCR expression results, but also suggested inactivation of NFAT by CSA as a possible mechanism underlying the synergy of KIT TKI and CNPI combination therapy.

We tested other KIT-mutant cell lines to determine whether constitutive NFAT activation was a common characteristic of mastocytosis cell lines. We also wanted to establish whether NFAT was maximally activated in KIT-mutant cell lines. In addition to P815 cells, we treated rat RBL2H3 and human HMC1.2 cells with 1μM CSA or 1μM ionomycin (IonM) plus 100nM 12-O-tetradecanoylphorbol-13-acetate (TPA) for two hours. Ionomycin and TPA synergize to activate calcium flux which leads to downstream activation of calcineurin and NFAT. Following incubation, the cells were fractionated and Western blotting was used to visualize NFAT phosphorylation and localization. Each NFAT species expressed in HMC1.2's was found to be constitutively active based on band size and protein localization (Figure 8). The same pattern of constitutively active NFAT was observed in RBL2H3 and HMC1.1 cells (data not shown). In each cell line we observed a minimal further translocation of NFAT species into the nucleus following induction of calcium flux, indicating maximal activation of NFAT species in KIT-mutant mast cells (data not shown). Due to a lack

of antibodies suitable to detect canine NFAT species by immunoblotting, NFAT activation phosphorylation and subcellular localization could not be evaluated in the BR and C2 cell lines.

Finally, to visually confirm the immunoblotting results we stained murine P815 cells and human HMC1.2 cells for NFAT species. In both cell lines we observed a high level of nuclear staining in untreated cells. The nuclear staining was diminished in cells treated with 1uM CSA (Figure 9). This shift in localization confirms the shift in localization that we observe with Western blotting techniques, and strengthens our conclusion that NFAT species are constitutively active in KIT-mutant mast cell lines.

Constitutive activation of NFAT represents a novel finding in KIT-mutant mast cells that has not been previously reported. Having characterized NFAT gene and protein expression in these cell lines, we sought to assess the regulation of NFAT-dependent transcriptional activity by mono- and combination therapy.

Monotherapy and combination therapy decrease NFAT transcriptional activity in KIT-mutant cells

NFAT is a transcription factor, so in addition to changes in localization and phosphorylation, single agent and combination treatment should also lead to changes in NFAT-dependent transcriptional activity. To investigate the modulation of NFAT transcriptional activity we stably transduced an NFAT promoter- reporter construct into the P815 cell line. In this construct, transcription driven from a tandem repeat of the NFAT consensus binding sequence (GGAAA) and a minimal CMV promoter regulates the expression of firefly luciferase. There was a substantial basal level of reporter expression in this cell line, confirming constitutive NFAT activity.

CSA treatment of the NFAT promoter-reporter-P815 cell line (NFAT-P815) induced a dose dependent decrease in NFAT transcriptional activity as assessed by the level of firefly luciferase (Figure 10A). We saw a similar decrease in reporter activity when the cells were treated with other calcineurin inhibitors including FK506, ascomycin, fenvalerate, and pimecrolimus (data not shown). Unexpectedly, treatment of NFAT-P815 cells with dasatinib also resulted in a dose-dependent decrease in NFAT-dependent transcriptional activity (Figure 10B). This effect was also seen with other KIT inhibitors such as imatinib and ponatinib (data not shown). Combination treatment with CSA and dasatinib significantly decreased NFAT-dependent transcriptional activity more than either drug alone (Figure 10C), suggesting an intersection between the KIT and NFAT signaling pathways.

These data confirm constitutive calcineurin-dependent activation of NFAT-dependent transcriptional activity in KIT-mutant mast cell lines. NFAT-dependent transcriptional activity was modulated by either calcineurin inhibitors or KIT inhibitors. Notably, combination therapy synergistically decreased NFAT- dependent transcriptional activity, suggesting regulation of NFAT-dependent transcriptional activity as a common downstream target of this combination treatment.

KIT inhibition of NFAT-dependent transcriptional activity is independent of intracellular calcium levels

In previously described models systems, NFAT is regulated by intracellular calcium levels that activate calmodulin/calcineurin. While KIT signaling can activate calcium influx [175, 176], it is unknown whether this aspect of KIT activity is responsible for the inhibition of basal NFAT-dependent reporter activity we observe. To determine whether KIT inhibitors were acting through the same calcium-dependent pathway

as calcineurin inhibitors, we evaluated NFAT localization, phosphorylation, and transcriptional activity following treatment with KIT inhibitors or calcineurin inhibitors. NFAT-P815 cells were treated with a combination of TPA and IonM for 2 hours in order to activate calcium flux-dependent signaling and increase NFAT-dependent reporter activity. There was a 10-20 fold increase in NFAT-dependent reporter gene expression following TPA/IonM treatment. This increase was completely inhibited by pre- treating the cells for 2 hours with a calcineurin inhibitor (CSA or FK506) (Figure 11A). To confirm these results, NFAT-P815 cells were also pre-treated with four different CNPIs (CSA, FK506, ascomycin, and pimecrolimus) followed by a two hour treatment with TPA/IonM (100nM and 1μM respectively). As previously described, all of these calcineurin inhibitors blocked the increase in NFAT-dependent reporter activity induced by TPA/IonM treatment; however there was only a partial effect of these inhibitors on basal NFAT-dependent reporter activity (Figure 11B).

NFAT-P815 cells were pre-treated with calcium channel inhibitors (YM58483, a CRAC channel inhibitor[177] or pyr3, a TRPC inhibitor[178]) followed by a two hour treatment with TPA/IonM. Both calcium channel blockers completely inhibited the induction of NFAT-dependent reporter activity (Figure 11C); however they had only a minimal effect on basal NFAT-dependent reporter activity. Finally, NFAT- P815 cells were treated with KIT inhibitors (dasatinib, ponatinib, or imatinib), followed by a two hour treatment with TPA/IonM (Figure 11D). In contrast to the case with CNPIs, KIT inhibitors only partially reduced the TPA/IonM induced increase in NFAT-dependent reporter gene expression, suggesting that KIT inhibitors do not effectively block induced calcium flux and subsequent calcineurin activation. However, the fact that KIT inhibitors affect basal NFAT signaling, whereas calcium channel blockers do not, suggests an alternative mechanism by which KIT inhibitors regulate basal and

induced NFAT signaling in KIT-mutant mast cells. It appears that induced NFAT transcriptional activity is completely calcium dependent, whereas basal NFAT transcriptional activity is modulated by additional KIT- dependent mechanisms, such as signaling through downstream KIT pathways.

One explanation for the synergy observed in our combination treatment studies is that inhibition of calcineurin signaling modulates NFAT and this in turn modulates KIT expression or activity. Alternatively, KIT kinase inhibitors could modulate NFAT subcellular localization and/or phosphorylation through an unidentified mechanism. This latter model would explain why KIT inhibitors modulate NFAT-dependent reporter activity in KIT-mutant mast cells. To test this hypothesis, P815 cells were treated with CSA or FK506 (10, 100, 1000nM). Protein lysates from treated cells were fractionated and probed for activation of phospho-KIT as well as the downstream KIT signaling targets ERK and AKT. CSA and FK506 had no effect on phospho-KIT, phospho-ERK, or phospho-AKT using doses that were sufficient to modulate NFAT activity and which had a synergistic effect in our cellular assays, indicating that CNPIs do not directly affect KIT kinase activity or proximal signaling pathways (e.g. MAPK, Figure 12A). In additional experiments, P815 cells were treated with dasatinib or imatinib (1, 10, 50 nM and 0.5, 1, 5 μM, respectively) before cellular fractionation and immunoblotting for NFAT2 and NFAT4. Inhibition of KIT signaling by dasatinib or imatinib did not cause a shift in NFAT species to the upper, highly phosphorylated state, nor did it cause any increase in cytoplasmic localization (Figure 12B).

Altogether, these data indicate that the effects of KIT inhibition on NFAT-dependent transcriptional activity and cell viability likely is exerted through an alternative mechanism, independent of calcium signaling or calcineurin activity. Despite the

lack of direct crosstalk, these two pathways seem to converge at the transcriptional level.

Calcineurin knockdown sensitizes p815 cells to dasatinib treatment

In order to determine the mechanism mediating the synergy of combination therapy, we tested whether the effects of combination therapy were calcineurin-dependent versus calcineurin-independent. As discussed above, CSA has additional off target effects besides its well characterized effect on inhibiting calcineurin phosphatase activity. To eliminate these off target effects as mechanisms behind synergy we used lentiviral transduction to deliver shRNA and create stable knockdown of the calcineurin subunit PPP3R1. Calcineurin is a heterodimer, composed of a catalytic subunit and a regulatory subunit. Knockdown of either subunit leads to enzyme inactivation. In addition to three unique catalytic subunit isozymes (PPP3CA, PPP3CB, PPP3CC), there are two regulatory isozymes (PPP3R1, PPP3R2). Only PPP3R1 is expressed in P815 cells, so we were able to use a single knockdown of PPP3R1 to inhibit calcineurin phosphatase activity.

We stably transduced P815 cells with a non-targeting mammalian shRNA or a PPP3R1 shRNA. Puromycin-resistant cells were selected for further analysis. Immunoblotting of cells stably transduced with a PPP3R1 shRNA demonstrated that knockdown of calcineurin lead to a shift in NFAT localization – similar to that observed with 1μM CSA treatment (Figure 13A). These effects were not seen with stable clones expressing a non-targeting shRNA (shNT). The stable shCN-P815 cells were tested with dasatinib, with and without CSA. The shCN knockdown cell line showed increased sensitivity to dasatinib treatment compared to shNT-P815 cells. The decrease in cell viability in the CN knockdown cells was comparable to the observed

cell viability following combination therapy in P815 cells (Figure 13B). This sensitivity was not observed in shNT cells treated with dasatinib.

Based on these results we conclude that the observed synergy is calcineurin dependent and not the result of inhibiting other CSA targets such as MDR1, or cyclophilin A.

NFAT specific inhibitors combine with KIT inhibitors to synergistically decrease cell viability and induce apoptosis

To further confirm that the observed synergy was both calcineurin- and NFAT-dependent, we tested the effects of two NFAT specific inhibitors (rocaglamide[179], tributylhexadecylphosphonium bromide (THPB)[180]), alone or in combination with dasatinib. Combination therapy with rocaglamide/dasatinib or THPB/dasatinib decreased cell viability more significantly than monotherapy (Figure 14A, B). The average calculated combination index value was 0.73 and 0.36 for rocaglamide plus dasatinib and THPB plus dasatinib, respectively, indicating synergy for both drug combinations.

To determine whether NFAT specific inhibitors induced apoptosis when combined with a KIT inhibitor, we tested the effects of monotherapy versus combination therapy on P815 cells. To assess apoptosis induction, caspase 3/7 was quantified after 48 hours of drug treatment (Figure 14C, D). For each NFAT inhibitor combination there was a significant increase in caspase 3/7, most notably at doses above 20nM rocaglamide and 100nM THPB.

Our data with NFAT specific inhibitors are in complete agreement with our results using calcineurin phosphatase inhibitors, or PPP3R1 knockdown, suggesting that the synergy between KIT inhibitors and calcineurin inhibitors is NFAT-dependent.

Discussion:

Despite the fact that targeted kinase therapy has transformed treatment of some KIT-mutant cancers, KIT-mutant SM patients have yet to fully benefit from these therapies. Unfortunately, most cases of human SM harbor the KIT D816V mutation, which is minimally or at best partially inhibited by clinically available KIT TKIs. Therefore, novel treatment options are needed to sensitize these cells to KIT TKI therapy. In this paper we present data indicating that calcineurin/NFAT inhibition sensitizes KIT-mutant mast cells to KIT TKIs. Synergy was seen even when the KIT TKI was used at doses that had only a minimal anti-proliferative effect as a single agent. This observation is of particular relevance to the treatment of SM with an associated D816V mutation.

Notably, we report for the first time that NFAT family members are constitutively activated in all KIT - mutant mast cell lines tested to date, including the HMC1.2 cell line harboring KIT V560G+D816V. This phenomenon has not previously been described and may contribute to the progression of mast cell disease. The cause of this constitutive NFAT activation is unknown, but NFAT activation and localization can be manipulated using calcineurin inhibitors (CSA and FK506). Calcineurin phosphatase inhibitors alone were not sufficient to decrease cell viability or induce apoptosis but combining KIT TKIs and calcineurin/NFAT inhibitors led to a synergistic anti-proliferative and pro-apoptotic effect in KIT- mutant mast cells. This suggests that CNPIs cooperate with KIT inhibition to affect cell viability and apoptosis. Additionally, we presented evidence that combination therapy may diminish disease persistence based on significantly reduced replating efficiency following simultaneous inhibition of KIT and calcineurin in KIT-mutant mast cell models.

It is known that calcineurin inhibitors such as CSA have other targets in addition to calcineurin. One such reported target is the drug efflux pump PgP, which mediates multidrug resistance (MDR) [41-43]. If synergy was mediated via the inhibition of PgP by CSA, then we would expect to see a further decrease in KIT activation following treatment of KIT-mutant cells with CSA/dasatinib when compared with single agent dasatinib. However, combination therapy did not further modulate KIT autophosphorylation compared with dasatinib alone (data not shown). In agreement with this observation, combination therapy and single agent dasatinib had identical effects on KIT-dependent signaling through the PI3K and MAPK pathways. To confirm that the observed synergy was in fact NFAT-dependent, we knocked down the expression of the PPP3R1 subunit of calcineurin. PPP3R1 knockdown sensitized P815 cells to dasatinib treatment, and eliminated the effect of adding 1μM CSA.

The fact that CN knockdown replaced the effects of adding CSA strongly supports our hypothesis that inhibition of calcineurin is required for the observed synergy. To further confirm these results we tested NFAT specific inhibitors in combination with KIT inhibitors. Our results replicated the results we saw with CSA combined with dasatinib, as determined by CI values; we therefore conclude that synergy between KIT inhibitors and CNPIs is NFAT-dependent.

We also found that KIT inhibitors did not affect NFAT phosphorylation or cellular localization. However, KIT inhibitors partially inhibited basal NFAT-dependent transcriptional activity in our NFAT-dependent promoter-reporter cell line, suggesting that these two pathways converge to regulate NFAT-dependent transcriptional activity. It has been reported that KIT signaling activates calcium signaling [181], so we hypothesized that inhibition of KIT signaling could affect NFAT through reduction of calcium flux. However, when we induced calcium influx with TPA and ionomycin,

KIT inhibitors were unable to fully block the resultant increase in NFAT-dependent transcriptional activity. On the other hand, either calcium channel blockers or calcineurin inhibitors were able to completely inhibit the increase in NFAT activity induced by increased calcium flux. Conversely, calcium channel blockers only minimally inhibited basal NFAT-dependent transcriptional activity, as assessed with our promoter-reporter cell line model. Finally, KIT inhibitors partially blocked basal NFAT- dependent transcriptional activity. We conclude that constitutive NFAT activity in mast cells is only minimally-dependent upon calcium flux.

In addition to KIT modulating NFAT-dependent transcriptional activity, we examined the possibility that NFAT activity could modulate KIT expression or kinase activity. However, we found no evidence that calcineurin inhibitors modulated levels of total or phospho-KIT (Figure S2). To further investigate the mechanism behind modulation of NFAT-dependent transcription by inhibitors of these distinct pathways, we examined the effects of KIT inhibition on NFAT localization and phosphorylation. We found that neither dasatinib nor imatinib affected NFAT localization or phosphorylation at doses that were sufficient to inhibit KIT signaling. It is known that NFAT transcriptional activity synergizes with certain DNA binding partners such as JUN [33, 34]. We hypothesize that KIT inhibition modulates one or more NFAT binding partners leading to the observed decrease in NFAT-dependent transcriptional activity.

Figures and Tables:

Table 3 - Summary of KIT-mutant mast cell characteristics

Cell Line	Species	KIT mutation	Media Conditions
p815	Murine	D814Y	DMEM+10% FBS, 1% pen strep, 1% L-Glut
RBL2H3	Murine	D817Y	MEM+10% FBS, 1% pen strep, 1% L-Glut
BR	Canine	L575P	DMEM+2% calf serum, .25g/L histidine, 25mL/L HEPES
C2	Canine	16bp insertion	DMEM+2% calf serum, .25g/L histidine, 25mL/L HEPES
HMC1.1	Human	V560G	DMEM+10% FBS, 1% pen strep, 1% L-Glut
HMC1.2	Human	V560G+D816V	DMEM+10% FBS, 1% pen strep, 1% L-Glut

Table 4 - Antibodies used in this study

Antibody	Concentration	Company	Catalog #
NFAT1	1:1000	Cell Signaling	4389
NFAT2	1:1000	Thermo Sci	MA3-024
NFAT3	1:400	Santa Cruz	sc-13036
NFAT4	1:400	Santa Cruz	sc-8321
B-actin	1:1000	Cell Signaling	4970
p-KIT	1:1000	Cell Signaling	3391
Total KIT	1:1000	Cell Signaling	3074
p-ERK	1:1000	Cell Signaling	9101
Total ERK	1:1000	Cell Signaling	9102
p-AKT	1:1000	Cell Signaling	9271
Total AKT	1:1000	Cell Signaling	9272
Lamin A/C	1:400	Santa Cruz	sc-7292
MYC	1:1000	Cell Signaling	5605
Pim2	1:400	Santa Cruz	sc-13514
p-STAT3	1:1000	Cell Signaling	9131
p-STAT5	1:1000	Cell Signaling	9351
Total STAT3	1:1000	Cell Signaling	9132
Total STAT5	1:1000	Cell Signaling	9352
B-tubulin	1:1000	Cell Signaling	2128

Table 5 - Summary of combination index values for KIT-mutant mast cell lines from CNPI+KIT inhibition Combination index (CI) values calculated following 48hr combination therapy**.** CI's calculated using the method of Chou and Talalay in Calcusyn.

Cell Line	KIT Inhibitor	Calcineurin Inhibitor	CI Value	Cell Line	KIT Inhibitor	Calcineurin Inhibitor	CI Value
p815	Dasatinib	CSA	0.438	**RBL2H3**	Dasatinib	FK506	0.61
p815	Dasatinib	Ascomycin	0.829	**RBL2H3**	Dasatinib	CSA	0.324
p815	Dasatinib	Pimecrolimus	0.652	**RBL2H3**	Dasatinib	Ascomycin	0.409
p815	Imatinib	FK506	0.659	**RBL2H3**	Dasatinib	Pimecrolimus	0.909
p815	Sunitinib	CSA	1.029	**RBL2H3**	Sunitinib	CSA	0.643
p815	Nilotinib	CSA	0.61	**RBL2H3**	Nilotinib	CSA	0.227
p815	Sorafenib	CSA	0.774	**RBL2H3**	Sorafenib	CSA	0.973
p815	Crenolanib	CSA	0.508	**RBL2H3**	Crenolanib	CSA	0.602
BR	Dasatinib	CSA	0.261	**RBL2H3**	Imatinib	CSA	0.657
BR	Dasatinib	Ascomycin	0.517	**HMC1.1**	Dasatinib	CSA	0.504
BR	Dasatinib	Pimecrolimus	0.465	**HMC1.1**	Dasatinib	Ascomycin	0.442
BR	Imatinib	FK506	0.425	**HMC1.1**	Dasatinib	Pimecrolimus	0.631
BR	Sunitinib	CSA	0.268	**HMC1.1**	Sunitinib	CSA	0.854
BR	Nilotinib	CSA	0.175	**HMC1.1**	Nilotinib	CSA	0.231
BR	Sorafenib	CSA	0.216	**HMC1.1**	Crenolanib	CSA	0.719
BR	Crenolanib	CSA	0.593	**HMC1.2**	Dasatinib	CSA	0.481
C2	Dasatinib	FK506	1.056	**HMC1.2**	Dasatinib	Ascomycin	0.861
C2	Dasatinib	CSA	0.546	**HMC1.2**	Dasatinib	Pimecrolimus	0.153
C2	Dasatinib	Ascomycin	0.682	**HMC1.2**	Sunitinib	CSA	0.509
C2	Dasatinib	Pimecrolimus	0.798	**HMC1.2**	Crenolanib	CSA	0.771
C2	Sunitinib	CSA	0.584				
C2	Nilotinib	CSA	0.232				
C2	Sorafenib	CSA	0.647				
C2	Crenolanib	CSA	0.142				
C2	Imatinib	CSA	0.466				

Table 6 - qRT-PCR analysis of NFAT expression in KIT-mutant mast cell lines

Cell Line	NFAT1	NFAT2	NFAT3	NFAT4
P815	X	X		X
HMC1.1	X	X		X
HMC1.2	X	X		X
BR		X		X
C2		X		X
RBL2H3	X	X		X

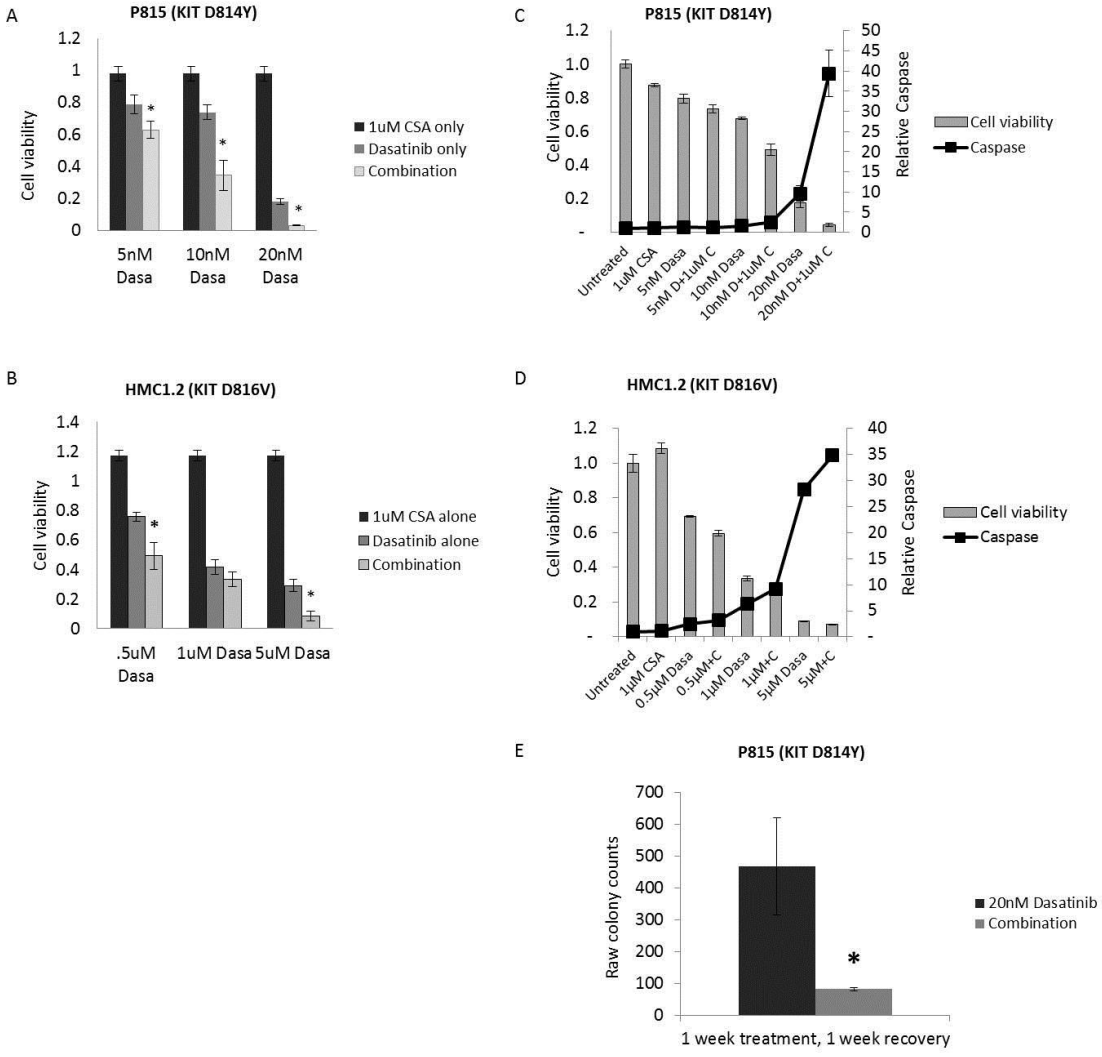

Figure 6 - Combination treatment in KIT-mutant mast cells with CSA and dasatinib leads to synergistic decrease in cell viability, induction of caspase 3/7, and decreased replating efficiency. "Dasa" or "D" = dasatinib, "C" = CSA. A) Combination treatment of a calcineurin phosphatase inhibitor (CSA) and a KIT inhibitor (dasatinib) for 48hrs caused a synergistic decrease in cell viability in P815 cell line. B) Combination treatment of a calcineurin phosphatase inhibitor (CSA) and a KIT inhibitor (dasatinib) for 48hrs caused a synergistic decrease in cell viability in HMC1.2 cell line. C) Combination treatment of a calcineurin phosphatase inhibitor (CSA) and a KIT inhibitor (dasatinib) for 48 hours led to caspase 3/7 induction in P815 cells. Relative cell viability is depicted using the left axis and relative caspase 3/7 level using the right axis. D) Combination treatment of a calcineurin phosphatase inhibitor (CSA) and a KIT inhibitor (dasatinib) for 48 hours led to caspase 3/7 induction in HMC1.2 cells. Relative cell viability is depicted using the left axis and relative caspase 3/7 level using the right axis. E) Colony growth of P815 cells treated with 20nM dasatinib alone or in combination with 1μM CSA. Cells were treated for a week, and allowed to recover for a week before colonies were quantified. 1μM CSA had no effect on colony growth (data

not shown, colonies too numerous to count). Error bars = SD, * denotes p< 0.05 compared to dasatinib treatment alone.

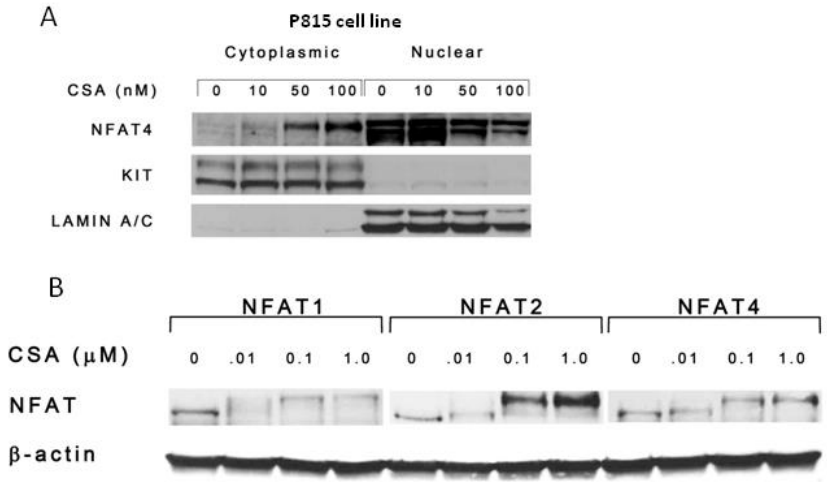

Figure 7- Immunoblotting of KIT-mutant mast cells reveals constitutively active NFAT species. A) Fractionation of p815 cells showed localization of NFAT4 in the nucleus of unstimulated cells. Treatment with CSA, a CNPI, caused inactivation of NFAT4 via increased phosphorylation and translocation into the cytoplasm. Total KIT is shown as a cytoplasmic loading control and Lamin A/C is shown as a nuclear loading control. B) All NFAT family members expressed in p815-cells (NFAT1, 2, and 4) showed constitutive activity, and inactivation following treatment with CSA. Cytoplasmic protein fractions are shown in panel B.

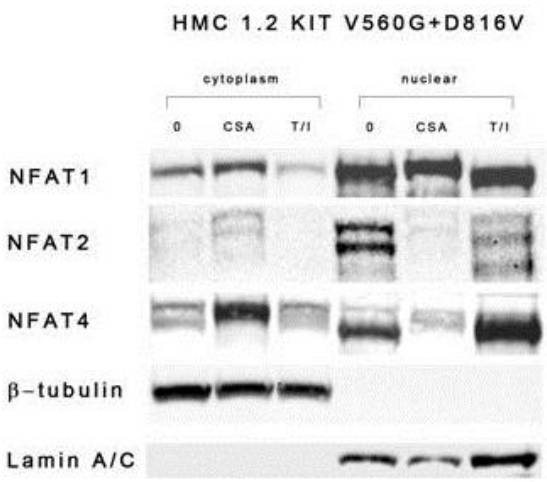

Figure 8- HMC1.2 cell line reveals constitutively active NFAT species. A) HMC1.2 cells treated for 2hrs with 1uM CSA or 100nMTPA+1uM IonM. Fractionation reveals constitutive activation of NFAT1, 2, and 4. NFAT3 was not detected by Western blotting.

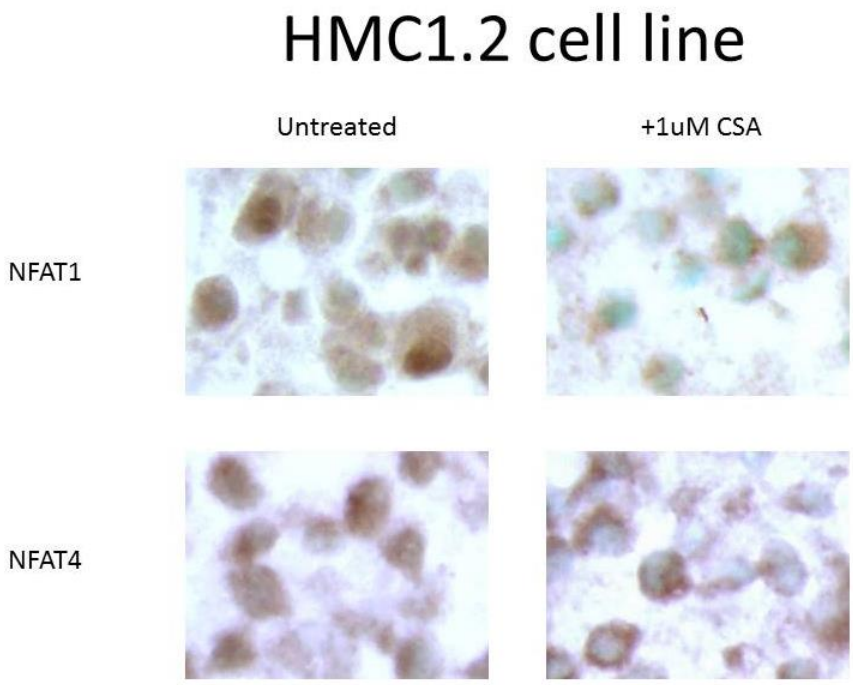

Figure 9- IHC staining of HMC1.2 cell line reveals constitutively active NFAT species. Untreated HMC1.2 cells show nuclear staining for NFAT1 and NFAT4 (left panels) HMC1.2 cells treated for 2hrs with 1uM CSA show a decrease in nuclear NFAT staining and an increase in cytoplasmic staining (Right panels). Nucleus stained with methyl-green.

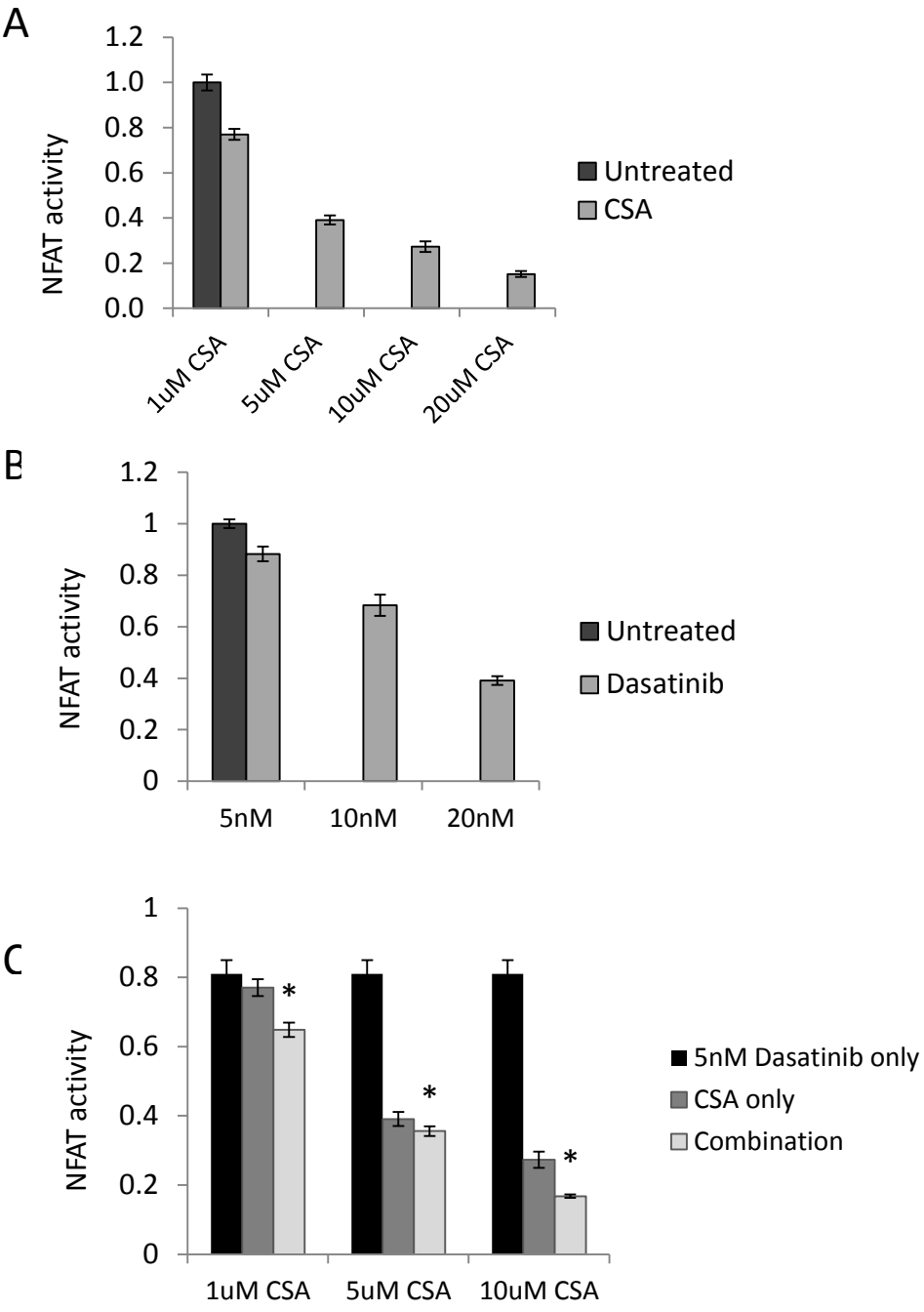

Figure 10- Monotherapy and combination therapy decrease NFAT transcriptional activity in KIT mutant cells. A) Treatment with CSA led to a dose-dependent decrease in NFAT transcriptional activity B) Treatment with dasatinib led to dose-dependent decrease in NFAT transcriptional activity. C) Treatment with CSA plus dasatinib combined to further decrease NFAT-dependent transcriptional activity. Error bars = SD, * denotes $p < 0.05$ compared to either mono-treatment.

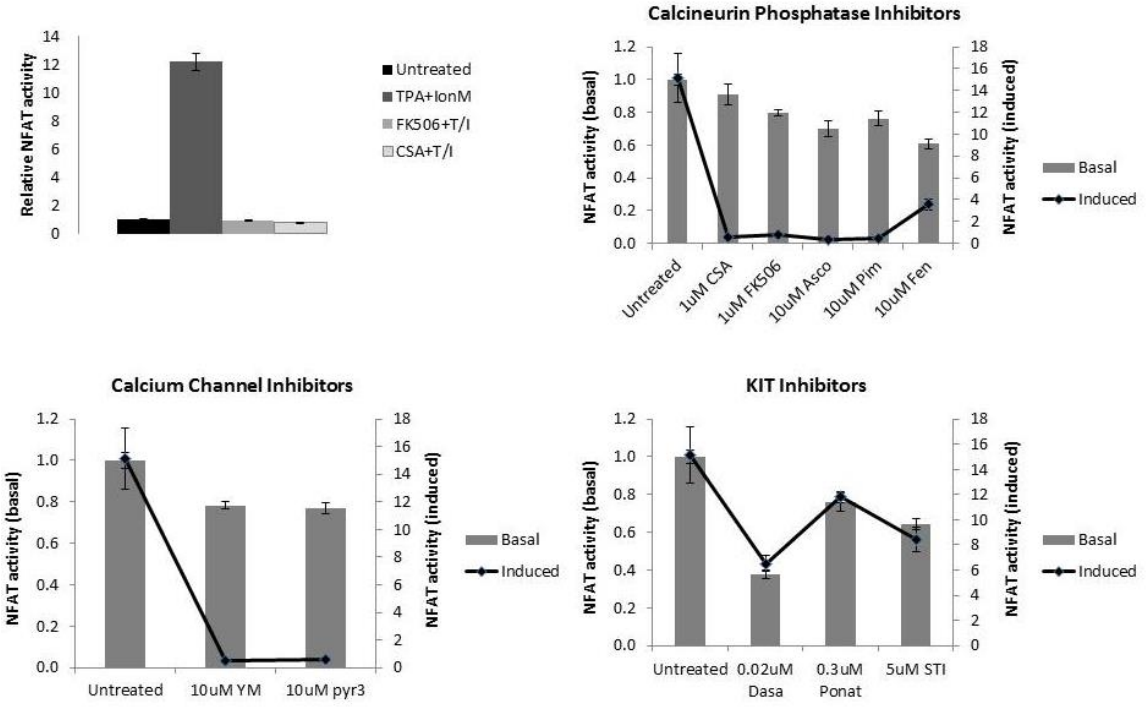

Figure 11- Monotherapy and combination therapy decrease NFAT-dependent transcriptional activity in KIT mutant cells. A) TPA/IonM (T+I) induced an increase in NFAT-dependent transcriptional activity. This increase was blocked by pre-treatment with a calcineurin inhibitor (CSA or FK506). B) The effect of calcineurin inhibitors on basal and induced NFAT-dependent reporter activity. Basal NFAT inhibition is shown at four hours post-treatment (gray bars, left axis). Induced NFAT activity shown after two hours of pretreatment, and 2 hours of TPA+IonM (black line, right axis). Calcineurin phosphatase inhibitors partially blocked basal activity and completely blocked calcium induced NFAT-dependent transcriptional activity. C) The effect of calcium inhibitors on basal and induced NFAT-dependent reporter activity. Basal NFAT inhibition is shown at 4hrs post-treatment (gray bars, left axis). Induced NFAT activity is shown following two hours of pretreatment, and 2 hours of TPA+IonM (blue line, right axis) Calcium channel blockers partially block basal NFAT-dependent transcriptional activity and completely block calcium induced activity. D) The effect of KIT inhibitors on basal and induced NFAT-dependent reporter activity. Basal NFAT inhibition is shown at four hours post-treatment (black bars, left axis). Induced NFAT activity shown following two hours of pretreatment, and 2 hours of TPA+IonM (blue line, right axis). KIT kinase inhibitors partially block both basal and calcium induced activity. Error bars = SD.

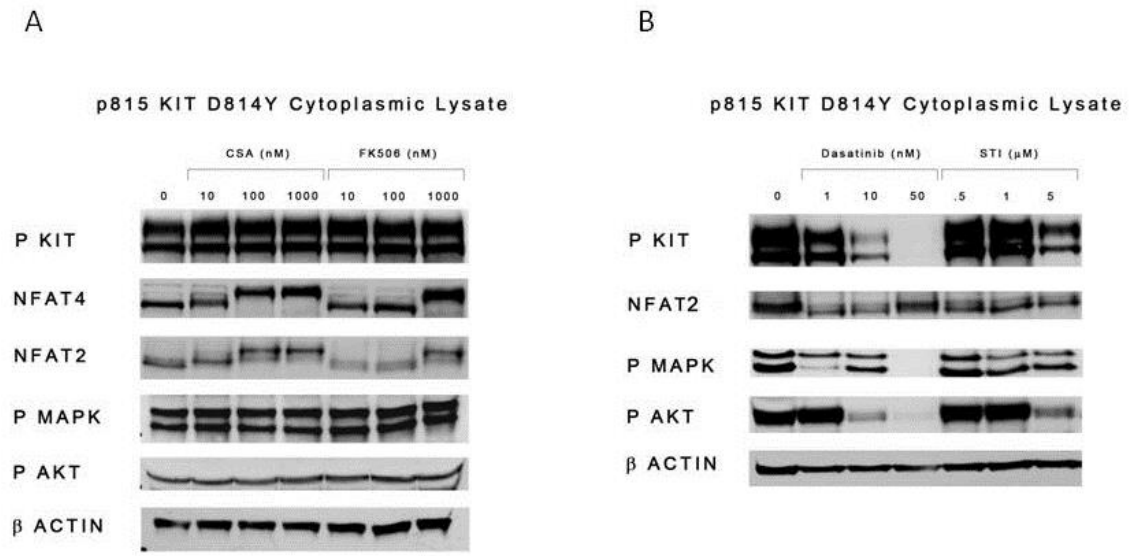

Figure 12- KIT inhibitors do not affect NFAT subcellular localization and CNPIs do not modulate KIT or downstream signaling pathways. A) P815 cells were treated with CSA or FK506 for 3 hours. Both CSA and FK506 caused a shift in NFAT from the lower, unphosphorylated band to the upper, phosphorylated band. This was accompanied by an increase in cytoplasmic NFAT localization. CSA and FK506 did not affect the level of p-KIT or of downstream KIT signaling targets (p-ERK, p-AKT). B-actin is shown as a loading control. **B)** P815 cells were treated with increasing doses of dasatinib or imatinib for 3 hours. Both dasatinib and imatinib caused a decrease in p-KIT as well as decreased activation of downstream KIT signaling targets (p-ERK and p-AKT). However, dasatinib and imatinib did not cause any change in NFAT2 phosphorylation (no band shift), and did not affect NFAT2 localization.

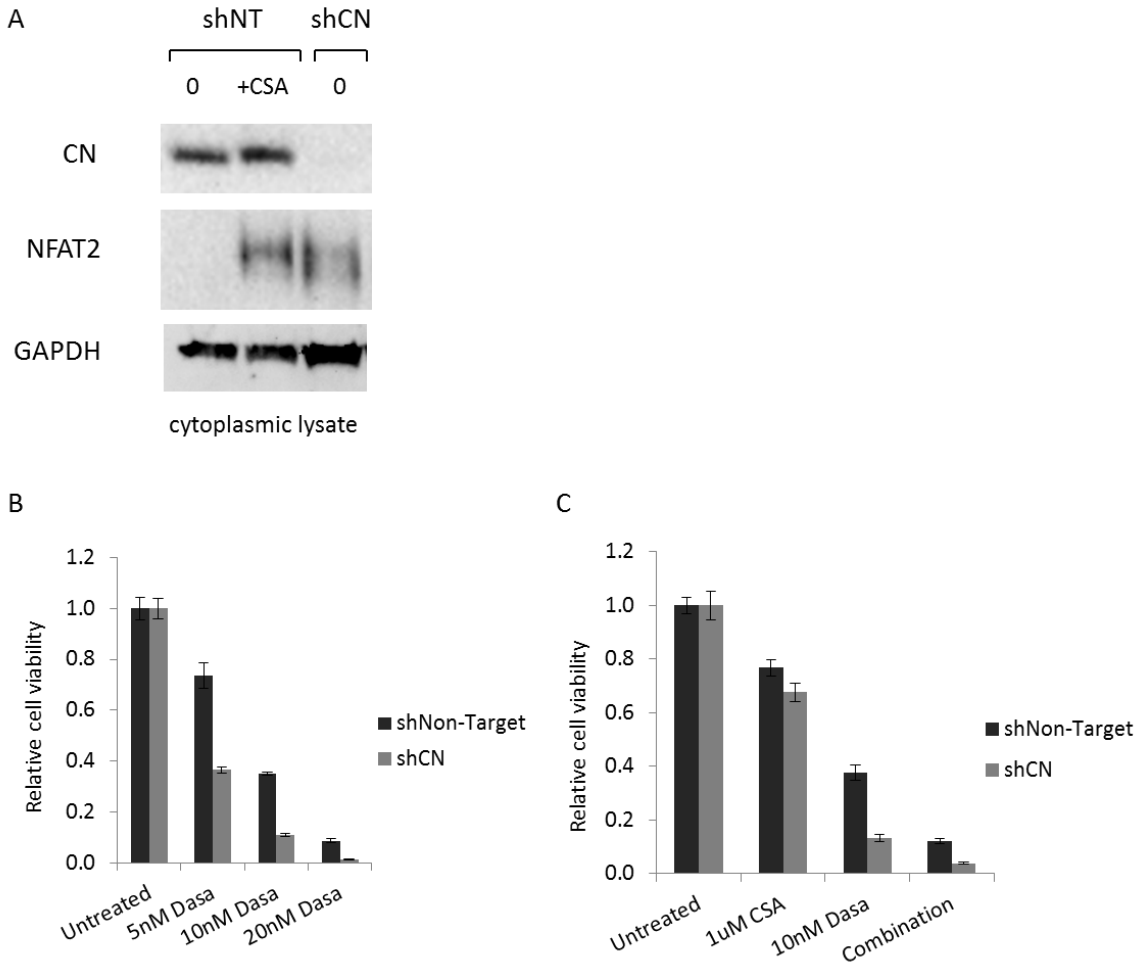

Figure 13- PPP3R1 knockdown sensitizes P815 cells to dasatinib treatment. A) Stable knockdown of calcineurin subunit PPP3R1 led to decreased calcineurin expression (shCN), and increased cytoplasmic localization of NFAT2. Cytoplasmic lysates are shown. B) P815 cells with stable PPP3R1 knockdown have increased sensitivity to dasatinib treatment – compared to parental shNT-P815 cells. The level of cell viability in shCN-P815 cells treated with dasatinib alone was comparable to parental shNT-P815 cells treated with 1μM of CSA plus dasatinib. Error bars = SD.

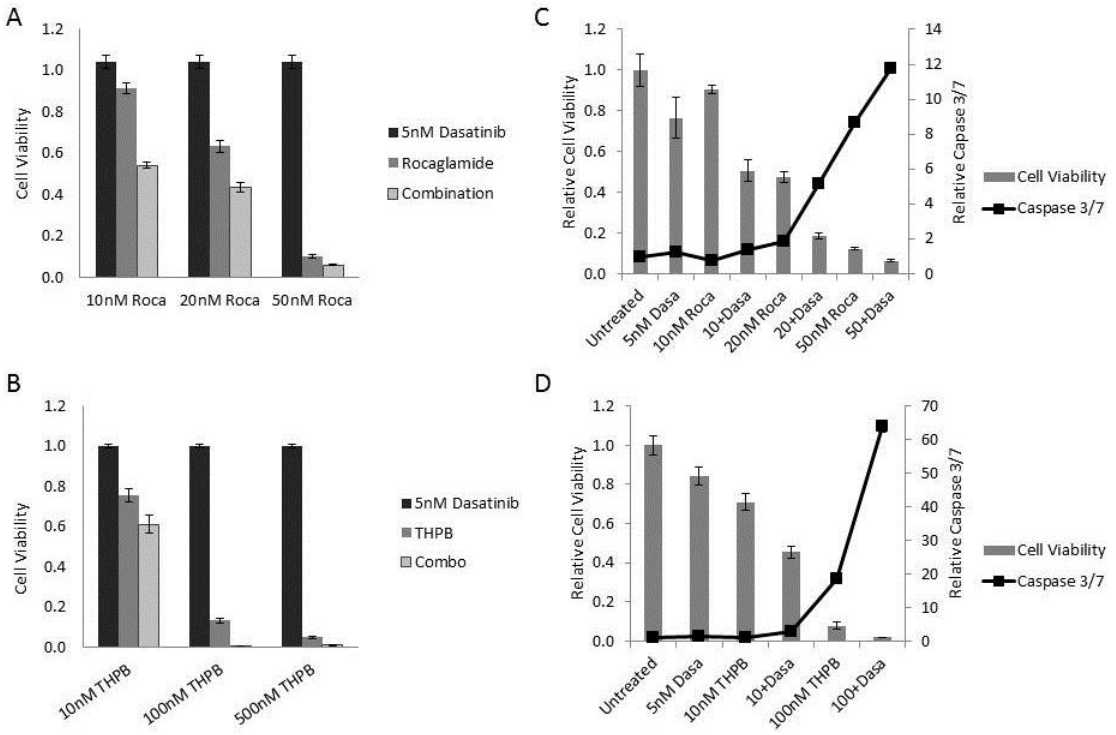

Figure 14- NFAT specific inhibitors combine with KIT inhibitors to synergistically decrease cell viability and induce apoptosis. A) Combination treatment with an NFAT specific inhibitor (Rocaglamide) and a KIT inhibitor (dasatinib) for 48hrs lead to a synergistic decrease in cell viability. B) Combination treatment with an NFAT specific inhibitor (THPB) and a KIT inhibitor (dasatinib) for 48hrs lead to a synergistic decrease in cell viability. C) Combination treatment with an NFAT specific inhibitor (Rocaglamide) and a KIT inhibitor (dasatinib) for 48hrs lead to a synergistic decrease in cell viability (gray bars) and caspase 3/7 induction (black line). D) Combination treatment of an NFAT specific inhibitor (THPB) and a KIT inhibitor (dasatinib) for 48hrs lead to a synergistic decrease in cell viability (gray bars) and caspase 3/7 induction (black line). Error bars = SD, * denotes $p < 0.05$ compared to mono-treatment.

Chapter 3: Modulation of the JAK-STAT Pathway Sensitizes Resistant KIT-Mutant Mast Cells to KIT Inhibition.

Introduction to RNA-Seq approach:

Following the results from our paper that demonstrated synergy between CNPIs and KIT TKIs we developed a number of models to explain the mechanism behind the observed synergy in KIT-mutant mast cells (Figure 15). These models allowed us to develop an RNA-Seq strategy that captured the downstream effects of combination therapy. Regardless of the mechanism underling synergy, our RNA-Seq experimental approach allowed us to monitor the downstream effects across the genome at the mRNA transcript level.

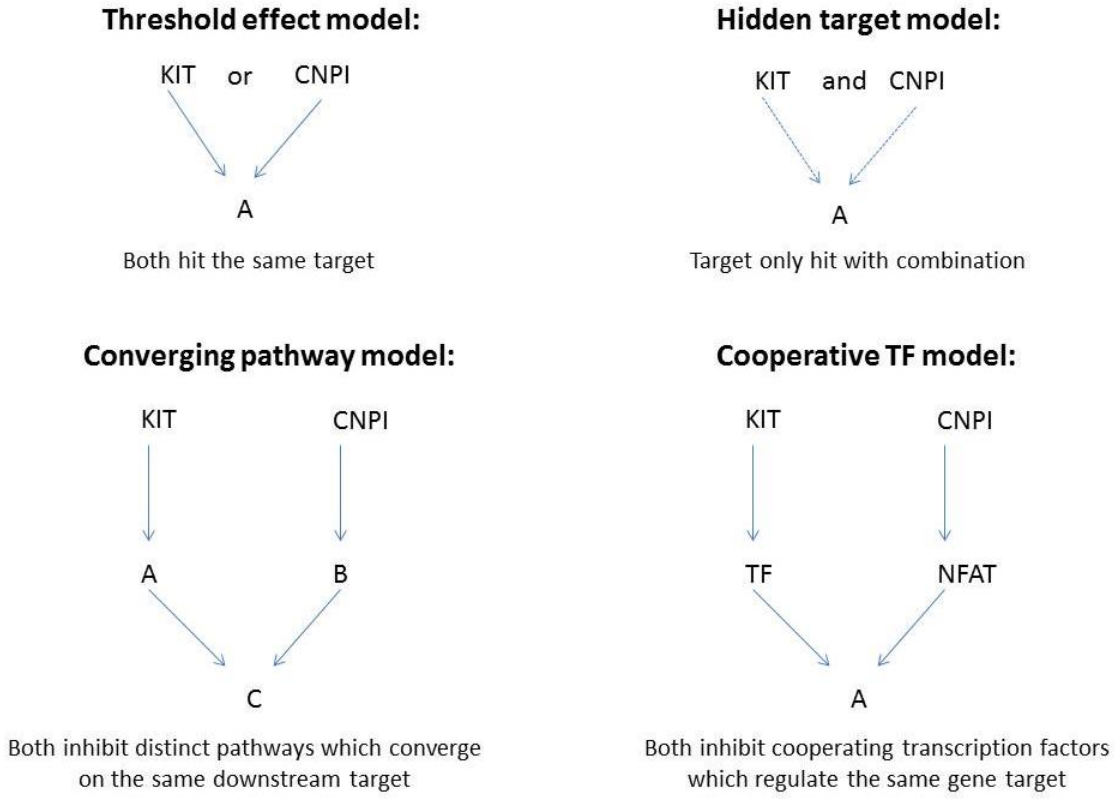

Figure 15 – RNA-Seq models. Proposed signaling models for CNPI+KIT TKI combination therapy.

In the *Threshold Effect Model* both the CNPI and TKI inhibit the same target, but co-targeting overcomes a "threshold" level of signaling that leads to changes in gene transcription that eventually manifest as decreased cellular viability and increased cellular apoptosis. An example would be both the CNPI and TKI modulating signaling of the MAPK pathway. In the *Hidden Target Model* both inhibition from the CNPI and TKI are required in order to see modulation of target transcription. An example of this type of signaling would require inhibition of two distinct targets in order for a third target to be indirectly modulated. This could involve phosphorylation of a target whereby CNPI treatment results in removal of an inhibitory phosphate and TKI treatment results in phosphorylation at an activating site. The *Converging Pathway Model* is a spin-off of the *Threshold Effect Model* where the inhibitors affect distinct signaling pathways, which directly converge on the same downstream target. An example of this would be the MAPK pathway and the AKT pathway both leading to downstream modulation of MYC levels. Finally the *Cooperative Transcription Factor (TF) Model* is a spin-off of the *Converging Pathway Model*. In this slightly more specific model, the two inhibitors regulate two distinct transcription factors that cooperate to regulate the transcription of a single downstream set of targets. This model is explored more in Chapter 6 – section 2 *NFAT-JUN interaction in KIT-mutant mast cells*.

Introduction:

The use of potent and specific tyrosine kinase inhibitors (TKIs) has revolutionized the treatment of cancers that are driven by constitutively active kinases. Perhaps the most notable example is the initial description of using imatinib to treat chronic myelogenous leukemia [182]. Based on the success of this treatment and the discovery of an increasing number of oncogenic mutant kinases in human cancers (e.g. EGFR

mutations in non-small cell lung cancer), additional TKIs have been developed and clinically validated for treatment of a variety of human cancers. Unfortunately not all patients respond to TKIs and those who do often develop secondary drug resistance over time. Therefore, there has been an effort in recent years to identify novel drug targets that when targeted in combination with an inhibitor of oncogenic kinase leads to a synergistic or even synthetic lethal treatment effect.

In the current study, we focus on the development of targeted therapy for systemic mastocytosis (SM). Notably, 90% of human SM cases harbor the activating KIT mutation D816V [66, 183]. This mutation is at best partially sensitive, and in most cases completely resistant, to currently available FDA approved KIT TKIs [150]. The goal of the current study was to identify synergistic drug combinations that would sensitize KIT D816V cells to KIT inhibition *in vitro* and that were suitable for advancing *in vivo* testing.

Historically RNAi screens have been used to identify synergistic or synthetic lethal combinations [184-186]; however we previously identified the synergistic combination of targeting KIT kinase and calcineurin phosphatase activity in KIT-mutant mast cell lines [132]. The first target, KIT, is a receptor tyrosine kinase that is commonly mutated in mast cell diseases and gastrointestinal stromal tumors [146, 187]. The other target, NFAT, is a transcription factor whose inhibition leads to downstream changes in gene transcription. Dephosphorylation of NFAT by the phosphatase calcineurin leads to NFAT nuclear translocation, DNA binding, and transcription promotion.

We recently discovered that NFAT species are constitutively active in a panel of KIT-mutant mast cell lines. Additionally, the simultaneous inhibition of calcineurin/NFAT and KIT led to a synergistic decrease in cell viability and long term replating potential, as well as a synergistic increase in caspase activity. Despite these promising results of the

NFAT/KIT combination therapy, NFAT inhibition requires the use of calcineurin phosphatase inhibitors (CNPIs) which are inherently immunosuppressive. In addition there are other safety concerns over the long-term use of these agents.

Originally introduced into the clinic in 1983, the CNPI cyclosporine A (CSA) is now a cornerstone immunosuppressant used in transplant patients to prevent acute organ rejection. Soon after, a second, distinct compound, FK506, was approved [99]. In addition to use in organ transplantation, CSA and FK506 are being used in a number of other immune-related health issues such as autoimmune disorders, rheumatoid arthritis, psoriasis, and chronic dry eye [188-190].

Although CSA and FK506 are distinct compounds they have similar side-effects associated with their chronic use including kidney/renal dysfunction which can result in chronic nephrotoxicity. They can also alter glucose metabolism leading to diabetogenesis, or neurotoxicity including encephalopathy. Finally, due to the immunosuppressive nature of CNPIs, patients have an increased incidence of infection and/or malignancy [102]. Notably, each of these conditions resolves when CNPI doses are reduced. Overall, in the context of organ transplant, the benefits of immunosuppressant agents outweigh the side-effects; however any alternative to long-term use should be explored both in clinic and in the research environment. In the current study, we used RNA-Seq to identify alternative drug targets that could inhibited in combination therapy with a KIT TKI to elicit the same beneficial effects seen when simultaneously inhibiting calcineurin/NFAT and KIT in KIT-mutant cancer cells[191, 192].

Materials and Methods:

Cell culture:

P815 [35] cells were grown in DMEM (10% FBS, 1% L-glut, 1% pen-strep). All cell lines were grown at 37°C and 5% CO2. Each cell line's morphology was monitored, and growth curve analysis and sequencing was performed bi-annually to ensure the identity of each line throughout the course of these studies. The P815 cell line was purchased from ATCC.

Immunoblotting Studies:

To prepare nuclear and cytoplasmic protein extracts, we used Thermo-Scientific NE-PER Nuclear Extraction Kit (#78833) and followed the manufacturer's instructions. Lysates were prepared using either the NE-PER kit or routine detergent lysis (RIPA lysis buffer: 50mM Tris-HCl, 1% IGEPAL, .25% deoxycholate, 150mM NaCl, 5mM EDTA, and 1:100 protease/phosphatase inhibitor cocktail). The antibodies used in our immunoblotting experiments are listed in Table 7.

shRNA knockdown cell lines:

P815 cells with JAK1, JAK2, CCND1, CCND2, or MYC knockdown or non-targeting knockdown (shNT) were created using pLKO.1 Mission lentiviral transduction particles from Sigma. Briefly, P815 cells were transduced overnight with 85.5uL media, 0.006ug polybrene, and 12.5uL of lentiviral particles. Following a 24 hour recovery, stably transduced clones were selected using 1ug/mL puromycin.

Cell Viability and Caspase assays:

Cells were plated at 10,000/well at the same time they were treated, in opaque, 96-well plates in a total volume of 50uL per well. Control and treated cells were incubated for 48

hours. Following incubation, 50uL of Cell Titer Glo substrate (Promega #G7571) was added to each well. Plates were rocked for 15 minutes and then analyzed using the “Cell Titer-Glo” program on a Microplate luminometer GloMax-96 (Promega). Alternatively, following incubation, 50uL of Caspase 3/7 (Promega #G8091) was added to each well. Plates were rocked for 60 minutes and then read using the “Caspase-Glo” program on a Microplate luminometer GloMax-96 (Promega).

RT-PCR:

Total RNA was extracted from P815 cells using a Qiagen RNAeasy Plus Mini Kit combined with the Qiagen RNase-Free DNase Treatment. Single-stranded cDNA was prepared from 1 µg of total RNA in a 50-µL reaction using 60 µmol/L random hexamer primers, 0.5 mmol/L dNTPs, 100 units RNaseOUT, 5 mmol/L DTT (DTT: dithiothreitol), 1× First Strand buffer, and 500 units SuperScript III reverse transcriptase following manufacturer's instructions (Invitrogen by Life Technologies, Grand Island, NY).

Real-time polymerase chain reaction (PCR) was carried out in a 50uL reaction using single stranded cDNA (corresponding to 1ug initial total RNA) and 19 probes Master MIX (Roche), with a FAM-labeled hydrolysis probe specific to the reference Glyceraldehyde 3-phosphate dehydrogenase (GAPDH). Cycling conditions on a Light-Cycler 480 instrument (Roche) included 10 min at 95oC followed by 40 cycles of 95oC for 10 sec and 60oC for 20 sec. CCND2, MYC, and GAPDH (mouse) were detected using commercial TaqMan Gene Expression assays (Applied Biosystems by Life Technologies): GAPDH assay Mm03302249_g1, GAPDH assay Mm99999915_g1, MYC assay Mm00487804_m1, CCND2 assay Mm00438070_m1.

Expression results were analyzed using the comparative C_T method (also known as the $2^{-\Delta\Delta CT}$ method)[193].

RNA-Seq:

RNAseq libraries were prepared using the TruSeq RNA preparation kit (Illumina). This kit was qualified for use with total RNA input from 0.1 to 4 µg. Briefly, total RNA quality was verified by examination on a Bioanalyzer (Agilent). Poly(A)+ RNA was recovered using oligo-dT -coated magnetic beads. Recovered RNA was then chemically fragmented. First-strand cDNA was generated from the fragmented RNA using random hexamer priming. The RNA template was removed and the second strand was generated. The ends of the resulting double stranded cDNA were repaired, after which a single 'A' nucleotide was added to the ends of both strands. Appropriate adaptors were ligated to the ends of the cDNA. Adaptors contained both flow cell binding sequences and indexing "barcodes". The cDNA was amplified using a limited number of cycles of PCR. Following amplification and clean-up, the library concentration was determined using real-time PCR. Samples were diluted to a concentration appropriate to generate 160 to 180 million clusters per lane on the HiSeq 2000 flow cell (Illumina). Following sequencing, the base call data was assembled using the CASAVA package (Illumina).

Data was analyzed using the software package DNAnexus which aligned the reads, and normalized to RPKM (reads per thousand million). Comparisons (p-values) between treatment groups were made using the R/Bioconductor packages edgeR and DESeq using a predicted false discovery rate of <5%. Excel was used to sort genes based on expression level.

Results:

Synergy in P815 cells informs RNA-Seq assay design

As described above, we have previously characterized the synergy that results from the simultaneous inhibition of constitutively active NFAT and KIT. We saw decreased proliferation, increased caspase activity and decreased long-term replating efficiency in a panel of six KIT-mutant mast cell lines. To interrogate downstream targets of this combination we designed and optimized an RNA-Seq assay. We started by repeating previous experiments to confirm the dose range and efficacy of CSA+dasatinib in P815 cells. These experiments included cell viability assays and caspase 3/7 assays (Figure 16A). Based on these results we chose to use 20nM dasatinib and 1uM CSA in our RNA-Seq experiments. We started with a pilot timecourse RNA-Seq experiment to determine the earliest timepoint resulting in dynamic changes in gene expression. We compared the results of the RNA-Seq timecourse to cell viability timecourse data in the P815 cell line. We examined the average top 100 downregulated targets across the three timepoints. We saw significant decreases at each progressive timepoint with the greatest decrease in transcript expression at the 6 hour timepoint (Figure 16B). This compared favorably with cell viability data which revealed a modest effect of combination therapy at 6 hours (Figure 16C). Taken together, we chose to use the 6 hour timepoint at a dose of 20nM dasatinib plus 1uM CSA in a triplicate RNA-Seq study.

RNA-Seq screen reveals JAK-STAT and MAPK pathway modulation following combination therapy

Given that NFAT is a transcription factor and modulation of NFAT activity is required for combination therapy activity, we hypothesized that the combination effect was mediated in large part by regulation of target gene transcription/RNA abundance. We further

postulated that these modulated transcripts may represent targets for pharmacologic intervention. Alternatively, the pattern of transcript modulation may uncover critical pathways that are modulated by combination therapy. RNA-Seq allows an unbiased assessment of transcriptome wide changes in gene expression following single agent or combination therapy. As a method for characterizing global changes in transcription, RNA-Seq is an attractive option because of the ability to quantify differences in mRNA abundance in response to various treatments and diseases. Compared to microarray techniques, RNA-Seq eliminates the need for prior species-specific sequence information and overcomes the technical challenges of detecting low abundance transcripts. In addition, RNA-Seq is very reliable in terms of technical reproducibility [191, 192]. Here, we used RNA-Seq to compare RNA transcript levels before and after inhibition of KIT and NFAT in a KIT-mutant mast cell line. Our previous results of combining CNPIs and KIT TKIs reproduced across all six KIT-mutant mast cell lines that we tested; however here we used P815 cells as a well described representative cell line model.

P815 cells were treated for 6 hours with 1uM CSA, 20nM Dasatinib, or a combination of both in triplicate sets. RNA was harvested from cells and subjected to RNA-Seq. All targets with an RPKM expression value of <0.8 were removed from the results as it was deemed their expression would be too low to accurately measure/study. We also removed uncharacterized genes from our candidate list, leaving 9,164 potential gene targets (Figure 17). Comparing untreated cells to combination treated cells, we removed targets whose expression change was associated with a p-value ≥0.002. Next, targets whose expression did not increase or decrease 2-fold or more following combination therapy were removed. Using these criteria we generated a candidate gene list with 221 down-regulated transcripts and 157 up-regulated transcripts (Tables 8,9).

These top down-regulated and up-regulated targets were entered in to the STRING software program[194]. String is an online database that provides direct and indirect, known and predicted, protein-protein interactions. It is a useful tool to elucidate connections between targets in genome-wide screens such as RNA-Seq or RNAi knockdown. In addition to our top gene candidates, NFAT family members and KIT were added to the network as sources of input from our pharmacological manipulations. All targets that were not part of a single interaction network (confidence score > 0.7) were removed from our genes of interest (Figure 18, top). This further reduced the candidate gene list to 49 (Table 10). Finally, we used the KEGG Pathways feature of the String program to identify which signaling pathways were over-represented by our remaining networked proteins. Aside from pathways that are part of the natural biology of mast cells such as the "Cytokine Signaling" pathway, the most highly over-represented pathway was the JAK-STAT pathway – a known downstream target of KIT signaling. A second over-represented pathway was "Pathways in Cancer" (Figure 18, bottom). We evaluated the physiological plausibility of each target within these two pathways to determine whether their up- or down- regulation made sense in our molecular context. For example, we found that SOCS1 was downregulated by 87% following combination therapy. However, SOCS1 is part of a negative-feedback loop that inhibits JAK-STAT signaling, so a decrease in this target would not be expected to mediate cell death. This type of analysis resulted in a further reduction of our list to 12 candidate genes across two pathways.

We chose to validate these 12 targets of interest with Taq-man RNA expression assays and confirmed the changes in transcript levels seen in our RNA-Seq experiment (CCND2 and MYC shown in Figure 19A). Based on these confirmatory results we chose to investigate the potential of three new combination therapies for their potential to

replace our original CNPI/KIT inhibitor combination – KIT plus + a JAK1-3 inhibitor, KIT inhibitor plus a MYC inhibitor, and a KIT inhibitor plus a CCND2 inhibitor.

Inhibition of novel targets synergizes with KIT inhibition to decrease cellular viability and increases apoptosis

We chose to further examine inhibitors of JAK1-3, MYC, or CCND1/2 for their potential to replace CSA in combination treatments using a KIT TKI backbone to inhibit the growth of KIT mutant mast cells. We treated P815 cells with Dasatinib or CSA alone or in combination for 6 hours. Cells were fractionated and lysates were probed for MYC, CCND2, and phospho-STAT3/5 (downstream target of JAK signaling). We found a decrease in MYC, phospho-RB and phospho-STAT3/5 protein expression, in agreement with changes in RNA expression seen in our RNA-Seq experiment (Figure 19B). Next, we treated P815 cells with a pan-JAK inhibitor (CYT387,[195]), a MYC inhibitor (I-BET151,[196]), or a CDK4/6 inhibitor (palbociclib,[197]) to identify inhibitory doses for each compound, to be used in combination studies.

I-BET151 is a bromodomain and extra-terminal BET inhibitor which displaces BET family members BRD3 and BRD4 from acetylated histone proteins where their binding promotes transcription. Global gene-expression analysis by Tolani et al.. revealed that I-BET151 decreased both MYC expression and expression of MYC-dependent target genes[198]. This finding explains the efficacy of I-BET151 in cancers where MYC is overexpressed such as multiple myeloma [199] and Burktitt's lymphoma[200].

Currently, there are no CCND1/2 specific inhibitors that have been clinically tested; however there are compounds that have been shown to decrease CCND2 expression. One of these compounds, crizotinib led to a 20% decrease in CCND2 expression in normal keratinocytes *in vitro* [201]. Another compound, fangchinoline was found to

inhibit growth in the CML cell line K562 [202], which correlated to a decrease in CCND2 expression. Unfortunately this downregulation was dose-dependent where 1uM led to a decrease while 10uM led to an increase in CCND2 expression. We chose to use a CDK4/6 inhibitor, palbociclib, to pharmacologically inhibit CCND2. CCND1 and CCND2 assemble with CDK6 to form active complexes which induces cell cycle progression through activation of RB. Therefore inhibition of CDK6 with palbociclib should lead to inhibition of CCND1 and CCND2 and its downstream targets (here, phospho-RB).

P815 cells were treated for 6 hours with increasing doses of CYT387, I-BET151 or palbociclib. Cytoplasmic and nuclear lysates were probed for P-STAT3/5, MYC and pRB. CYT387 treatment decreased JAK signaling as evidenced by a dose dependent decrease in P-STAT3/5 (Figure 19C). As previously reported, I-BET151 decreased MYC expression in a dose dependent fashion(Figure 19D). Finally, increasing doses of palbociclib led to a dose-dependent decrease in p-RB indicating inhibition of CCND2 (data not shown).

The overall goal of our study was to identify compounds that could replace CSA in a combination therapy that incorporated a KIT inhibitor backbone. Based on the results in Figure 19 and preliminary cellular viability experiments (not shown), inhibitor doses were chosen for use in combination studies that led to approximately 10% decrease in cellular viability. P815 cells were treated with I-BET151 (200nM), Palbociclib (100nM) or CYT387 (500nM) alone or in combination with increasing doses of dasatinib (5, 10, 20nM). After 48 hours, cellular viability was measured and combination index (CI) values were calculated. The mean CI values across at least six independent experiments are shown in Figure 20A. The mean CI value for dasatinib plus CSA is shown for comparison (CI=0.42). The mean CI value for dasatinib plus CYT387 (P=0.47), was not statistically different than the CI value for dasatinib plus CSA as

assessed by student's t-test; however the CI value for I-BET151 and palbociclib were significantly higher (P=0.0001, P= 0.01). These data indicated that the synergy between CSA and dasatinib (with respect to cellular viability) was equivalent to the synergy seen when combining a pan-JAK with a KIT inhibitor. While the effects of combining a MYC or CCND2 inhibitor with a KIT TKI were not as potent as the CNPI plus KIT TKI combination, the CI values were still less than 1.0 (0.78, and 0.64 respectively) indicating synergy.

We previously (as shown in Figure 16) found that combining a CNPI with a KIT inhibitor led to a significant increase in caspase 3/7 activity compared to a KIT inhibitor alone. We evaluated the ability of these combinations to induce caspase 3/7 activity as an indication of apoptosis. P815 cells were treated for 48 hours with I-BET151 plus dasatinib, palbociclib plus dasatinib, or CYT387 plus dasatinib. Caspase 3/7 was measured with Caspase-Glo reagent (Promega) using a luminometer (Glomax 96, Promega) and readings were normalized to cell viability. As shown in Figure 20B, 200nM I-BET151 did not synergize with 20nM dasatinib to increase caspase 3/7. On the other hand, treating P815 cells with 100nM palbociclib plus 20nM dasatinib resulted in a 32-fold increase in caspase 3/7 levels compared to 20nM dasatinib alone (Figure 20C). Similarly, treating cells with 500nM CYT387 plus 20nM dasatinib caused a 77-fold increase in caspase 3/7 levels compared to 20nM dasatinib alone (Figure 20D). These results were confirmed across five independent experiments. The combinations with CYT387 or palbociclib plus dasatinib showed similar caspase 3/7 induction compared to what we saw when we combined CSA with dasatinib. Again, this supports the use of either CYT387 or palbociclib to replace CSA in a combination therapy strategy.

JAK or CCND inhibition sensitizes cells to KIT inhibition and decreases long-term growth KIT-mutant mast cells

In vitro as well as clinical treatment of KIT mutant cancer with KIT inhibition have shown that despite inhibition of proliferation, induction of apoptosis, and long term clinical responses, treatment does not eradicate all KIT mutant cells. Persistent disease in this setting necessitates the clinical need for continuous treatment and represents a population of cells that can further mutate to become drug-resistant. This phenomenon can be modeled in vitro using prolonged drug exposure followed by drug washout and enumeration of surviving cells in a replating assay. We have previously demonstrated that the combination of dasatinib and CSA significantly decreases the number of cells with replating capacity compared with single agent dasatinib alone (Ch 2, Figure 6E)

To further test the efficacy of our novel combination treatments, we evaluated the effects of these combinations on the long term replating efficiency of P815 cells. P815 cells were treated with 20nM of dasatinib alone or in combination with 1uM CSA (positive control for comparison), 500nM CYT387, 100nM palbociclib, or 200nM I-BET151. Cells were treated for 1 week, then removed from drug, washed, and replated. Cells were allowed to recover for an additional week, before colonies were stained with crystal violet and quantified.

In agreement with our cellular viability and caspase 3/7 data, palbociclib plus dasatinib and CYT387 plus dasatinib performed similarly to, or better than CSA plus dasatinib across four experiments. Representative wells from a single experiment are shown in Figure 21A. The average colony counts for this experiment are shown in Figure 21B. These data demonstrate that CYT387 plus dasatinib and palbociclib plus dasatinib decrease the number of P815 cells that survive combination treatment; however

treatment with I-BET151 plus dasatinib was no better than dasatinib alone with respect to inhibition of replating efficiency in P815 cells.

Knockdown of JAK1, JAK2, or CCND2 sensitizes cells to KIT inhibition

To confirm the effects we saw in our cellular viability, apoptosis, and long term replating assays were the result of specific inhibition of JAK, or CCND, we created P815 cell lines with stable shRNA knockdown of each target. We used lentiviral transduction to deliver shRNA particles to P815 cells and selected for stable clones with puromycin. Stable shRNA knockdown cell lines were created for JAK1, JAK2, CCND1, CCND2, and non-targeting (NT). Based on preliminary experiments with alternative JAK inhibitors we eliminated JAK3 as a potential target mediating synergy.

We used these stable cell lines to test their sensitivity to dasatinib treatment. Each cell line, including P815-shNon-targeting (NT) cells were treated for 48hr with 1uM CSA, 10nM dasatinib, or a combination of both. Cellular viability was quantified as before, with the Cell Titer-Glo reagent (Promega) and measured with a luminometer. We found that knockdown of JAK1 or JAK2 sensitized cells to dasatinib treatment (Figure 22A, B). Treatment of shJAK1 or shJAK2 cell lines with 10nM dasatinib led to decreased cell viability compared to the same treatment in shNT cells. This decreased cell viability was similar to the level of cell viability observed in the shNT cell line following combination treatment with CYT387 plus dasatinib. Similarly, we found that knockdown of CCND2 sensitized cells to dasatinib treatment (Figure 22 C). The cell viability of treating the shCCND2 cell line with 10nM dasatinib was equivalent to the cell viability of treating shNT-P815 cells with 10nM dasatinib plus 0.1uM palbociclib. In contrast, knockdown of CCND1 did not sensitize cells to dasatinib treatment compared to shNT-P815 cells (Figure 22D).

These experiments reveal that JAK1, and JAK2, are likely the targets of CYT387 that are responsible for the observed synergy between CYT387 and dasatinib in P815 cells. Also, CCND2 is likely an indirect target of palbociclib through CDK4/6 inhibition, accounting for the observed synergy between palbociclib and dasatinib in P815 cells. Finally, inhibition of JAK1, JAK2, or CCND2 is sufficient to sensitize P815 cells to dasatinib treatment.

Discussion:

To target both resistance and persistence in KIT-mutant SM we have focused on improving the efficacy of current KIT TKIs by identifying novel combination therapies. Combination therapy using CNPIs and KIT TKIs has synergistic effects on cellular proliferation and apoptosis of KIT mutant mast cells. However, there are potential concerns over the use of immunosuppressive drugs in cancer patients [103, 203-208]. Therefore, we designed RNA-Seq experiments to uncover new drug targets that would combine with KIT inhibition and cause similar effects on cellular proliferation and apoptosis as the combination of KIT TKIs and CNPIs. Although a large number of gene transcripts were significantly upregulated or downregulated, downstream components of the JAK-STAT and “Cancer” pathways were the most overrepresented amongst the list of modulated transcripts.

Follow-up studies on three of these targets (JAK, CCND2, and MYC) demonstrated that combining commercially available JAK inhibitors with a KIT TKI resulted in a similar degree of synergy as our original combination of dasatinib plus CSA. Although the CI value for palbociclib plus dasatinib was not statistically equivalent to the CI value of CSA plus dasatinib, it performed as well as the CSA combination with respect the caspase 3/7 induction, and replating efficiency. On the other hand, inhibiting MYC in combination

with KIT failed to perform as well as CSA plus dasatinib in cell viability, caspase 3/7 and replating efficiency assays.

Interestingly, both JAK2 and CCND2 have been found to be over expressed in cases of aggressive non-Hodgkin lymphoma [209]. Subsequently, Walz et al.. showed that treating JAK2-mutant erythroid leukemia cells (HEL cell line with JAK2 V617F) with a JAK inhibitor led to cell cycle arrest and decreased CCND2 expression. These results were confirmed in another cellular model by transfecting JAK2 V617F into Ba/F3 cells [210]. It has also been shown that STAT5 binds to the CCND2 promoter [211] which could provide a link between JAK activity and CCND2. These data suggest that the efficacy of our JAK/KIT and CCND2/KIT combinations may be the result of hitting the same critical signaling pathway.

The fact that knockdown of either JAK1 or JAK2 sensitized cells to dasatinib treatment suggests that incomplete inhibition of the JAK-STAT pathway is sufficient for synergy with a KIT inhibitor. It also suggests redundant function amongst JAK proteins within P815 cells. This explanation is conceivable given that JAK proteins interact at receptors tyrosine kinases to autophosphorylate each other. Although we did not specifically test TYK2 involvement, we would not be surprised if we saw similar sensitization of P815 cells to dasatinib treatment following knockdown of TYK2 (another member of the JAK family). Conversely, only inhibition of CCND2 was able to recapitulate the effects of treating cells with palbociclib and dasatinib. This suggests that CCND2 plays a critical, unique role that is not shared by CCND1 in P815 cells. Comparison of mRNA transcript levels, using RNA-Seq, of shCCND1-P815 cells and shCCND2-P815 cells may shed light on the downstream targets of synergy.

We believe the CCND2 inhibitor + KIT TKI and JAK inhibitor + KIT TKI combinations both warrant further *in vivo* characterization to determine their potential as treatment options for KIT-mutant mast cell neoplasms. If validated by further studies, these combination treatments could represent a significant clinical advance for patients with advanced mast cell neoplasms by overcoming the current limitations of KIT kinase inhibitors.

The discovery that JAK-STAT signaling is critical to KIT-mutant mast cell survival was greatly facilitated by our use of RNA-Seq and the String database. Combining RNA-Seq with String allowed us to uncover a signaling pathway that was not necessarily mutated or even deregulated, but nevertheless critical to the survival of KIT-mutant mast cells. We believe this approach could be used to interrogate any kinase-driven cancer in order to identify synergistic drug combinations. We plan to expand these studies to include other models of KIT-mutant cancer (such as KIT-mutant GIST) to uncover novel synergistic and synthetic lethal combinations to treat these diseases.

Figures and Tables:

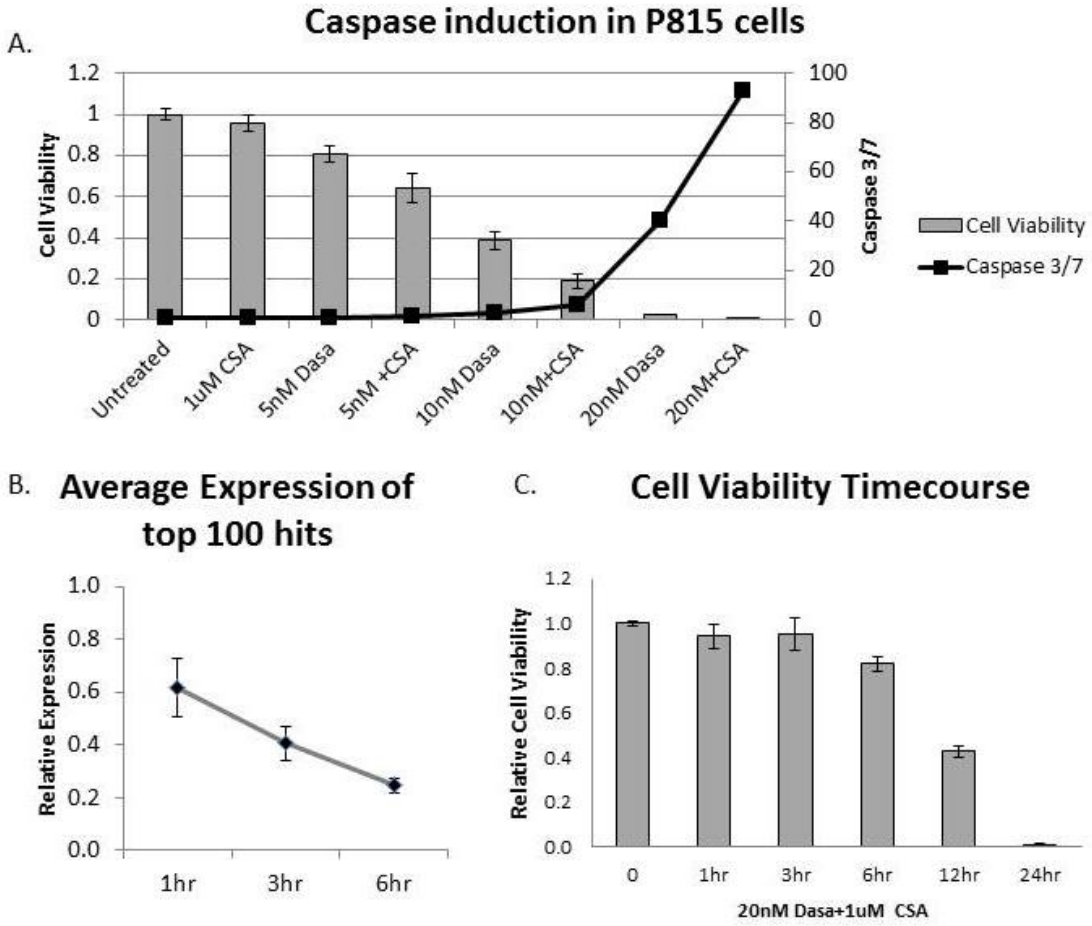

Figure 16: RNA-Seq timecourse informs design of triplicate RNA-Seq experiment. A) Cell viability and caspase 3/7 assays in P815 cells reveal significant synergy at 20nM dasatinib plus 1uM CSA in cells treated for 48hr. B) RNA-Seq timecourse shows time-dependent decrease in mRNA transcripts levels of top 100 downregulated hits from 1-6hrs. C) Combination treatment of P815 cells shows major impact of combination therapy on cell viability at 12 hours.

A.

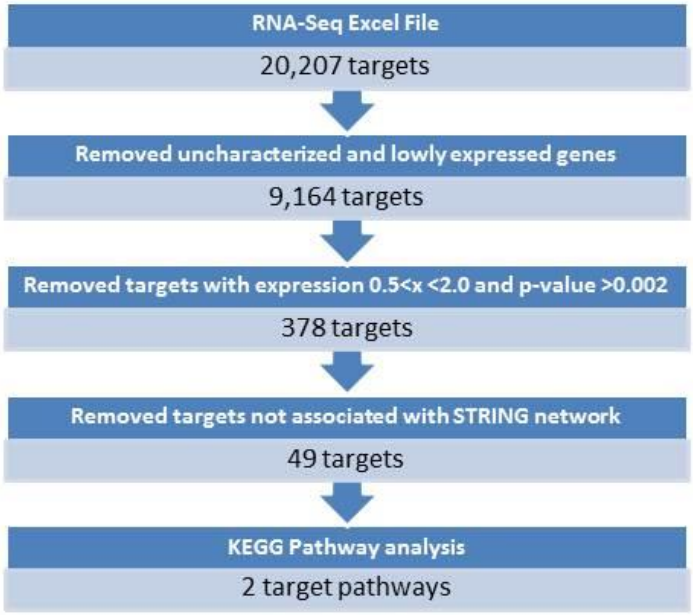

B.

KEGG Pathway	Target
JAK-STAT	MYC, BCL2L1, CCND2, OSM, CISH, SOCS1, IL2RA, IL21R, IL7R, CBLC
"Cancer"	FOS, CCND1, VEGFA, MMP2, MYC, BCL2, BCL2L1, CBLC, PDGFRA

Figure 17 – RNA-Seq data analysis. A) Flow-chart describing the RNA-Seq data analysis process including Excel sorting, and STRING analysis. **B)** KEGG pathways identified by STRING analysis of top 49 target candidates. Included are the gene candidates from each pathway.

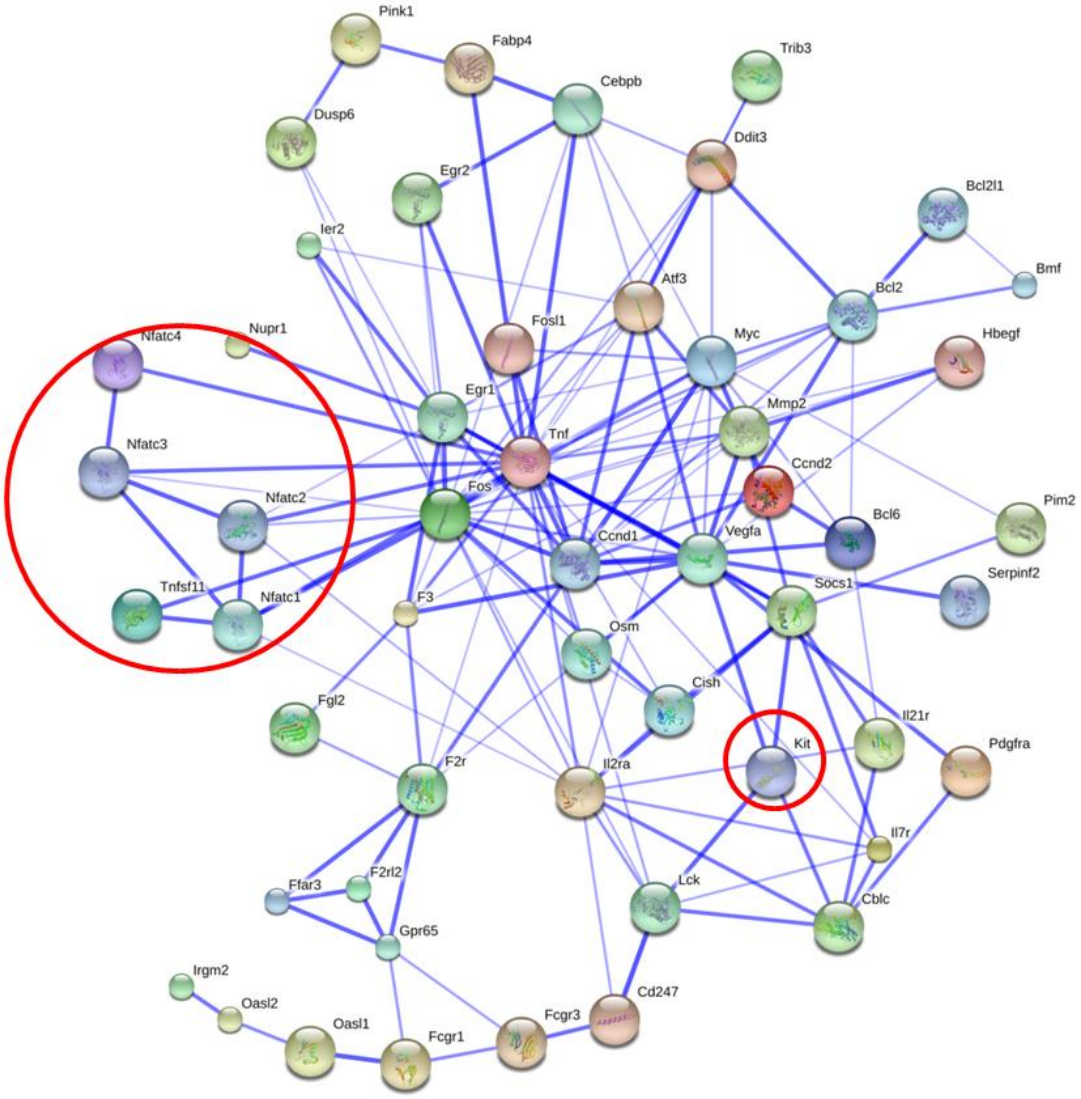

KEGG Pathway	Target
JAK-STAT	MYC, BCL2L1, CCND2, OSM, CISH, SOCS1, IL2RA, IL21R, IL7R, CBLC
“Cancer”	FOS, CCND1, VEGFA, MMP2, MYC, BCL2, BCL2L1, CBLC, PDGFRA

Figure 18- String analysis of top up-regulated and down-regulated hits from Tables 7. String network from top candidates in Tables 7 and 8 (top). Red circles indicate points of pharmacologic input from CSA and dasatinib. KEGG pathways identified by STRING analysis of targets in table 9 (bottom). Included are the gene candidates from each pathway.

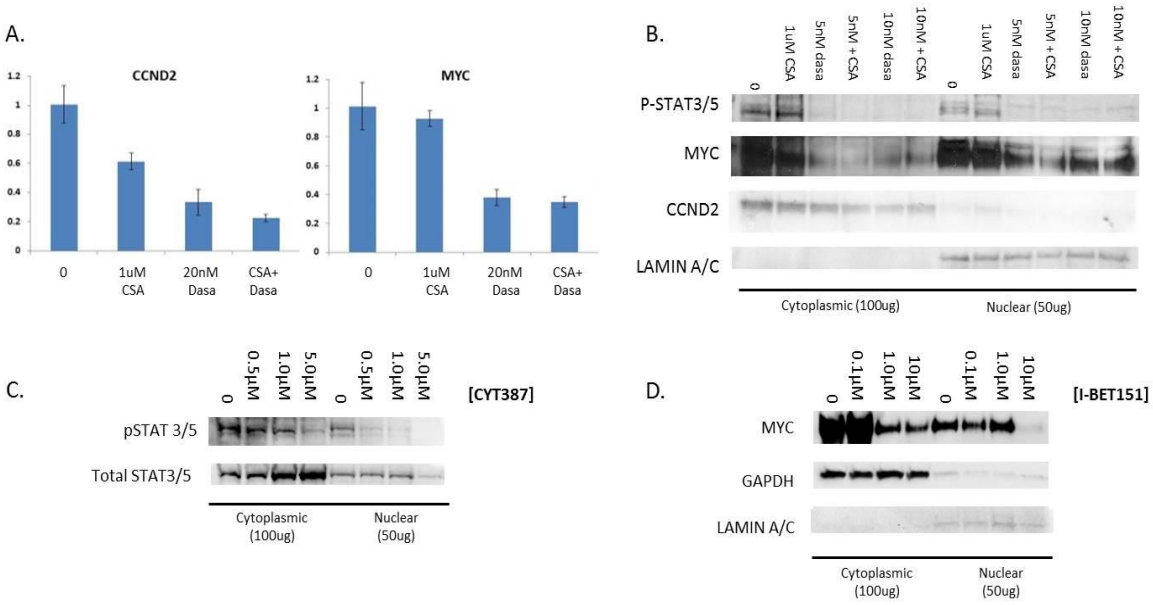

Figure 19 – Confirmation of top targets from RNA-Seq screen. A) P815 cells were treated with control media, CSA (1 µM), dasatinib (20 nM), or both for 6 hours. RNA was harvested and analyzed by qRT-PCR for quantitation of CCND2 or MYC and control gene (GAPDH) transcript levels. Data was analyzed using the comparative Ct method. Y-axis denotes the fold-change in transcript levels compared with untreated cells. Error bars indicate ± 1 standard deviation. **B)** P815 cells were treated with 1uM CSA, dasatinib, or a combination of the two for 6 hours. Cytoplasmic and nuclear fractions are shown. Probing with phospho-STAT3/5, MYC, or CCND2 reveals decrease in protein expression following treatment with dasatinib and/or combination therapy. **C)** P815 cells were treated with CYT387, a JAK inhibitor, for six hours. Cytoplasmic and nuclear fractions are shown. Increasing doses of CYT387 decreased phospho-STAT3/5 expression in both cytoplasmic and nuclear fractions. **D)** P815 cells were treated with I-BET151, a MYC inhibitor, for six hours. Cytoplasmic and nuclear fractions are shown. Increasing doses of I-BET151 decreased MYC expression in both cytoplasmic and nuclear fractions.

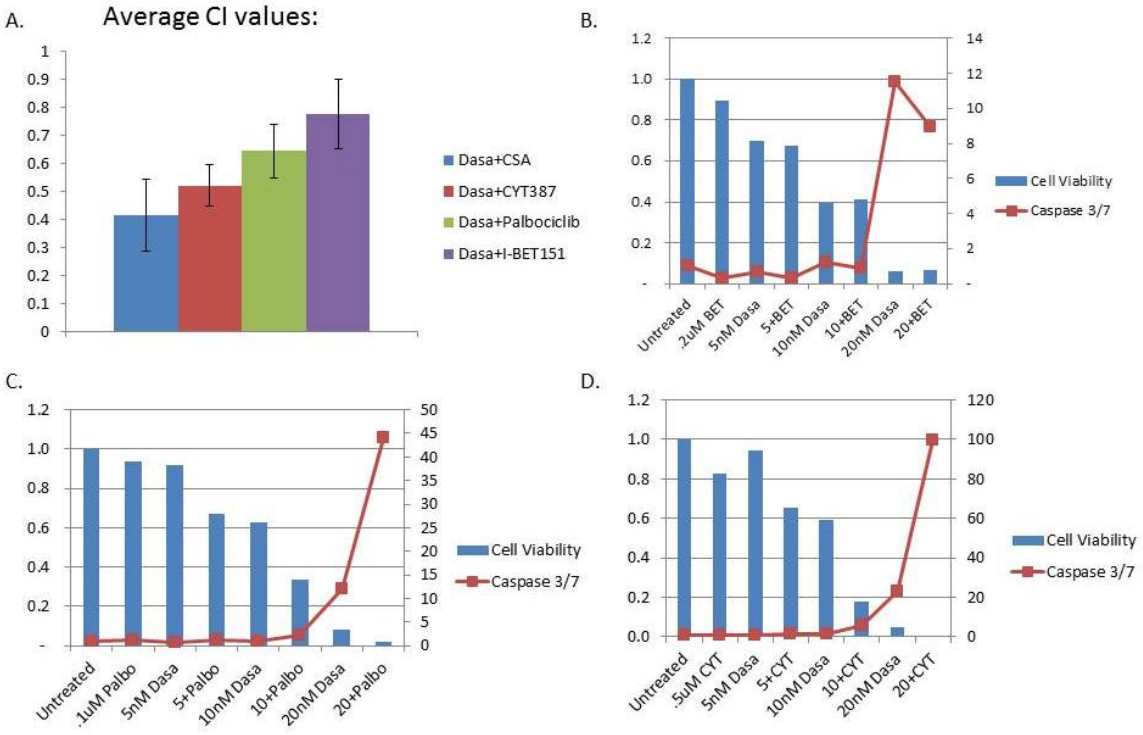

Figure 20- JAK-STAT or MYC inhibition combined with KIT inhibition reduced cell viability. A) Following combination treatment in P815 cells for 48 hours, cell viability was measured and combination index values (CI) were calculated as shown. For comparison, the original CI value for CSA plus dasatinib in P815 cells is shown. The palbociclib and I-BET151 combinations were statistically different from the CSA plus dasatinib combination as assessed by student's t-test. **B)** Combination treatment using a MYC inhibitor (I-BET151) and dasatinib (Dasa) for 48hrs led to a synergistic decrease in cell viability(left axis, blue bars), but did not synergistically increase caspase 3/7 activity (right axis, red line). **C)** Combination treatment using a pan-JAK inhibitor (CYT387) and dasatinib (Dasa) for 48hrs led to a synergistic decrease in cell viability (left axis, blue bars), and a synergistic increase caspase 3/7 activity (right axis, red line). **D)** Combination treatment using a CDK4/6 inhibitor (palbociclib) and dasatinib (Dasa) for 48hrs led to a synergistic decrease in cell viability (left axis, blue bars), and a synergistic increase caspase 3/7 activity (right axis, red line).

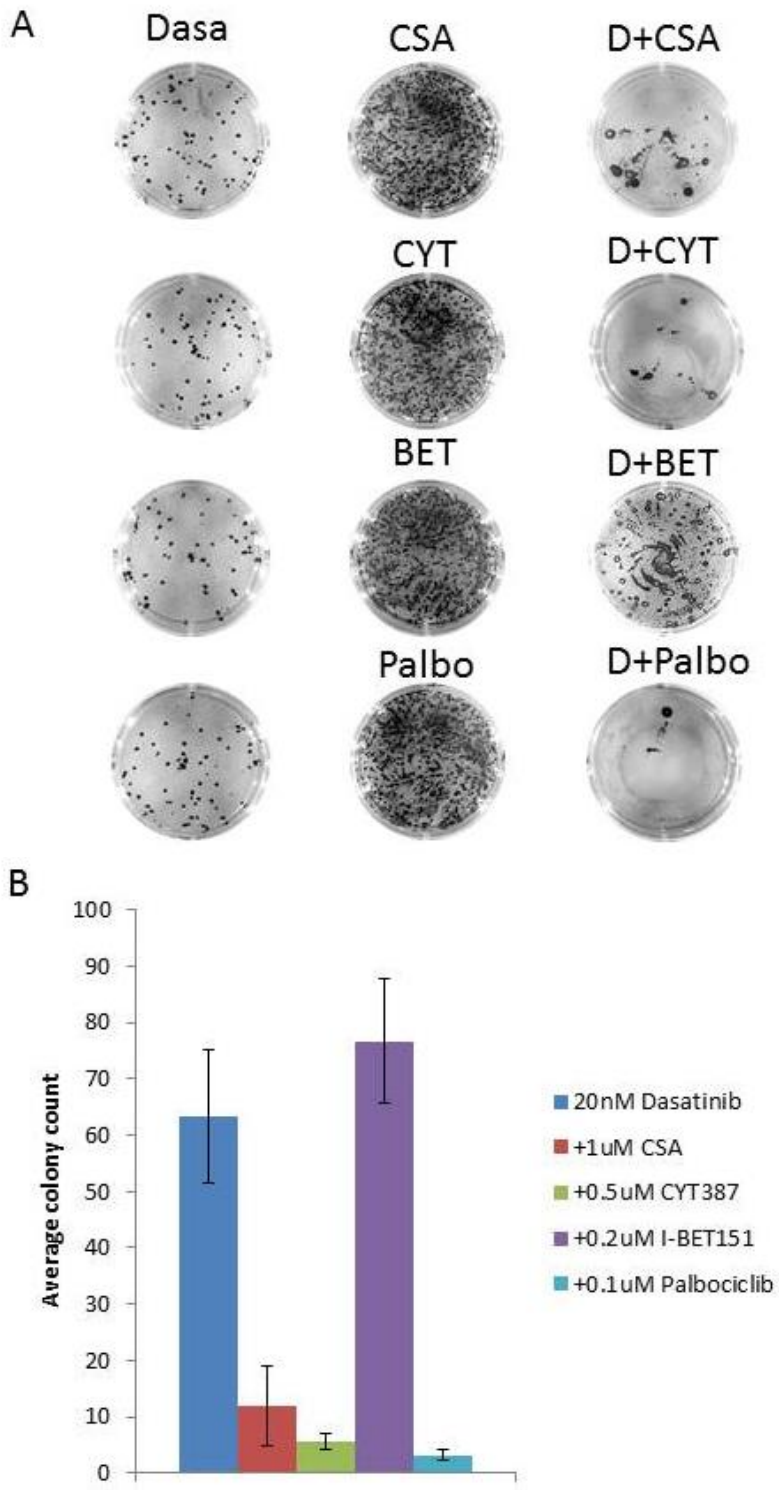

Figure 21- Novel combination therapies decrease long-term replating efficiency of P815 cells. A) P815 cells treated for 1 week with 20nM dasatinib, 1000nM CSA, 500nM CYT387, 200nM I-BET151, or 100nM palbociclib, or in combination. Wells shown are representative of four independent replicate wells, and three independent experiments. **B)** Quantitation of the entire experiment shown in panel A.

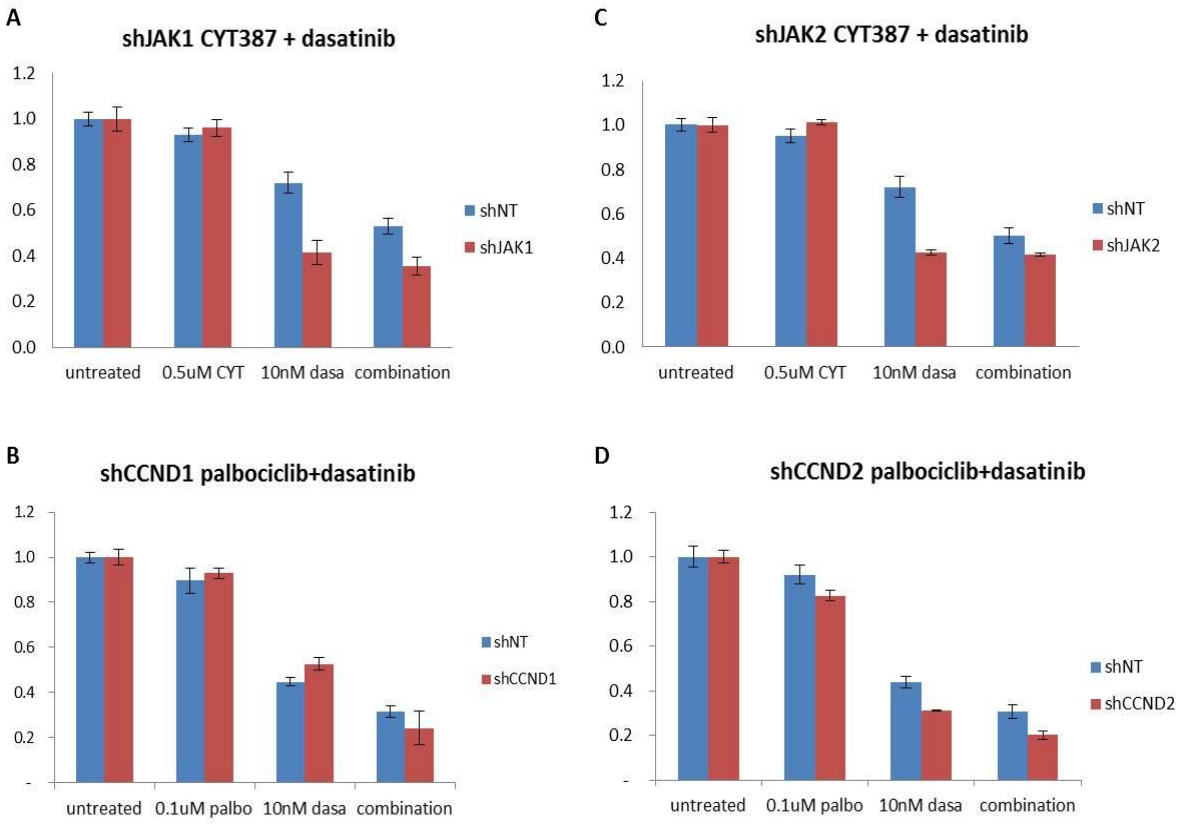

Figure 22- KD of JAK sensitizes cells to dasatinib treatment. A,B) P815 cells containing stable knockdown of JAK1 (A) or JAK2 (B) were treated with dasatinib, CSA or a combination of the two for 48 hours. Cell viability was measured and JAK1 and JAK2 knockdown sensitizes P815 cells to dasatinib treatment. **C)** Blot showing KD of JAK1/2 in P815 cells **D/E)** CTG showing cellular viability following combination treatment in CCND1/2 KD lines and blot showing KD of CCND1/2 in P815 cells **F/G)** CTG showing cellular viability following combination treatment in MYC KD line and blot showing KD of MYC in P815 cells.

Table 7- Antibody list

Antibody	Concentration	Company	Catalog#	2°
B-actin	1:1000	Cell Signaling	4970	Rb, 1:10,000
p-RB	1:400	Santa Cruz	sc-12901	Gt, 1:10,000
total RB	1:400	Santa Cruz	sc-50	Rb, 1:10,000
total JAK1	1:400	Santa Cruz	sc-277	Rb, 1:7500
total JAK2	1:1000	Cell Signaling	3230	Rb, 1:7500
CCND2	1:1000	Cell Signaling	3741	Rb, 1:7500
p-STAT3	1:1000	Cell Signaling	9131	Ms,Rb 1:10,000
total STAT3	1:1000	Cell Signaling	9132	Ms,Rb 1:10,000
p-STAT5	1:1000	Cell Signaling	9351	Ms,Rb 1:10,000
total STAT5	1:1000	Cell Signaling	9352	Ms,Rb 1:10,000
Lamin A/C	1:1000	Cell Signaling	2032	Rb, 1:5000
MYC	1:1000	Cell Signaling	5605	Rb, 1:7500
GAPDH	1:2000	Cell Signaling	2118	Rb, 1:10,000

Table 8 - Transcripts down regulated by two-fold or greater and p<0.002.

GENE	FOLD Δ	GENE	FOLD Δ	GENE	FOLD Δ	GENE	FOLD Δ	GENE	FOLD Δ	GENE	FOLD Δ	GENE	FOLD Δ
Egr1	0.0172	Nupr1	0.2673	Lck	0.3350	Aim1	0.3871	Polr3d	0.4298	Txk	0.4675	Fkbp7	0.4929
Rhbdl3	0.0330	Tlr1	0.2688	Ccnd2	0.3377	Slc20a2	0.3883	Ears2	0.4316	Wars	0.4687	Gfi1	0.4938
Per2	0.0684	Cd247	0.2695	Osm	0.3384	Nop58	0.3902	Polr3h	0.4318	Rrp12	0.4690	Amz1	0.4939
Tnfsf11	0.0818	Actr3b	0.2700	Serpina3h	0.3395	Lrrn3	0.3906	Ptpn9	0.4343	Cnga1	0.4691	Vegfa	0.4973
Fos	0.0901	Pcdh7	0.2708	Serpina3g	0.3422	Atf3	0.3951	Zdhhc21	0.4347	Qtrtd1	0.4692	St8sia4	0.4974
Cd226	0.0925	Kcnh2	0.2735	Lrp12	0.3463	Nedd9	0.3960	Dus2l	0.4352	Cspg4	0.4712	Rad1	0.4974
Angptl3	0.1264	Shroom3	0.2746	F2r	0.3469	Snupn	0.4018	Cd300lf	0.4405	Gpatch4	0.4737	Gypc	0.4981
Serpinb2	0.1324	Aqp9	0.2747	Podxl	0.3483	Them4	0.4037	Nsun3	0.4420	Tmem185b	0.4743	Dusp5	0.4983
Socs1	0.1328	Trmt61a	0.2765	Slc1a4	0.3489	Mettl11a	0.4039	Ankrd36	0.4440	Cacna1d	0.4744	Ublcp1	0.4984
Trib3	0.1332	Mdfic	0.2793	Etv5	0.3490	Slc25a32	0.4056	Wnt10a	0.4463	Mett10d	0.4762	Gpr113	0.4987
Spry4	0.1345	Id1	0.2796	Mc1r	0.3494	Lin28b	0.4071	Polr1b	0.4469	Fam43a	0.4762	Ccnd1	0.4999
Fzd9	0.1419	Fam89a	0.2810	F3	0.3544	Bcl2	0.4073	Pglyrp2	0.4472	Cdca7	0.4767		
Pde3b	0.1521	Slamf1	0.2925	Kcnk5	0.3545	Bank1	0.4091	Tmem20	0.4486	Cd244	0.4771		
Fhl4	0.1544	Dph1	0.2943	Slc15a1	0.3582	Rrs1	0.4092	Mag	0.4487	Prmt7	0.4772		
Mfsd2	0.1576	Zc3h8	0.2976	Spry1	0.3585	Nop56	0.4106	Slc35f2	0.4488	Ifrd2	0.4789		
F2rl2	0.1577	Ier2	0.2978	Zfp697	0.3593	Wdr43	0.4124	Cdkl2	0.4490	Tnfrsf13b	0.4790		
Sh2d4a	0.1651	Btla	0.3028	Ccdc137	0.3594	Tnfrsf9	0.4128	Exod1	0.4499	Nfe2l1	0.4803		
Gvin1	0.1690	Dus4l	0.3050	Ddit3	0.3597	Got1	0.4134	Sema4g	0.4500	Epb4.9	0.4809		
Hbegf	0.1711	Pus7l	0.3059	Fbxo47	0.3610	Nek6	0.4137	Rtn4ip1	0.4507	Batf3	0.4840		
Lipg	0.1766	Bend6	0.3089	Extl1	0.3625	Cebpb	0.4140	Pcyox1l	0.4510	Ccdc116	0.4862		
Dusp6	0.1864	Gbp4	0.3118	Ffar3	0.3656	Tox	0.4146	Dhodh	0.4521	Gpr155	0.4863		
Chac1	0.2010	Bcl2l1	0.3118	Cish	0.3679	Cd3eap	0.4157	Zdhhc23	0.4529	Wdr4	0.4867		
Il2ra	0.2025	Fosl1	0.3148	Rcbtb2	0.3680	Reep6	0.4163	Slc29a2	0.4532	Tnfsf8	0.4871		
Ttll11	0.2044	Serpina3f	0.3163	Dkc1	0.3686	Dtx4	0.4166	Ccrn4l	0.4549	Xpo4	0.4881		
Slamf9	0.2085	Plxnc1	0.3172	Nr1h4	0.3688	Apobec1	0.4179	Slc25a29	0.4563	Aldh18a1	0.4882		
Irgm2	0.2098	Rrm2b	0.3199	Slc7a1	0.3756	Gemin4	0.4187	Jph1	0.4571	Dhdh	0.4886		
Pim2	0.2099	Rrp1b	0.3208	Hk2	0.3768	Egr2	0.4217	B3galt6	0.4581	Fam136a	0.4888		
Fcgr1	0.2133	Taf4b	0.3256	Piga	0.3769	Amica1	0.4229	Nolc1	0.4584	Fam118b	0.4894		
Car12	0.2186	Fam5c	0.3267	Rpp38	0.3786	Mettl13	0.4249	Slc7a11	0.4593	Tnfrsf18	0.4895		
Mmp2	0.2367	Hsd17b7	0.3300	Fgl2	0.3787	Relt	0.4253	Dok2	0.4595	Xrcc2	0.4897		
Tnf	0.2429	Gpr65	0.3313	Slc25a33	0.3795	Tsr1	0.4255	Srl	0.4596	Tha1	0.4899		
Eda2r	0.2481	Tnfrsf21	0.3322	Rhbdd1	0.3797	Ankrd6	0.4257	Pi16	0.4621	Fancf	0.4902		
Slc19a1	0.2596	Gpt2	0.3333	Myc	0.3807	Gemin6	0.4266	Casq2	0.4622	Lrrc66	0.4905		
Il21r	0.2602	Fam60a	0.3338	Mtrr	0.3829	Btn2a2	0.4277	Zmat1	0.4642	Hhip	0.4917		
Adora2b	0.2635	Map3k8	0.3349	Zc3h6	0.3856	Bxdc1	0.4298	Gnl3	0.4652	Fam72a	0.4928		

Table 9 - Transcripts upregulated by two-fold or greater (p<0.002).

GENE	FOLD Δ	GENE	FOLD Δ	GENE	FOLD Δ	GENE	FOLD Δ	GENE	FOLD Δ
Entpd7	2.0035	Pdgfra	2.1138	Fabp4	2.2799	Mon2	2.5360	Atp6v0d2	3.2349
Patz1	2.0040	Pdzk1ip1	2.1171	Hspa8	2.2847	M6prbp1	2.5403	Oasl2	3.3222
Fcgr3	2.0047	Supt4h1	2.1243	Acrbp	2.2866	Plekho1	2.5588	Rab3il1	3.3904
Sec24d	2.0087	Lhfpl2	2.1257	Tmem216	2.2877	Cpne8	2.5713	Tubb2b	3.4289
Syvn1	2.0094	Zfp775	2.1295	Pisd	2.2939	Fam109b	2.5743	Mrpl10	3.4409
Zswim4	2.0143	Bmf	2.1344	Tmod4	2.3004	Wdr81	2.5777	Agtr1a	3.5212
Map1lc3b	2.0230	Lin37	2.1349	Dhdds	2.3027	Sphk1	2.5998	Apobec2	3.6896
Acss2	2.0256	Usp14	2.1392	Cnnm3	2.3147	Ypel3	2.6167	Dhrs3	3.7489
Zfp120	2.0297	Ip6k1	2.1408	Ndst2	2.3157	Hspa13	2.6179	Lrrc46	3.7979
Dbx2	2.0342	Atp1b3	2.1415	Plekhf1	2.3201	Ctns	2.6519	Il7r	4.0685
Hbp1	2.0344	Vps11	2.1418	Snx21	2.3206	Snhg6	2.6573	Pik3ip1	4.3332
Cma1	2.0353	Sec61b	2.1469	Ctdsp2	2.3248	Sema6c	2.6602	Gabrd	4.4122
Rrad	2.0372	Cat	2.1482	Mmp27	2.3344	Clec18a	2.6653	Cd7	5.4916
Aggf1	2.0404	Nudt22	2.1537	Bckdha	2.3361	Dnajb9	2.6735	Gstp2	5.5293
Frmd4a	2.0477	Arx	2.1558	Cpt1a	2.3525	Pink1	2.7024	Trim63	6.4339
Tbc1d15	2.0481	Tmem71	2.1567	Frmpd1	2.3574	Cma2	2.7147	Gngt1	6.8109
Phldb3	2.0493	Osbpl5	2.1685	Hexim1	2.3635	Bcl6	2.7572	Nyx	10.8774
Dedd2	2.0502	Csn1s2b	2.1742	Rab9	2.3654	Nfatc4	2.7573		
Cblc	2.0504	Gmfg	2.1754	Pcmtd2	2.3712	Ulk1	2.8181		
Eif2c4	2.0526	P2ry14	2.1825	Cd300lb	2.3769	Spint1	2.8208		
Flcn	2.0547	Rnf181	2.1917	Fam189b	2.3849	Pnrc1	2.8360		
Fn3k	2.0555	Gimap6	2.1933	Efna4	2.3882	Aff3	2.8458		
Maged1	2.0716	Stx5a	2.2087	Acot11	2.4114	Csrp3	2.9121		
Nat2	2.0803	Ddx55	2.2208	Mpp4	2.4242	Nfatc1	2.9171		
Ccdc114	2.0826	Wdr45	2.2232	H47	2.4251	Pnpla7	2.9282		
Mns1	2.0842	Cnn2	2.2302	Spata2L	2.4258	Calcoco1	2.9600		
Crygn	2.0861	Ypel1	2.2419	Ticam1	2.4313	Serpinf2	2.9722		
Cir1	2.0909	Adfp	2.2442	Hmha1	2.4442	Aqp11	2.9937		
Pear1	2.0930	Stk36	2.2565	Fnbp1	2.4501	Mcpt9	3.0393		
Arfgap3	2.0972	Kcnk6	2.2631	Atg2a	2.4632	Tcp11l2	3.0633		
Il8rb	2.0974	Sesn1	2.2676	Tbc1d17	2.4905	Kifc2	3.0698		
Cd97	2.0981	Urod	2.2679	Itpkb	2.4963	Mlycd	3.0956		
Sec14l1	2.0982	Ttyh2	2.2698	Klhl24	2.5011	Abtb1	3.1463		
Tmem151a	2.1024	Tns3	2.2746	Oasl1	2.5270	Mycl1	3.1865		
Tnfsf12	2.1125	Xpa	2.2751	Mettl7a1	2.5333	Tbx6	3.2160		

Table 10 - Top 49 candidates from String analysis. P-value compares gene expression level before and after combination treatment for 6 hours inP815 cells.

Gene	Fold Δ	p-value	Gene	Fold Δ	P-value
Atf3	0.395	3.63E-07	**Gpr65**	0.331	7.34E-12
Bcl2	0.407	3.88E-10	**Hbegf**	0.171	4.07E-14
Bcl2l1	0.312	2.58E-15	**Ier2**	0.298	4.85E-16
Bcl6	2.757	1.50E-11	**Il21r**	0.260	9.80E-19
Bmf	2.134	3.63E-07	**Il2ra**	0.203	2.87E-23
Cblc	2.050	9.61E-05	**Il7r**	4.068	1.60E-11
Ccnd1	0.499	0.00052	**Irgm2**	0.210	9.81E-23
Ccnd2	0.338	1.50E-08	**Lck**	0.335	1.77E-10
Cd247	0.269	0.00025	**Mmp2**	0.237	2.73E-06
Cebpb	0.414	3.19E-06	**Myc**	0.381	2.14E-11
Cish	0.368	2.68E-10	**Nfatc1**	2.917	1.48E-07
Ddit3	0.360	2.44E-12	**Nupr1**	0.267	1.93E-09
Dusp6	0.186	1.23E-27	**Oasl1**	2.527	2.28E-06
Egr1	0.017	2.26E-28	**Oasl2**	3.322	0.00011
Egr2	0.421	0.0009	**Osm**	0.339	1.00E-12
F2r	0.349	2.23E-13	**Pdgfra**	2.114	1.68E-05
F2rl2	0.158	1.92E-25	**Pim2**	0.210	3.35E-24
F3	0.354	0.00033	**Pink1**	2.702	4.48E-11
Fabp4	2.280	9.80E-05	**Serpinf2**	2.972	0.00187
Fcgr1	0.213	4.05E-14	**Socs1**	0.133	1.25E-37
Fcgr3	2.005	6.20E-06	**Tnf**	0.243	4.35E-05
Ffar3	0.366	0.00013	**Tnfsf11**	0.082	6.72E-07
Fgl2	0.379	3.84E-11	**Trib3**	0.133	8.93E-36
Fos	0.090	9.06E-38	**Vegfa**	0.497	1.57E-06
Fosl1	0.315	8.27E-06			

Chapter 4: Experimental Methods

4.1 Cell Culture:

Cells were maintained at 37 degree C with 5% CO2.

Table 11 - Cell line details and media composition

Cell Line	Species	KIT mutation	Media Conditions
p815	Murine	D814Y	DMEM+10% FBS, 1% pen strep, 1% L-Glut
RBL2H3	Murine	D817Y	MEM+10% FBS, 1% pen strep, 1% L-Glut
BR	Canine	L575P	DMEM+2% calf serum, .25g/L histidine, 25mL/L HEPES
C2	Canine	16bp insertion	DMEM+2% calf serum, .25g/L histidine, 25mL/L HEPES
Gist T1	Human	ΔV550-Y578	IMDM+15% FBS, 1% pen strep, 1% L-Glut, plated on fibronectin
HMC1.1	Human	V560G	DMEM+10% FBS, 1% pen strep, 1% L-Glut
HMC1.2	Human	V560G+D816V	DMEM+10% FBS, 1% pen strep, 1% L-Glut

4.1.1 P815 cell line:

The P815 mastocytoma cell line was created by treating a male DBA/2 mouse with methylcholanthrene– a highly carcinogenic compound [166]. It contains the KIT D814Y mutation which is homologous to the D816V mutant commonly found in humans [69]. P815s were originally described as a suspension cell line; however, in my hands the P815 cell line is primarily adherent until it reaches confluency at which point cells continue to proliferate, detach, and occupy the media. The derivation of this cell line from DBA/2 mice makes them an excellent tool for *in vivo* studies. Indeed they have been used extensively to study host-tumor interactions [212, 213]. P815s can be injected intraperitoneally, in which case colony forming assays or cellular viability assays can be performed at various timepoints post-injection. Additionally these cells can be

implanted subcutaneously, where solid tumors form. P815 cells have also been useful for studying cytokine signaling *in vitro* based on their derivation from a mast cell [214].

In addition to the parental P815 cell line several P815 variants have been created. One variant, the P1.HTR cell line was designed to be highly transfectable [215]. It was created by selection of transfected cells for thymidine kinase (TK) uptake with HAT media whereby only cells that were TK+ survived. The TK+ cells were slowly removed from HAT and allowed to recover. Next, TK- cells were selected with BrdU. BrdU is only able to incorporate into nucleic acids if it has been previously phosphorylated by thymidine kinase. Therefore, TK- cells would not be sensitive to BrdU/UV treatment. This process of enriching for P815 cells that were transfectable was repeated four times until the resulting cells were approximately 100-fold more transfectable. This new cell line – P1.HTR – has been used extensively *in vivo* and *in vitro* to transiently or stably introduce genes of interest into P815s. It has also been shown to form better tumor masses than parental P815s when injected subcutaneously [213].

Another set of P815 variants are the tum- P815 cell lines. These were created through *in vitro* mutagenesis and elicit a strong immunogenic response. Comparison of these cells with the parental P815 cells has provided a model for studying the molecules and mechanisms mediating anti-tumor immune responses [216].

There are several drawbacks to using the P815 cell model. First, as implied above, P815s are highly resistant to transfection. I have confirmed this numerous times through transfection optimization studies with this and other KIT-mutant cell lines. The transfectability of this cell line was addressed by the creators of the P1.HTR cell line; however it is unclear what the impact of selection would be on NFAT expression and activity. If we continue to study NFAT, the P1.HTR cell line may be a useful tool to

acquire. Another drawback is the rapid doubling rate of P815s. Over time, this could lead to the acquisition of additional, random mutations and eventual genetic drift. To avoid these issues I thaw new P815 cells approximately every month. (To date, we have not observed any obvious changes in doubling rate, or cell morphology.)

4.1.2 RBL2H3 cell line:

The rat basophilic leukemia cell line RBL1 was created via the use of a carcinogen – ICI 42464 by Eccl et al. in 1971 [217]. The carcinogen gave rise to a granulocytic leukemia which eventually killed the host. Cultured cells from the animal maintained the ability to initiate tumors following subcutaneous injection [218], but were later abandoned as a research tool, but not before valuable variants of the RBL1 cell line were established. One cell line, RBL-HR+, was found to have increased levels of histamine release, and through limiting dilutions to reduce cellular heterogeneity, the RBL2H3 cell line was isolated[218].

Many years after its original discovery, the RBL2H3 cell line was found to harbor the activating KIT D817Y mutation[70], which gave rise to our interest in the cell line as a model of signaling pathways in KIT mutant cells. In addition to being a tool to study KIT activation, the RBL2H3 cell line has been used extensively to study basophil degranulation, inflammation, allergy, and immunologic phenomenon. Although it is commonly referred to as a mast cell line, RBL2H3 cells are of basophilic origin and exhibit cellular characteristics somewhere in between a true basophil or mast cell [168, 218].

4.1.3 BR and C2 cell lines:

The BR and C2 cell lines were obtained from canine mastocytomas. In particular, the mastocytoma that eventually gave rise to the C2 cell line was obtained during final illness which was associated with mast cell leukemia [169]. The cell lines were propagated in athymic mice [219] before being successfully cultured *in vitro.* These cell lines represented an important milestone in mast cell research, because they were the first cultured canine mast cells. This was noteworthy because despite the creation of rodent mast cell lines (P815 and RBL2H3), human mast cells were observed to be more closely related to canine mast cells rather than rodent mast cells. At the time of their creation, there were also no continuously cultured human cell lines available either.

It was later discovered that the BR cell line contains a KIT L575P point mutation while the C2 cell line contains a short duplication in KIT exon 11. Both mutations lead to constitutive activation of KIT as assessed by immunoblotting for phospho-KIT [71]. Although we have not been able to confirm NFAT status in BR and C2 cells lines due to a lack of suitable antibodies to detect canine NFAT species, we have confirmed KIT activation via immunoblotting and NFAT species expression via qRT-PCR.

4.1.4 HMC1.1 and HMC1.2 cell lines:

The HMC1 cell line was the first human mast cell line to be successfully cultured. It originated from a mast cell leukemia patient, and exhibits characteristics of an immature mast cell line [167]. Subsequently, a group studying KIT expression in human and murine hematopoietic organs and cell lines found KIT mRNA expression in the HMC1 cell line [220].

Two sublines of the HMC1 cell line were isolated – one was found to harbor a KIT V560G point mutation and is referred to in this document as HMC1.1. The other cell line harbored dual KIT mutations – KIT V560G+D816V [221]. To date, only two other human mast cell lines have been established (LAD2 and LUVA).

4.1.5 NFAT-P815 cell line:

This cell line was created using the Cignal Lenti NFAT Reporter from SABioscience (catalog # 336851, CLS-015L). P815 cells were plated at 10,000 cells per well in a clear-bottom 96-well plate. Cells were transduced with 78uL DMEM media (+15% FBS, 1% P/S, 1% L-Glut), 6ug/ml polybrene (2uL/well at .3ug/ul), and 20uL Cignal Lenti NFAT reporter. The cells were incubated overnight and the following morning the transduction media was removed and replaced with DMEM media. Cells were incubated for an additional 48 hours. After 48 hours, the cells were selected for puromycin resistance at a concentration of 1ug/ml (as determined by previous puromycin dose titration experiments in p815 parental cells.) Cells were selected for 4 days before being tested with the Luciferase Assay System (Promega, #E1501) for firefly luciferase expression.

4.2 Cellular fractionation:

Cytoplasmic and nuclear fractions from control and inhibitor treated cells are prepared using a commercial kit (#78833, Thermo Sci). Briefly, cells are scraped and spun down in 15mL conical tubes at 1500 RPM for 5 minutes. The media is aspirated, and pellets are resuspended in 100uL of CER I reagent (plus protease/phosphatase inhibitors) and incubated on ice for 10 minutes. Next, 5.5uL of CER II reagent is added and each sample is vortexed briefly and incubated for an additional minute on ice. Lysates are transferred to a 1.5mL tube and spun down at maximum speed in a bench-top centrifuge

for five minutes. The cytoplasmic fraction is transferred to a new 1.5mL tube, and the nuclear pellets are resuspended in NER I reagent (plus protease/phosphatase inhibitors). Samples are vortexed for 15 seconds and incubated on ice for 10 minutes. This process is repeated four times for a total of 40 minutes of incubation. Finally, samples are spun down in the bench-top centrifuge for 5 minutes at maximum speed. The samples can then be frozen at -20°C or quantified with Bradford reagent for immediate use in Western blotting applications.

4.3 Immunoblotting:

Cells were lysed as described above with the Thermo-Pierce fractionation kit, or using a traditional RIPA lysis buffer: 50mM Tris-HCl, 1% IGEPAL, .25% deoxycholate, 150mM NaCl, 5mM EDTA, 1:100 protease/phosphatase inhibitor cocktail. Following lysis, protein concentration is quantified with Bio-Rad Protein Assay Dye Reagent Concentrate: dye, phosphoric acid and methanol as measured at 595nm with a BioMate 3 spectrophotometer (Thermo Scientific). For immunoblotting, we typically use 100-200 µg and 50-100 µg of cytoplasmic and nuclear protein lysate, respectively.

Equivalent amounts of protein lysate are mixed with 20uL of Laemmli buffer, and boiled at 95°C for 10 minutes. Samples are then loaded into a Criterion 10% polyacrylamide gel, and run at 110volts for 125 minutes for standard gels, or at 300volts for 25 minutes for TGX Stain-free gels (Cat #567-8033). Once the gels are run, they are transferred to nitrocellulose at 300mA for 2 hours or at 2A for 10 minutes using the Trans Blot Turbo Transfer System (Bio-Rad). Nitrocellulose membranes are blocked in 5% milk or BSA for 1 hour and rocked in primary antibody overnight. A list of primary antibodies used in these studies is found below. Secondary antibodies include mouse, rabbit, and goat,

and are typically used at 1:7500 for 30 minutes. Blots are developed with standard Western blotting detection reagents such as ECL from Amersham (Cat #RPN2209). Blots are visualized using film or with the Bio-Rad Chemi-Doc system (Image Lab software from Bio-Rad).

Table 12 - Antibody list

Antibody	Concentration	Company	Catalog#	2°
NFAT1	1:1000	Cell Signaling	4389	Ms, 1:7500
NFAT2	1:1000	Thermo Sci	MA3-024	Rb, 1:7500
NFAT3	1:400	Santa Cruz	sc-13036	Rb, 1:7500
NFAT4	1:400	Santa Cruz	sc-8321	Rb, 1:7500
B-actin	1:1000	Cell Signaling	4970	Rb, 1:10,000
p-KIT	1:1000	Cell Signaling	3391	Rb, 1:5000
total KIT	1:1000	Cell Signaling	3074	Rb, 1:7500
p-ERK	1:1000	Cell Signaling	9109	Rb, 1:7500
total ERK	1:1000	Cell Signaling	9102	Rb, 1:7500
p-AKT	1:1000	Cell Signaling	9271	Rb, 1:7500
total AKT	1:1000	Cell Signaling	9272	Rb, 1:7500
p-RB	1:400	Santa Cruz	sc-12901	Gt, 1:10,000
total RB	1:400	Santa Cruz	sc-50	Rb, 1:10,000
p-JAK1	1:400	Santa Cruz	sc-16773	Gt, 1:10,000
total JAK1	1:400	Santa Cruz	sc-277	Rb, 1:7500
p-JAK2	1:1000	Cell Signaling	3776	Rb, 1:7500
total JAK2	1:1000	Cell Signaling	3230	Rb, 1:7500
CCND2	1:1000	Cell Signaling	3741	Rb, 1:7500
calcineurin	1:1000	Cell Signaling	2614	Rb, 1:7500
p-STAT3	1:1000	Cell Signaling	9131	Ms,Rb 1:10,000
total STAT3	1:1000	Cell Signaling	9132	Ms,Rb 1:10,000
p-STAT5	1:1000	Cell Signaling	9351	Ms,Rb 1:10,000
total STAT5	1:1000	Cell Signaling	9352	Ms,Rb 1:10,000
Lamin A/C	1:1000	Cell Signaling	2032	Rb, 1:5000
MYC	1:1000	Cell Signaling	5605	Rb, 1:7500
Pim2	1:400	Santa Cruz	sc-13514	Ms, 1:7500
B-tubulin	1:1000	Cell Signaling	2128	Rb, 1:10,000
GAPDH	1:2000	Cell Signaling	2118	Rb, 1:10,000
JUN	1:1000	Cell Signaling	9165	Rb, 1:7500

4.4 Cellular Proliferation Assays:

P815, RBL2H3, BR, C2 and HMC cells are plated at 5,000-20,000/well at the same time they are treated with inhibitor or control media, in an opaque 96 well plate in a total volume of 50uL and incubated for 48-72 hours. GIST cell lines (e.g. GIST T1, GIST 882, GIST 48) are plated at 20,000 cells/well on fibronectin-coated, opaque 96-well plates and incubated overnight. The next day, cells are treated with inhibitor or control in a total volume of 50uL/ well and incubated for 48-72 hours. Following the drug treatment period, 50uL of Cell Titer Glo substrate (Promega #G7571) is added to each well. Plates are rocked for 15 minutes and read using the Cell Titer-Glo program on a GloMax-96 Microplate luminometer (Promega). As an alternative (or to verify results), we can use XTT-based assays or manual cell counting.

Cell Titer Glo is a luminescent cell viability assay developed at Promega for use in cellular proliferation, cytotoxicity, and cellular viability experiments. The assay quantifies ATP as an indication of viable cells present in a sample. The Cell Titer Glo reagent lyses cells within the well and generates a luminescent signal that is proportional to ATP present in the sample (Figure 23). By directly adding the reagent to each well, errors due to washing and multiple pipetting steps are eliminated. Based on the high level of metabolic activity and proliferation of our KIT-mutant cancer cell lines we felt this assay would be a good tool to monitor the effects of pharmacologic inhibition on cell growth and viability.

4.5 Caspase 3/7 Assay:

Cells are treated as described above for the proliferation assays. Following incubation, 50uL of Caspase-Glo 3/7 Assay reagent (Promega, #G8091) is added to each well. Plates are incubated for 90min and then read using the Caspase-Glo program on a

GloMax-96 microplate luminometer (Promega). These assays can be complemented by performing immunoblotting for cleaved and non-cleaved forms of PARP (PARP antibody #9542, Cell Signaling Technology) or flow cytometric measurement of apoptosis induction using Annexin V-FITC/7-AAD staining.

The Caspase-Glo reagents from Promega are designed to quantify caspase content in samples of adherent or suspension cells. The reagent contains a pro-luminescent caspase substrate (Z-DEVD in the case of caspase 3/7) which is cleaved to release a substrate of luciferase, used in the light producing reaction seen in Figure 24. As with the cell viability assay, the reagent lyses the cells, and reacts with substrate to create light, which is read by the luminometer. The assay reaches steady state within one hour and remains stable for several hours, making it ideal for high throughput experiments with multiple 96-well plates.

4.6 NFAT Transcriptional Activity Assay:

P815-NFAT cells are plated at 10,000/well at the same time they are treated with inhibitor or control media in an opaque 96 well plate with a total volume of 50uL Cells are treated with inhibitors at the desired concentration for 1-24 hours depending upon the type and concentration of inhibitor. Following treatment, media is aspirated from the cells, and 20uL of Passive Lysis Buffer (Promega) is added to each well. Plates are rocked for 15 minutes at room temperature and then loaded into a GloMax-96 microplate luminometer. The plates are read using the “Luciferase Assay System with Injector” program which injects 100uL of firefly luciferase reagent into each well before quantifying luciferase protein present. The luciferase readout is used as an indication of NFAT transcriptional activity and is typically normalized to cell viability (CTG Assay) if the drug incubation lasting longer than 3 hours (to control for changes in cell number with prolonged incubation).

4.7 RT-PCR:

Real-time polymerase chain reaction (PCR) was carried out in a 50-µl reaction using single stranded cDNA (corresponding to 1µg initial total RNA) and 19 probes Master MIX (Roche), with a FAM-labeled hydrolysis probe specific to the reference Glyceraldehyde 3-phosphate dehydrogenase (GAPDH). Cycling conditions on a Light-Cycler 480 instrument (Roche) included 10 min at 95oC followed by 40 cycles of 95oC for 10 sec and 60oC for 20 sec. Genes of interest were detected using commercial TaqMan Gene Expression assays (Applied Biosystems by Life Technologies):

Gene expression (mouse) was detected using commercial TaqMan Gene Expression assays (Applied Biosystems by Life Technologies**): NFAT2** assay Mm00479445_m1, **NFAT1** assay Mm00477776_m1, **NFAT4** assay Mm01249200_m1, **NFAT3** assay Mm00452375_m1, **GAPDH** assay Mm03302249_g1, **GAPDH** assay Mm99999915_g1, **Ccl3** assay Mm00441259_g1, **Ccl4** assay Mm00443111_m1, **Ccng2** assay Mm00432394_m1, **Cish** assay Mm01230623_g1, **Dusp5** assay Mm01266106_m1, **Dusp6** assay Mm00518185_m1, **Fzd9** assay Mm01206511_s1, **Socs1** assay Mm00782550_s1, **MYC** assay Mm00487804_m1, **Etv5** assay Mm00465816_m1, **Il6** assay Mm00446190_m1, **Tnf** assay Mm00443260_g1, **Ccnd2** assay Mm00438070_m1, **Id2** assay Mm00711781_m1, **Ccnd1** assay Mm00432359_m1, **Hif1a** assay Mm00468869_m1, **Egr1** assay Mm00656724_m1, **Pim2** assay Mm00454579_m1, **Id1** assay Mm03676649_s1, **Ccne2** assay Mm00438077_m1, **Pim1** assay Mm00435712_m1, **Hbegf** assay Mm00439306_m1, **Bcl6** assay Mm00477633_m1

Expression results were analyzed using the comparative C_T method (also known as the $2^{-\Delta\Delta CT}$ method) [193]. This method quantifies changes in gene expression, normalized to a housekeeper gene, such as GAPDH, and relative to the expression of a calibration gene. The target expression = $2^{-\Delta\Delta CT}$, where $-\Delta\Delta CT = -(\Delta C_T - \Delta C_R)$, where ΔC_T is the

difference between the threshold cycles for the target and the reference gene, and ΔC_R is the difference between the threshold cycles for the calibration gene and the reference gene. In our experiments were used the expression of the target gene in untreated cells as our calibration gene.

4.8 shRNA:

We ordered shRNA lentiviral particles from Sigma for stable transduction of P815 cells.

Table 13 - Sigma MISSION shRNA clone list

Target	Clone ID
NFAT2	NM_016791.2-1985s1c1
PPP3R1	NM_024459.1-278s1c1
JAK1	NM_146145.1-2364s1c1
JAK2	NM_008413.1-2499s1c1
CCND2	NM_009829.2-821s1c1
CCND1	NM_007631.1-511s1c1
MYC	NM_010849.2-1807s1c1
Non-target (NT)	SHC002V

Each cell line was created from the P815 parental cell line via lentiviral transduction with pLKO.1 Mission lentiviral transduction particles from Sigma (see table above). P815 cells were plated at 5,000/well in a clear-bottom 96-well plate. Cells were allowed to settle onto the surface for approximately 2 hours. Once cells became adherent, as determined by visual inspection under a microscope, they were transduced overnight with 85.5uL media, 0.006ug polybrene, and 12.5uL of lentiviral particles. Cells were washed and incubated with fresh media for 24 hours. Following recovery, stably transduced clones were selected using 1ug/mL puromycin. Several stable colonies from each transduction were expanded and tested for knockdown efficiency. Immunoblotting was used to quantify the degree of knockdown as assessed by comparison to both parental P815 cells and NT-P815 cells.

4.9 Co-Immunoprecipitation:

In order to detect protein-protein interactions between NFAT and JUN, I used a co-IP strategy. Nuclear cell lysates were incubated overnight with 500uL wash buffer (DPBS+1:1000 protease and phosphatase inhibitors) plus 20uL of NFAT agarose conjugated beads (Santa Cruz, #sc-7294 AC) or JUN agarose conjugated beads (Santa Cruz, #sc-1694 AC) plus nuclear lysate. Samples are rocked and incubated at 4°C overnight. Next, samples are spun down for five minutes at 5,000 RPM, washed with 500uL of wash buffer, and repeated. Laemlli buffer (20uL) is added to each sample and tubes are boiled for 10 minutes at 95°C. For immunoblotting methods please see immunoblotting section above.

4.10 NFAT-DNA binding assay:

To interrogate the effects of calcineurin and KIT inhibition on the interaction between NFAT and DNA we used an ELISA-based KIT from ActiveMotif (http://www.activemotif.com/catalog/222/transam-nfatc1). This assay can be adapted to use any NFAT antibody; however we primarily used it to probe for NFATc1 as the kit was originally intended. This ELISA assay is marketed by ActiveMotif as an “NFATc1” assay; however NFATc1 is equivalent to NFAT2, so this assay and results will henceforth be referred to as NFAT2 for consistency with the nomenclature throughout the rest of this document.

Nuclear lysates were isolated using the ActiveMotif Nuclear Extract Kit (#40010) . Cells are scraped and spun down for five minutes at 500 RPM, 4°C. Supernatant is removed and cells are resuspended in 250uL of hypotonic buffer transferred to a 1.5mL tube, and incubated on ice for 15 minutes. Detergent (25uL) is added to each sample and samples are vortexed for 10 seconds. Next, they are spun down for 30 seconds at

14,000*g* on a bench-top microcentrifuge. Supernatant (cytoplasmic fraction) is discarded and nuclear pellets are resuspended in 25uL of complete lysis buffer. Samples are vortexed and incubated/rocked at 4°C for 30 minutes. Samples are then vortexed for 30 seconds and centrifuged for 10 minutes at 14,000*g.* Lysates are frozen at -80°C or quantified for use in the NFAT-DNA TransAM assay.

Nuclear lysates are quantified as described above (“*Immunoblotting”)*. 40uL of Binding Buffer AM1 is added to each well of the TransAM NFAT2 plate. 7ug of nuclear lysate sample (diluted in Complete Lysis Buffer to 10uL) is loaded per well and 5ug of positive control (Jurkat nuclear extract) per well (diluted in Complete Lysis Buffer to 10uL). Negative control wells are loaded with 10uL of extra Complete Lysis Buffer. The plate is incubated for one hour at room temperature with gentle rocking (100 RPM). The wells are washed three times with 200uL of wash buffer per well. Primary NFAT2 antibody (100uL at 1:500) is added to each well and the plate is incubated for an additional hour at room temperature. Wells are washed three times again, and secondary anti-mouse HRP-conjugated antibody (100uL at 1:1000). Following one hour incubation, wells are washed four times and 100uL of developing solution is added to each well. The plate is incubated away from direct light for approximately 10 minutes at which point 100uL of Stop Solution is added to each well. Samples are read at 450nm on a spectrophotometer, and data is exported into Excel for further analysis.

4.11 RNA-Seq:

RNA-Seq is a novel approach to transcriptome profiling that improves upon traditional sequenced based methods. The approach uses next-generation sequencing to capture a snapshot of mRNA transcript levels within a sample. Next-generation sequencing (NGS) is a new alternative to classic Sanger sequencing. Like classic sequencing, it relies on identification of bases within small fragments of DNA/RNA. However, NGS is

able to process millions of signals in parallel, allowing for rapid sequencing across an entire genome. As a sequence-based method, RNA-Seq doesn't require a pre-fabricated capture array, so it is able to find novel mRNA transcripts. In addition, because it is not restricted to signal detection from a microarray, RNA-Seq eliminates low level noise as well as upper limit saturation. It therefore has a large dynamic range and is better able to measure genes expressed at low levels [192] .

Multiplexing allows large numbers of samples to be sequenced simultaneously during a single run. "Barcodes" are added to each unique sample so that they can be differentiated during data analysis.

For the Illumina platform used in our studies, DNA or RNA is purified, chemically fragmented and turned into a library of cDNA. Adapters are ligated onto the ends of the fragments with barcodes for subsequent identification of unique sample data. The cDNA is amplified using PCR, purified, and quantified using real-time PCR. Appropriate concentrations of DNA are run on a sequencer (the HiSeq 2000 Illumina Sequencing System in our case). The library of probes is washed across a flowcell and the cDNA fragments randomly bind to its surface becoming immobilized. Both ends of the fragment bind, forming a "bridge." Surface adapters on the flow cell enable elongation along bound DNA fragments to create double stranded bridges. These new bridges are denatured and the process is repeated in order to amplify the cDNA library which creates dense clusters of DNA on the flow cell. Finally, the sequence of each cluster is read base by base. This is accomplished by adding labeled reversible nucleotide tags which are excited with a laser and captured as G, T, C, or A. Each base is read sequentially and aligned to a reference sequence or aligned *de novo.*

In order to go from image capture to quantifiable data researchers use software packages like CASAVA. These types of software take the raw images and create intensity scores, base calls, and align the sequences for downstream analysis. The next step in data creation is to use a software service such as DNAnexus to normalize the reads to RPKM (reads per thousand million). . This software takes individual sequence reads and maps them to genes. It also normalizes the coverage to total reads and gene size, by calculating RPKM (reads per thousand million). The “million” part normalizes to total reads per sample. For example, if one sample had 20 million sequence reads and another sample had 10 million total reads, then gene expression would be skewed by 2-fold just due to differences in the total read counts per sample. This is corrected for by RPKM. On the other hand, the “thousand” part normalizes to gene length. The sequence reads are approximately 100 base pairs long. So, if a gene were 30kb in length and another gene were 10 kb in length, then the reads per gene would be off by a factor of three just because one gene is three times as long as the other. This too is controlled for in RPKM.

Next, comparisons between treatment groups were made using the R/Bioconductor packages edgeR and DESeq. These software packages allowed us to calculate p-values associated with each comparison. Finally, Excel was used to sort genes based on expression level.

Brief protocol for our RNA-Seq study, performed by the OHSU MPSSR Core:

RNAseq libraries were prepared using the TruSeq RNA preparation kit (Illumina). This kit was qualified for use with total RNA input from 0.1 to 4 µg. Briefly, total RNA quality was verified by examination on a Bioanalyzer (Agilent). Poly(A)+ RNA was recovered using oligo-dT -coated magnetic beads. Recovered RNA was then chemically fragmented.

First-strand cDNA was generated from the fragmented RNA using random hexamer priming. The RNA template was removed and the second strand was generated. The ends of the resulting double stranded cDNA were repaired, after which a single 'A' nucleotide was added to the ends of both strands. Appropriate adaptors were ligated to the ends of the cDNA. Adaptors contained both flow cell binding sequences and indexing "barcodes". The cDNA was amplified using a limited number of cycles of PCR. Following amplification and clean-up, the library concentration was determined using real-time PCR. Samples were diluted to a concentration appropriate to generate 160 to 180 million clusters per lane on the HiSeq 2000 flow cell (Illumina). Following sequencing, the base call data was assembled using the CASAVA package (Illumina).

Data was analyzed using the software package DNAnexus. This software aligns the reads, and normalizes to RPKM (reads per thousand million). Excel was used to sort genes based on expression level. In order to further hone our results, we entered all of the targets that decreased by 2.0 fold or greater into the online database *String.*

4.12 String: String[194] is an online database that provides direct and indirect, known and predicted, protein-protein interactions. It is highly useful in elucidating connections between targets in genome-wide screens such as RNA-Seq or RNAi knockdown. The user inputs proteins of interest and the String algorithm mines online databases and literature to create a protein network. The network is interactive, with references for each protein interaction as well as advanced features such as identifying targets within a biological pathway, with the same molecular function, or within the same cellular component. We have used String to reduce the noise in our RNA-Seq results, and to identify targets within physiologically relevant pathways that may be contributing to the observed synergy.

Chapter 5: Preliminary Data

5.1 Synergy in other cell lines

NFAT is a relatively newly characterized, deregulated target within the cancer world; therefore the full scope of its involvement across human cancers is unknown. We are excited about the possibility that this form of combination strategy may be beneficial to other types of KIT-mutant cancer, or even other types of kinase-driven cancers. To investigate this possibility we performed preliminary experiments in eight other cancer cell lines. We were encouraged to see that a number of these other models respond to kinase inhibition plus calcineurin inhibition. Although thorough investigation of alternative cancer models was outside the scope of my thesis project, we believe that follow-up studies in these models are warranted to determine whether such a combination treatment approach would be beneficial in cancers such as leukemia, melanoma, or other mast cell diseases.

The preliminary studies shared below consisted of cellular viability combination experiments using CTG as a readout. In a few instances we have cellular fractionation data showing NFAT localization and phosphorylation.

5.1.1 MC/9 murine mastocytosis cell line

The MC/9 cell line was originally derived from fetal murine hematopoietic tissue [222]. The cells resemble immature mast cells based on morphology and histamine content. They have normal karyotypes and have been shown to closely resemble *in vivo,* immature mast cells [223]. While there have been no reported KIT mutations in this cell line, in our hands, we observed p-KIT activation in the absence of SCF as determined by immunoblotting (data not shown). Regardless of the mechanism of KIT activation, the

fact that KIT is activated in this cell line suggests that these cells might be susceptible to KIT inhibition. Previously, it has been shown that KIT signaling rescued MC/9 cells from apoptosis induced by FK506 or CSA (in the absence of IL-3) [224]. The fact that CSA and FK506 inhibited KIT-mediated rescue of MC/9 cells from apoptosis supports an unknown mechanism of crosstalk between KIT and calcineurin signaling pathways.

While the MC/9 cell line isn't derived from neoplastic tissue, it is a mast cell model and could be used to establish the basis for the use of KIT and calcineurin inhibitors in other diseases associated with mast cells such as psoriasis [189], asthma [225], autoimmune diseases , or mastocytosis.

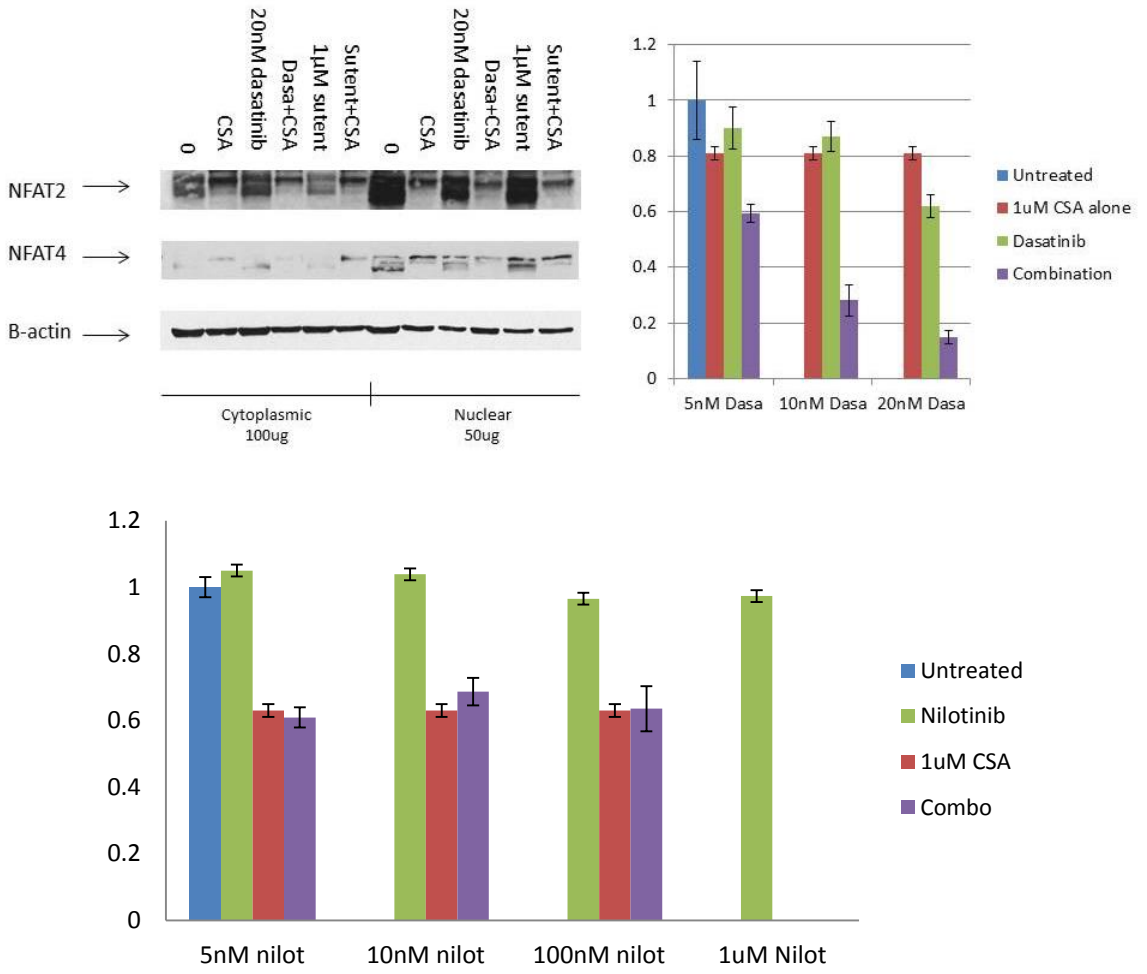

Figure 23 – MC/9 Preliminary data. NFAT species show nuclear localization in untreated MC/9 cells. CSA treatment leads to cytoplasmic translocation and band shift (top, left). MC/9 cells show extreme sensitivity to simultaneous CNPI and dasatinib treatment (top, right). MC/9 cells show no combination effect following treatment with CNPI+nilotinib (bottom).

Shown above are immunoblotting data and cellular proliferation data for the MC/9 cell line. In our immunoblotting studies, CSA treatment caused a band shift in both NFAT2 and NFAT4. This was accompanied by decreased NFAT nuclear localization. It is unclear why there isn't greater increase in cytoplasmic localization given the marked decrease in nuclear localization. We speculate that NFAT proteins may be degraded upon entry into the cytoplasm. Regardless, there is clear evidence of constitutive NFAT

activation in this cell line based on nuclear localization and phosphorylation species present in untreated cells, and the effects of CSA treatment on these characteristics. This data supports our findings in cellular proliferation experiments in MC/9 cells. We consistently saw synergy between CSA and dasatinib in MC/9 cells in the presence or absence of SCF (Figure 27). I also tested CSA in combination with nilotinib (Figure 27), sorafenib, or sunitinib (data not shown) and I saw no combination effect. These results may indicate novel mast cell biology whereby inhibition of a different dasatinib target (not KIT), such as Src, is critical to KIT-WT mast cell survival.

5.1.2 K562 human leukemia cell line

The K562 cell line was derived from a CML patient and is positive for the Philadelphia chromosome (BCR:ABL) [226]. These cells have been extensively used to study CML including a number of pre-clinical studies that established the inhibitory effects of imatinib on BCR-ABL signaling [227] [228]. In fact, the K562 cell line was the cell line that Gregory et al. [132] used in their RNAi-based synthetic lethal screen with imatinib, which gave rise to our original hypothesis that inhibiting KIT in combination with calcineurin may be synergistic in KIT-mutant cell lines.

During our initial combination experiments in P815 cells, we also sought to reproduce the synergy that Gregory reported in the K562 cell line with imatinib and CSA. Unfortunately, although we saw a modest combination effect (not significant), we did not see synergy in the K562 cell lines (Figure 28). We believe that this is due to the low level of NFAT activation in these cells. Not only does NFAT appear to be highly phosphorylated in the cytoplasm and nucleus, but treatment with TPA+IonM leads to an accumulation of NFAT in the nuclear fraction, indicating less than maximal NFAT activation (data not shown). We believe that NFAT activation is required for synergy

between NFAT/calcineurin inhibitors and KIT inhibitors, so the lack of synergy in the proliferation studies is not surprising to us. We predict that only cell lines exhibiting constitutive NFAT activation would respond well to combined NFAT and kinase inhibition.

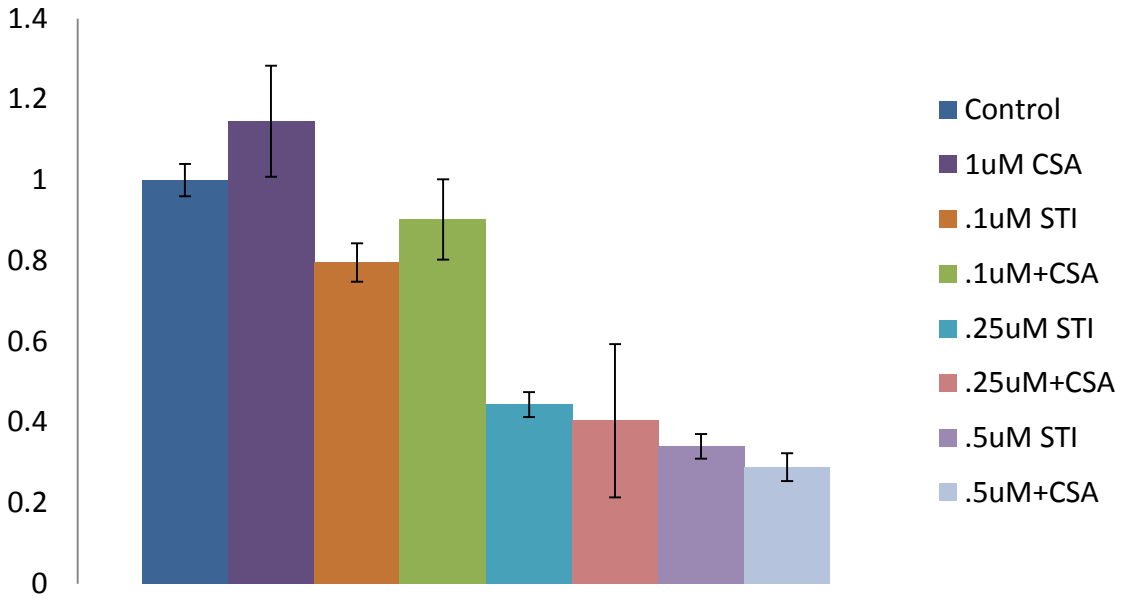

Figure 24 – K562 preliminary data. K652 cells treated for 48hours with increasing doses of CSA, imatinib, or both do not show synergy between CSA and imatinib.

5.1.3 Human GIST cell lines: T1, 882, 48

The GIST 882 cell line was established by Dr. Jonathan Fletcher from an untreated human GIST with a KIT exon 13 K642E mutation [22]. The Gist 48 cell line was established from a patient who progressed on imatinib treatment and expressed a KIT exon 11 V560D mutation and a secondary KIT exon 17 D820A mutation [229]. The GIST T1 cell line was established by Dr. Takahiro Taguchi from an untreated, metastatic GIST containing a 57 base pair deletion in KIT exon 11 [230]. Each of these cell lines is

dependent on KIT signaling, but only GIST 882 and T1 are sensitive to imatinib treatment at low doses.

We found that despite KIT inhibition by various KIT inhibitors, these cell lines did not synergize with calcineurin inhibitors (Figure 29, top 3 panels). To determine the cause for this we examined whether NFAT species were expressed in these cell lines. We found that contrary to KIT-mutant mast cell lines, the GIST cell lines predominantly expressed only NFAT4 (Figure 30). However, we were unable to determine whether NFAT4 was constitutively active in these cell lines because of a lack of suitable NFAT antibodies. We speculate that NFAT4 expression is below the level of detection in these cell lines.

I expanded the studies in the GIST T1 cell line to include the putative MYC inhibitor I-BET151 as well at the NFKB inhibitor BAY-11 (Figure 29, bottom 2 panels). This MYC inhibitor actually inhibits BET proteins which are known to recognize and bind to acetylated histone, recruiting transcriptional machinery to chromatin. It has been shown by Tolani et al.. and confirmed by our own research that inhibition of BET proteins leads to downregulation of MYC expression [198]. We saw much better response following combination of dasatinib with the BET inhibitor in GIST T1 cells, possibly pointing to alternative targets in GIST cancer models. Although BAY-11 combined nicely with dasatinib, I have been unable to confirm the inhibition of NFKB via immunoblotting.

The GIST 882s and 48s have both performed poorly in synergy studies throughout my studies. These graphs are representative of the vast majority of the data I have in these cell lines (Figures 31, 32). They do not appear to respond to simultaneous KIT and calcineurin/NFAT inhibition. I was not able to test other novel target inhibitors such as the MYC inhibitors or the JAK inhibitors in these cell lines.

Overall, I would recommend an adapted RNA-Seq approach in the GIST cell lines whereby treatment with a KIT inhibitor would hopefully uncover novel downstream targets that could be used in combination treatment strategies. Also, given the promising preliminary data with the MYC inhibitors in the GIST T1's I would expand these studies to include the 882 and 48 cell lines.

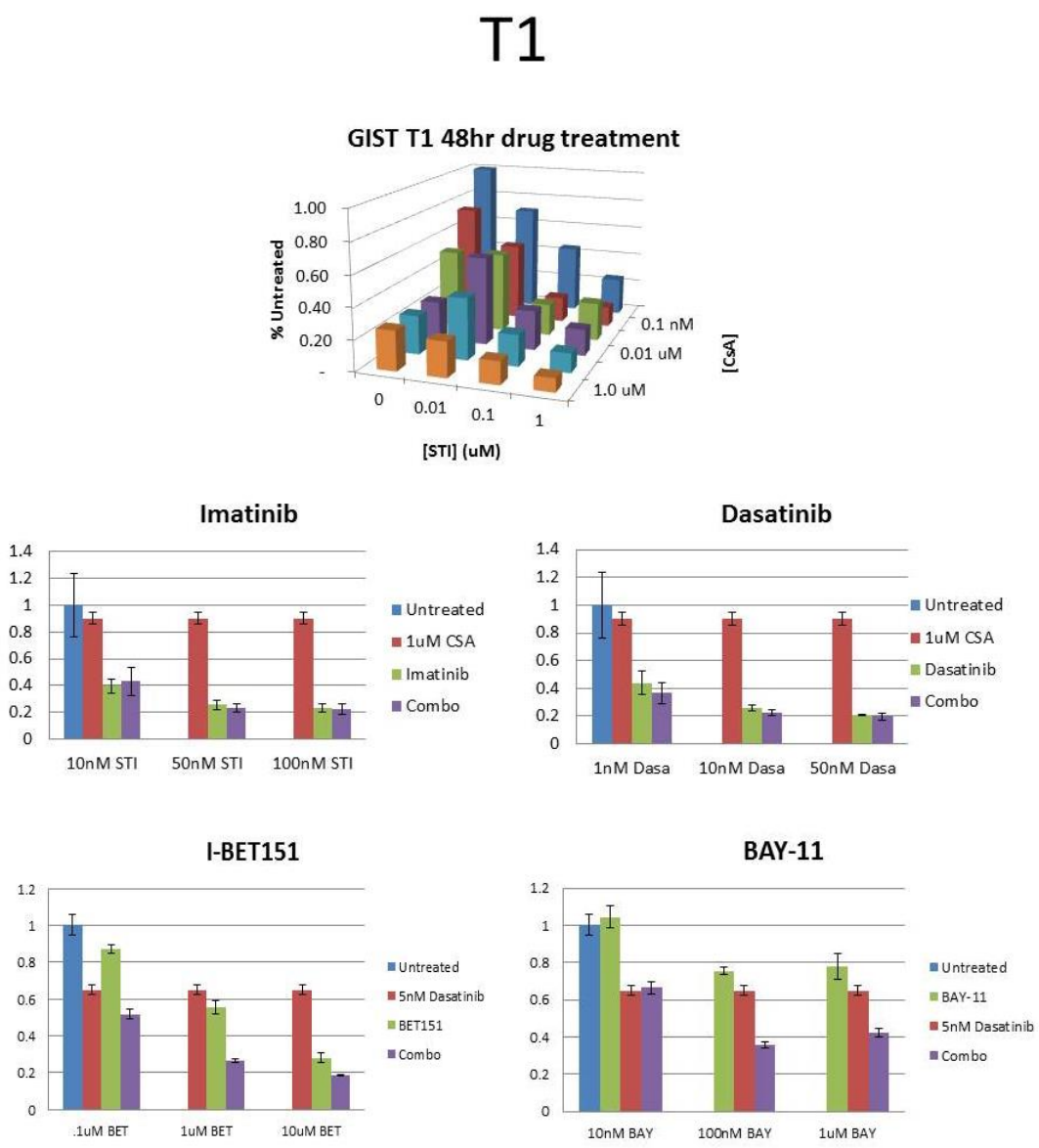

Figure 25 – Preliminary GIST T1 data. GIST T1 shows minimal combination effect following treatment with CNPI+KIT TKI (top 3 graphs). GIST T1 show significant combination effect following treatment with a KIT TKI plus either a BET inhibitor (I-BET151) or an NFKB inhibitor (BAY-11).

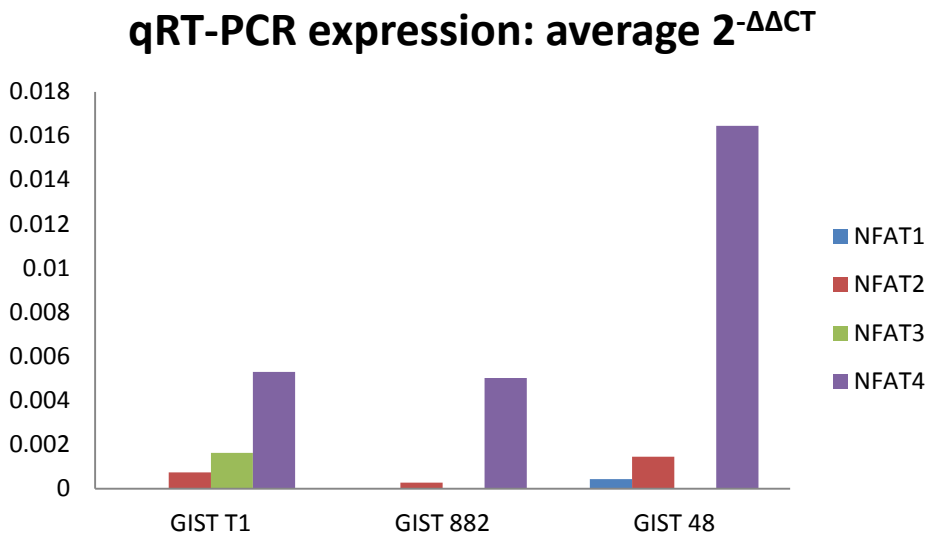

Figure 26 – NFAT species expression in GIST cell lines as assessed by qRT-PCR.

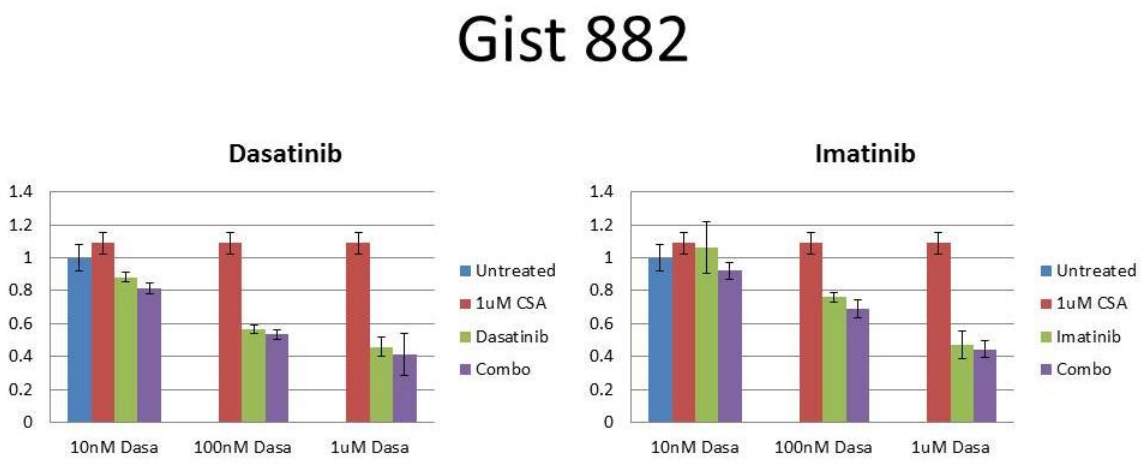

Figure 27 – Preliminary GIST 882 data. The GIST 882 cell line shows minimal combination effect following 48 hour treatment with a CNPI+KIT TKI.

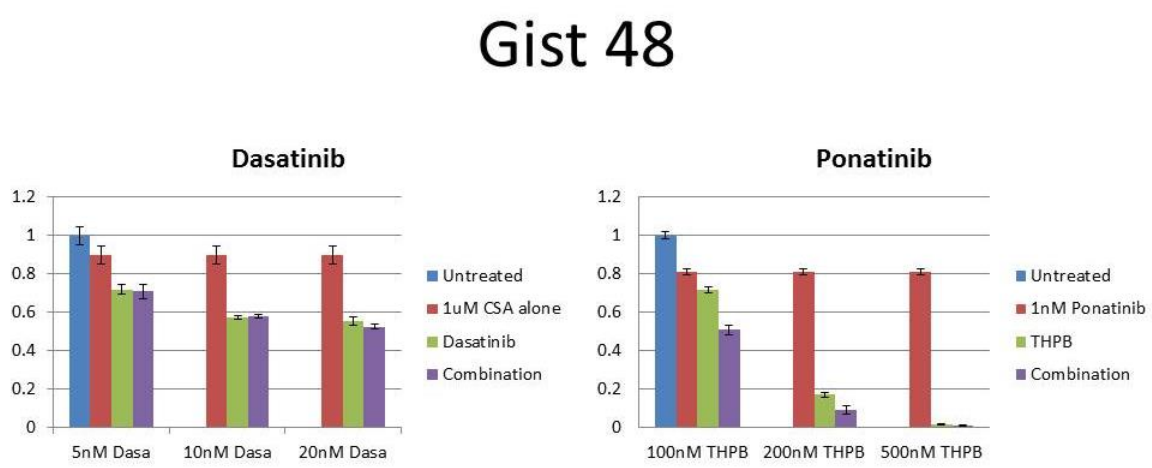

Figure 28 – GIST 48 preliminary data. The GIST 48 cell line shows no combination effect following treatment with CSA plus dasatinib (left). GIST 48 shows a significant combination effect following treatment with a different KIT TKI – ponatinib – in combination with CSA (right).

5.1.4 Human AML cell lines: MOLM 13, MOLM 14

The MOLM13 and MOLM14 cell lines were established from peripheral blood of a patient with acute monocytic leukemia (AML-M5a) which had evolved from myelodysplastic syndrome. At the point when these cell lines were established the patient had just relapsed following chemotherapy. The two cell lines harbor equivalent mutations such as the deletion of Cbl exon 8 [231], but differ in their cell surface antigen expression [232]. Our interest in these cell lines comes from the fact that they both harbor the same FLT3 ITD mutation [233]. There are a number of FLT3 inhibitors on the market, such as sunitinib, which could be combined with a calcineurin inhibitor, should NFAT turn out to be constitutively active in AML cancer models.

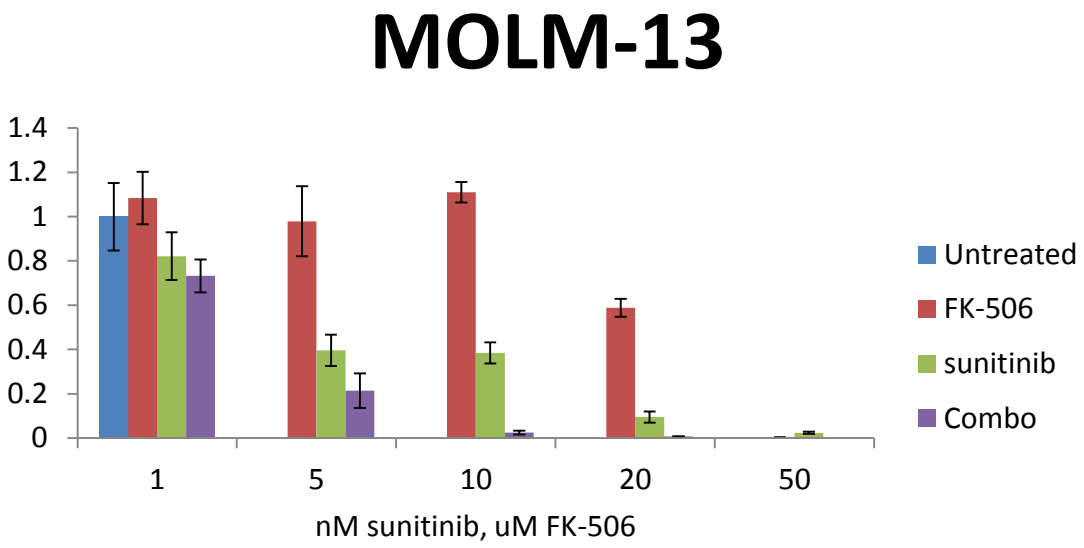

Figure 29 – Preliminary data for MOLM-13 cell line. MOLM-13 cell line shows a significant combination effect following treatment with a CNPI and a FLT3 inhibitor (sunitinib).

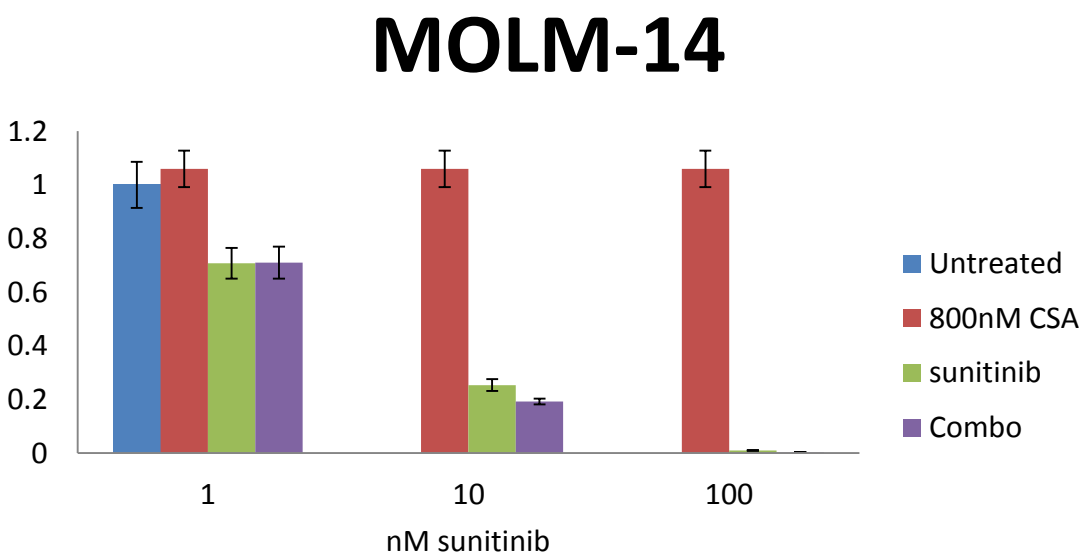

Figure 30 – Preliminary data for MOLM-14 cell line. MOLM-14 cell line shows a minimal combination effect following treatment with a CNPI plus a FLT3 inhibitor.

As we would expect, the MOLM 13 cells respond nicely to sunitinib at low nanomolar levels. Additionally, when combined with FK506, we see a synergistic reduction in cell viability (Figure 33). Based off of this data alone, I would hypothesize that NFAT is constitutively active in MOLM 13 cells. What is puzzling is that despite similar mutations in the MOLM 13 and MOLM 14 cell lines, the MOLM 14 cells did not respond well to combination treatment (Figure 34). As a negative control, I used dasatinib in combination with CSA and saw similar levels of cell viability compared with the sutent/CSA combination (data not shown). Notably, I ran fewer experiments with the MOLM 14 cells, so potentially following further optimization of CSA or FK506 doses, this cell line may respond to combination treatment. A good first step would be to fractionate these cells to determine whether NFAT is constitutively active.

5.1.5 EOL-1 human leukemia cell line

The EOL-1 cell line was established from the peripheral blood of a patient with Philadelphia negative eosinophilic leukemia. Notably, the cell line has a similar morphology to the original leukemic blasts. As such, this cell line is a unique tool to study mechanisms of malignancy in eosinophilic cells [234]. In addition to EOL-1, EOL-2 and EOL-3 cell lines were established from the distinct clones derived from the same patient blood sample. All three lines express the same cell surface markers, however in culture the EOL-1 cells form a monolayer while of the EOL-2 and EOL-3 cells form clusters. In this preliminary study, my experiments only utilized the EOL-1 cell line.

It was subsequently discovered that patients with hypereosinophilic syndrome responded to imatinib treatment, suggesting a RTK mutation behind the disease. In 2003, Cools et al. showed that a fusion protein, FIP1L1:PDGFRα, was present in over half of the patients who responded to imatinib treatment [235]. Since then, only the

EOL-1 cell line has been shown to harbor this same FIP1L1:PDGFRα fusion, making it the only current *in vitro* model for studying the effects of small molecule inhibitors on FIP1L1:PDGFRα positive chronic eosinophilic leukemia [236].

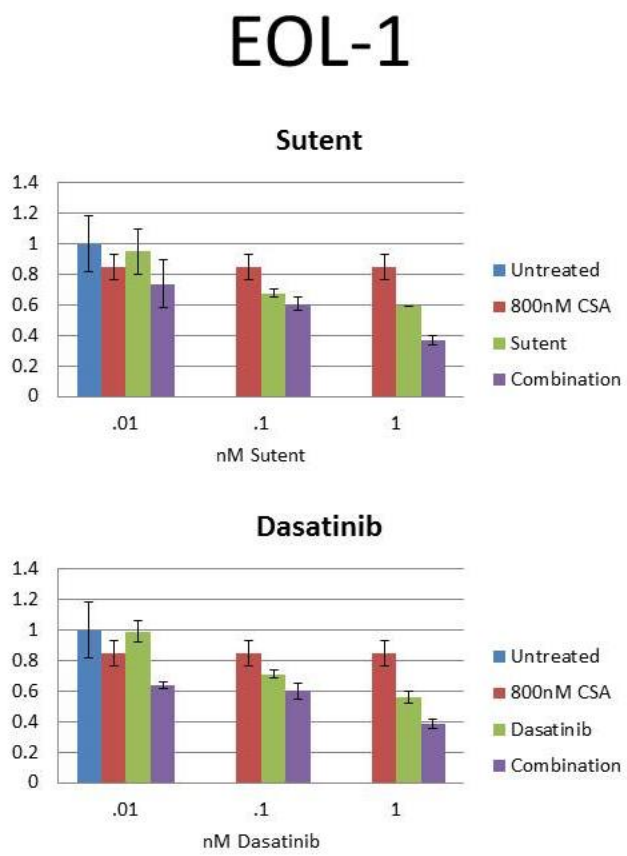

Figure 31 – Preliminary data for EOL-1 cell line. EOL-1 cell line shows significant combination effect following treatment with and CNPI plus either a FLT3 (top) or KIT inhibitor (bottom).

Given that EOL-1 cells harbor a PDGFRA fusion protein, we tested drugs that are known to have activity against other PDGFRA mutations. Sunitinib is FDA approved as a second-line therapy for GIST patients with PDGFRA mutations. Dasatinib (Sprycel) is not explicitly approved for the treatment of PDGFRA-mutant cancers (KIT and PDGFRβ are approved), however there are reports of dasatinib being effective *ex-vivo* and *in-vitro*

at low nM levels against PDGFRA^{D842V} and PDGFRA$^{\Delta DIM842-844}$ [237]. We chose to test both of these inhibitors in combination with CSA. Both inhibitors perform nearly identically in the cellular proliferation assay following 48hrs incubation in the EOL-1 cells (Figure 36). These levels of inhibition are promising and I would strongly encourage follow-up studies of this cell line to determine NFAT activation status.

5.1.6 SK Mel28

The SK-Mel-28 cell line was established from a patient with malignant melanoma during a study to identify distinct melanoma cell surface markers. The SK-Mel-28 cell line was noted due to a high level of reactivity between the patient sera and the autologous cultured melanoma cells [238]. It was later determined that the SK-Mel-28 cell line harbors a BRAF V600E mutation as well as a CDK4 R24C mutation. This particular CDK4 mutation has been shown to abrogate the binding of p16 with CDK4, however the presence of the this mutation does not seem to affect the cell line's sensitivity to BRAF inhibitors [239]. Currently this cell line is mainly used to test the effects of small molecule inhibitors on kinase activity of V600E.

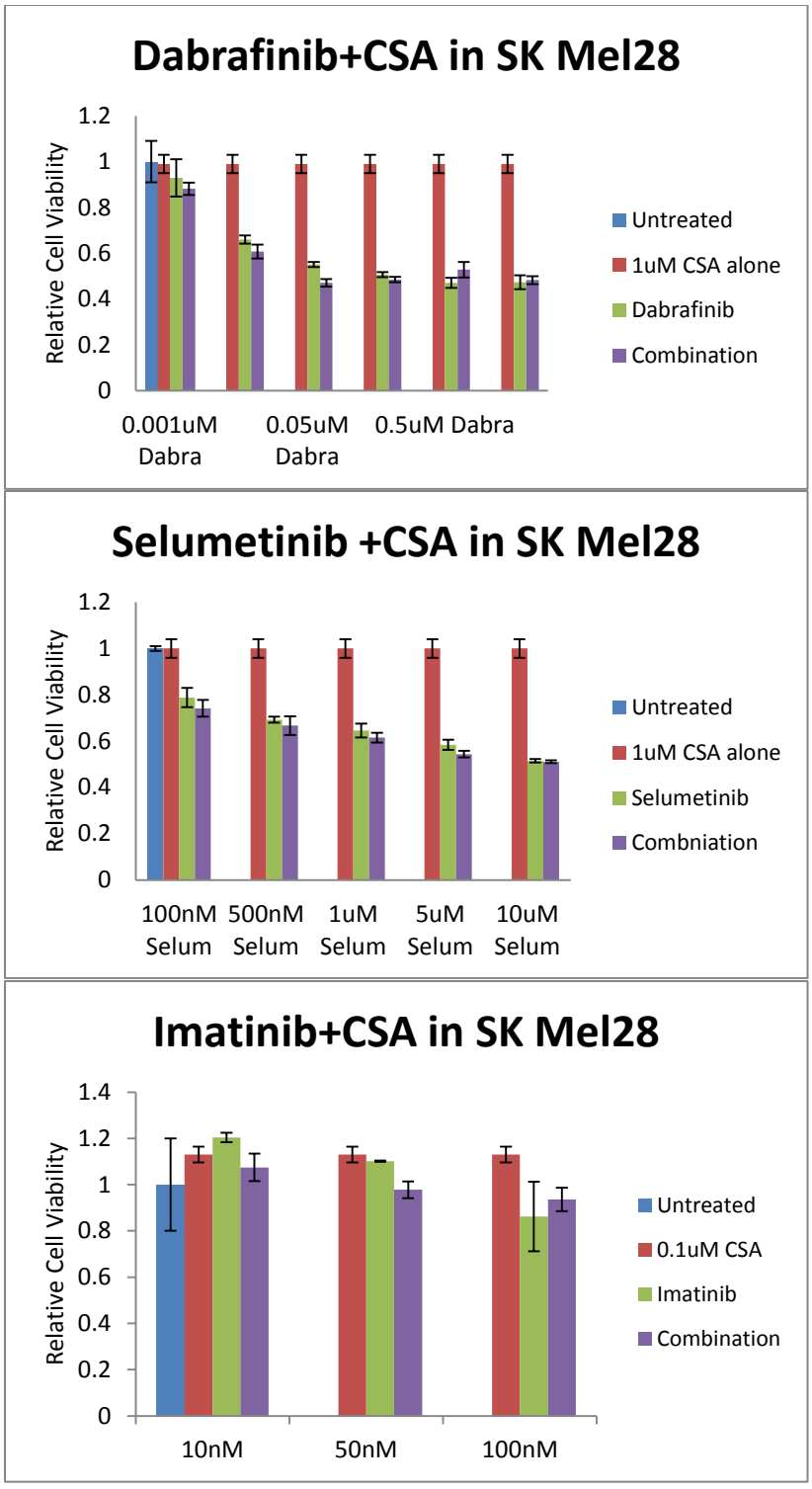

Figure 32 – Preliminary data for SK Mel 28 cell line. SK Mel 28 cells show a minimal combination effect following treatment with a CNPI plus either a Braf V600E inhibitor (dabrafenib) or a MEK inhibitor (selumetinib). SK Mel 28 cells show no combination effect following treatment with a CNPI plus a KIT TKI (bottom panel).

I dosed cells for 48 hours with the BRAF V600E inhibitors PLX-4032, or dabrafenib in combination with CSA. Additionally, I also tested the MEK inhibitor selumetinib which acts downstream of BRAF. None of these combinations showed additive or synergistic effects when combined with CSA (Figure 37). For comparison I treated cells with a KIT inhibitor combined with CSA. As expected, there was no combination effect. This experiment further demonstrates that combining a KIT inhibitor with a calcineurin inhibitor is only efficacious in cell lines with constitutive KIT and NFAT activation, as opposed to generally lethal in all cell types.

5.1.7 CHO and HEK293 cell lines

In an effort to identify a negative control cell line which did not contain constitutively active NFAT species, we tested CHO and HEK293 cells. We eventually determined that the K562 cell line had minimally active NFAT species, but CHO and HEK293 cells were both found to contain highly active NFAT species as evidenced by the immunoblotting experiment below. The P815 cell line was used as a positive control.

The CHO cell line is a widely used line that was established from Chinese hamster ovary cells. It was originally cultured as a tool to study the effects of various agents on chromosomal change and stability in cells cultured *in vitro* [240]. CHO cells are used for their rapid growth rate and high protein yield. They are used extensively in our laboratory to transiently express mutant KIT proteins for screening of novel small molecule KIT inhibitors.

The human embryonic cell line 293 (HEK293) was transformed from human embryonic cells with adenovirus type 5. The resulting cells continue to divide after reaching confluency, however they have low capacity to induce tumors when injected sub-cutaneously into nude mice [241]. This was the first successful transformation of a human cell line with virus. They are not representative models of either “normal” or cancer cells, but like CHO cells, HEK293 cells are used primarily as a tool to study transient or stable protein expression.

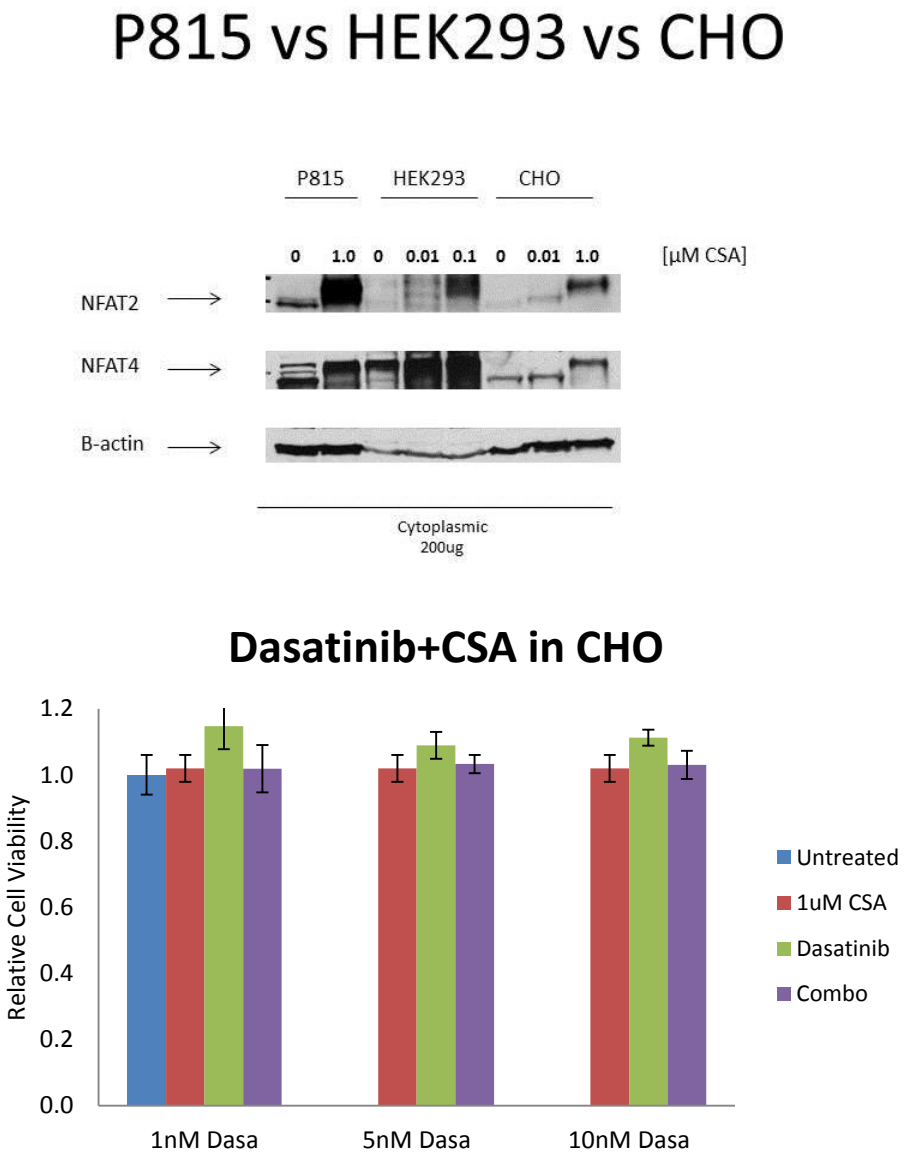

Figure 33 – Preliminary data for CHO and HEK293 cell lines. Immunoblotting of CHO and HEK293 cells reveals constitutive NFAT species as revealed by low levels of cytoplasmic NFAT in untreated cells, and increasing cytoplasmic localization of NFAT following CSA treatment (top). CHO cells show no combination effect following treatment with CNPI plus KIT TKI.

Despite the fact the NFAT appears to be constitutively active based on phosphorylation and localization within CHO and HEK293 cells (Figure 38, top), we would not expect to

see a combination effect in these cells lines because they lack constitutively active KIT signaling. To confirm this I treated CHO cells with dasatinib, CSA, or a combination of both. As shown in figure 38 (bottom), this combination had no synergistic effect on CHO cells. In line with this observation, CHO cells were less sensitive to high doses of either KIT inhibitors or calcineurin inhibitors compared to P815s, BRs, C2, etc.

CHO and HEK293 cells could be used in future experiments to interrogate NFAT signaling and activation mechanisms given the fact that NFAT is inherently constitutively active in these cells lines. These cell lines could prove to be useful tools, especially if transfectable cell lines are required to interrogate a specific aspect of NFAT biology.

5.2 Upstream activation of NFAT

Aside from studying the downstream consequences of combination therapy *in vivo* and in other cancer models, there are a number of unanswered questions upstream of combination therapy and at the point of crosstalk between the inhibitory targets. One question that I tried to address, unsuccessfully, was the upstream mechanisms leading to constitutive NFAT signaling. We believe, based on other studies, and our NFAT-reporter assay studies, that NFAT is not active as the result of activating mutations as is the case with KIT, but rather that some other upstream signaling mechanism is activating NFAT in otherwise “basal” conditions.

One hypothesis was that deregulated Wnt and Frizzled signaling was leading to activation of NFAT based on findings in the Gregory et al. paper [132], where their RNAi screen identified FZD8, FZD2, and WNT5A. Based on this hypothesis we created another reporter cell line for Wnt signaling which contained tandem repeats of the TCF/LEF DNA binding sequence. TCF/LEF is used as a readout for Wnt signaling

because Wnt signaling leads to the dephosphorylation, stabilization, and nuclear translocation of β-catenin. In the nucleus, stabilized β-catenin binds to the TCF/LEF transcription factors to regulate target gene expression. Like the NFAT reporter, the TCF/LEF reporter had a firefly luciferase readout.

Following creation of the WNT-P815 cell line, I tested it for basal reporter activity. Notably, in the NFAT-p815 cell line I consistently saw a high level of basal activity (>100,000 RLUs) due to the fact that NFAT was constitutively active in P815 cells. However, in the WNT-P815 cell line I only saw background levels of firefly luciferase in untreated cells (~5,000 RLUs).

In order to modulate Wnt signaling we purchased a dishevelled inhibitor (Dvl II). Dishevelled is a protein that acts directly downstream of frizzled receptors. It is a common node downstream of all frizzled proteins, which eliminated the need for individual frizzle inhibitors. While there are three distinct dishevelled proteins, the inhibitor we purchased was a pan-dishevelled inhibitor that works by disrupting the interaction between frizzled and dishevelled[242]. Treatment of WNT-P815 cells with increasing doses of Dvl II for six hours lead to a modest decrease in WNT signaling. Treatment of WNT-P815 cells with 20uM Dvl II lead to a 20% decrease in WNT reporter activity.

Next, I tried to activate WNT signaling by incubating cells with WNT ligand. From our RNA-Seq data we identified that P815 cells express both WNT10B and WNT3 were both expressed, albeit at low levels. Treatment of WNT-P815 cells with WNT10B overnight led to a modest increase in WNT reporter activity (20% increase at 2.0μg/mL). Increasing the inhibition to 72 hours did not increase WNT activity. I repeated the same experiment with WNT3 and again found no increase in WNT reporter activity.

To test whether inhibiting Wnt/Fzd signaling affected NFAT reporter activity I treated NFAT-p815 cells overnight with increasing doses of Dvl II. I found that 10uM of Dvl II led to a 13% decrease in NFAT reporter activity while 20uM of Dvl II led to a 18% decrease in NFAT-reporter activity (Figure 39, right). There was a very modest effect of combining 10nM dasatinib with 10uM Dvl II. There was a similarly modest effect of this combination on NFAT-P815 cellular viability (Figure 39, left).

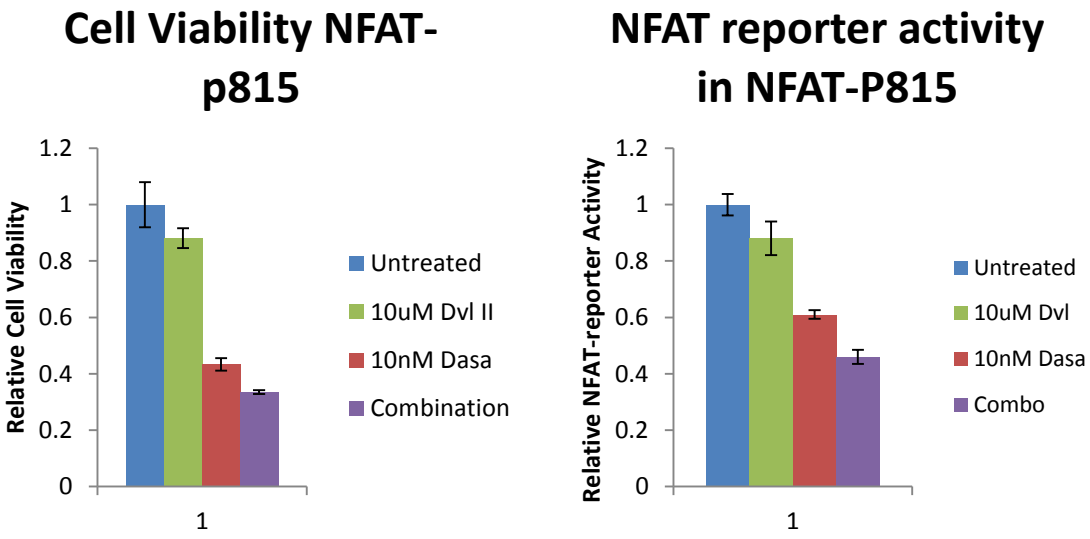

Figure 34 – Effects of a dishevelled inhibitor in P815 cells. P815 cells show a modest combination effect, with respect to cell viability, following treatment with a KIT TKI plus a dishevelled inhibitor (left). NFAT-reporter activity shows a similar combination effect following combination treatment with a KIT TKI plus a dishevelled inhibitor (right).

Due to the low level of basal WNT reporter activity, the fact that we were unable to activate WNT signaling in the P815 cellular context, and a lack of synergy between Dishevelled and KIT inhibitors we chose to focus on the downstream consequences of combination therapy as well as the source of crosstalk between NFAT and KIT pathways.

5.3 NFAT-JUN interaction in KIT-mutant mast cells

As described above, the transcription factor JUN (as part of AP-1) is a well-known binding partner of NFAT. NFAT physically interacts with AP-1 on composite AP-1:NFAT-DNA binding sites. AP-1 is actually a dimer made up of homo- or hetero-dimers of JUN family (JUN, JUNB, JUND), Fos family (Fos, FosB, Fra-1, Fra-2), ATF family (ATFa, ATF2, ATF3) and JDP family (JDP1, JDP2). These proteins are structurally and functionally related – all containing a BZIP domain. The BZIP domain consists of a basic (B) DNA-binding domain and a leucine zipper (ZIP) which is responsible for dimerization. Dimerization must occur before DNA-binding can occur [243].

The most highly studied and characterized member of AP-1 is JUN (formerly c-jun). This protein is regulated primarily through the MAPK signaling pathway via the kinases ERK, and JNK. Phosphorylation sites near the N-terminus are activating phosphorylation sites and enhance transactivation and DNA-binding of AP-1. Phosphorylation sites near the C-terminus, just upstream of the DNA-binding domain are inhibitory and block DNA binding. GSK3 (among other proteins) phosphorylates the C-terminus of JUN leading to a decrease in JUN-DNA binding and thus, a decrease in AP-1 activity. ERK activates JUN by phosphorylating p70 S6 which in turn phosphorylates and inactivates GSK3. This indirectly leads to the activation of JUN through the dephosphorylation of the C-terminal phosphates. Alternatively, activated JNK proteins translocate to the nucleus where they phosphorylate the N-terminus of JUN [243, 244].

Our interest in JUN comes from its regulation by the MAPK pathway. This pathway is activated downstream of KIT signaling and could provide a source of crosstalk between the KIT and calcineurin pathways. We previously found that KIT inhibitors such as dasatinib and imatinib were able to modulate NFAT-dependent reporter activity in P815 cells suggesting a point of crosstalk between KIT and NFAT

signaling pathways (see Chapter 1). We hypothesized that inhibition of NFAT and an unknown binding partner could account for the synergy we see in KIT-mutant mast cells following simultaneous inhibition of KIT and NFAT pathways. To explain this synergy we proposed the following model:

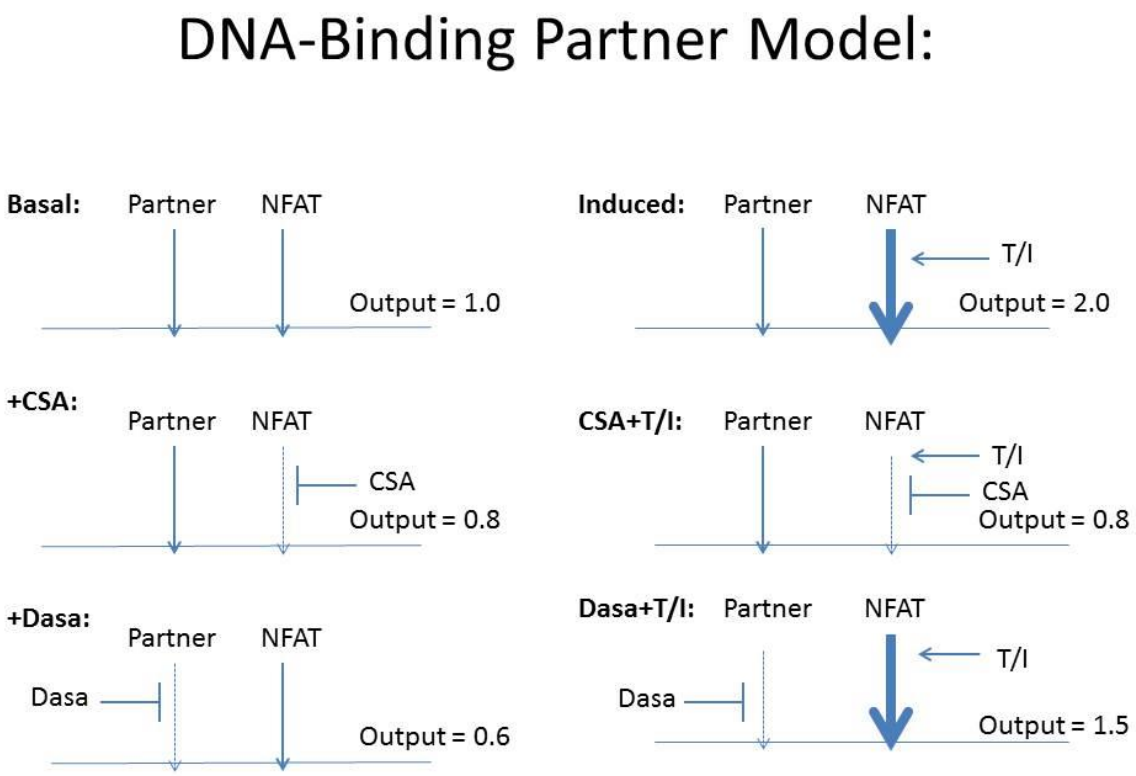

Figure 35 – DNA-binding partner model. Proposed model for an unknown NFAT-DNA binding partner that could account for the observed synergy and NFAT-reporter activity seen following treatment with CNPI, KIT TKI, or a combination of both.

In the basal scenario (untreated cells) both NFAT and the unknown binding partner bind DNA and drive NFAT-dependent transcriptional activity. In the induced scenario, cells are exposed to TPA and ionomycin (T/I) to induce calcium influx. Theoretically this should induce NFAT-dependent transcriptional activity, and it does, however we only see a 2-fold increase in the NFAT binding to DNA in the NFAT-DNA

ELISA assay (Figure 41, left) and a similar increase in the COX2-luciferase reporter system (Figure 42, right). (For more information on the NFAT-DNA binding assay please see Chapter 4. Briefly, the NFAT-DNA binding assay measures NFAT2 binding to GGAAA sequences which coat the wells of the ELISA plate.) We did see a significant increase in luciferase readout from the NFAT-P815 reporter cell line following treatment with T/I (Ch 2, Figure 11), but this drastic increase is unique to this particular reporter system and has not been seen in any other reporter system we have used. The drastic increase in NFAT activity has also not been reflected in data from the NFAT-DNA binding assay, or immunoblotting experiments in any KIT-mutant mast cell line tested to date. For example, exposing cells to T/I does not result in significant translocation of NFAT to the nucleus or further dephosphorylation (Figure 42). As illustrated in the DNA-binding partner model, T/I treatment leads to an increase in NFAT activity for a total output of 2.0.

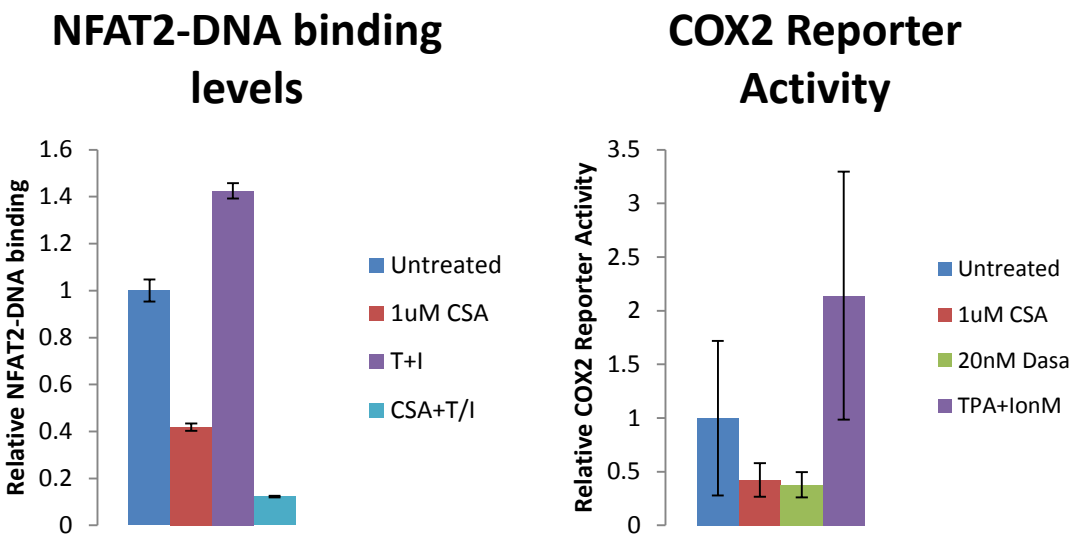

Figure 36 – Confirmation of NFAT-reporter results in other systems. A transfectable COX2 reporter system was transfected into P815 cells. Treatment with CSA, dasatinib, or TPA+IonM shows similar reporter activity to that of the NFAT-reporter system with respect to general trend. However, the magnitude of the reporter increase following treatment with TPA+IonM is much less in the COX2-reporter than the NFAT-reporter (left). An NFAT2-DNA binding ELISA assay performed on P815 cells shows a decrease in NFAT binding following CSA treatment; and an increase in NFAT binding following TPA+IonM treatment. This increase is blocked by pre-treatment with CSA (right).

Treating with 1uM CSA in the basal scenario decreased NFAT-dependent activity, but does not affect the unknown binding partner. Treatment with 1uM CSA blocks NFAT activation, resulting in a 30-50% decrease in NFAT-dependent activity as seen in the NFAT-P815 reporter system or the COX2-P815 reporter system (Figure 41), but has no effect on the binding partner. This inactivation of NFAT can also be monitored with immunoblotting which reveals a translocation of NFAT from the nucleus to the cytoplasm following 1uM CSA treatment. This is accompanied by a shift from the lower unphosphorylated to the upper highly phosphorylated band. While CSA appears to cause a significant change in NFAT localization and phosphorylation we only see a 20% decrease in NFAT-dependent reporter activity. This could be due to other transcription factors binding to our reporter constructs, or NFAT-DNA binding sites could

be so highly saturated in the nucleus that removing >50% of NFAT from the nucleus only causes a modest decrease in overall NFAT transcriptional activity. Either way, the effects of 1uM CSA on NFAT activity is sufficient to synergize with dasatinib and kill KIT-mutant mast cells.

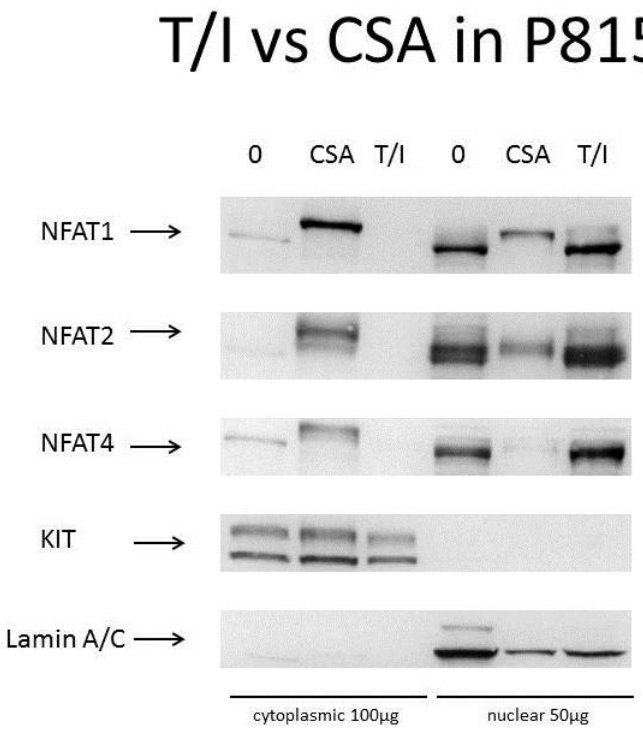

Figure 37 – NFAT response to CNPI inhibition and calcium activation. Fractionation of P815 cells reveals nearly 100% activation of NFAT species as assessed by nuclear localization. Treatment with TPA+IonM causes nuclear translocation of remaining NFAT protein. KIT and Lamin A/C are shown as cytoplasmic and nuclear loading controls, respectively.

In the induced scenario, pre-treatment of P815 cells with 1uM CSA followed by treatment with T/I blocks any increase in NFAT activity that would have resulted from T/I alone. This is because CSA inhibits calcineurin which is downstream of calcium signaling.

Finally, treatment of P815 cells in the basal scenario with 20nM dasatinib causes an ~40-60% decrease in NFAT transcriptional activity; however we do not see a corresponding decrease in NFAT-DNA binding activity nor a translocation of NFAT into the cytoplasm, nor a change in NFAT phosphorylation status (Figures 41, 12). This suggests to us that dasatinib inhibition is not acting through NFAT, but instead through an unknown cooperative DNA binding partner.

Data from the induced scenario supports this hypothesis. If dasatinib were acting though the same calcium/calcineurin/NFAT pathway as CSA we would expect to see a similar block of T/I effect when cells were pre-treated with dasatinib. However, pre-treatment of P815 cells with dasatinib does not block this increase (Ch 2, Figure 11). Although we see partial inhibition of the T/I increase, dasatinib is not exerting all of its effect on NFAT-dependent signaling through the same calcium/calcineurin/NFAT pathway. This hypothesis is further supported by immunoblotting data which reveal that increasing doses of dasatinib have no effect on NFAT phosphorylation or subcellular localization (Ch 2, Figure 12). Overall these data support the existence of an unknown cooperative binding partner that affects NFAT-dependent transcriptional activity by modulating the impact of NFAT rather than modulating the activation of NFAT itself.

To investigate whether JUN could account for the observed synergy and NFAT-dependent reporter data, we tested whether JUN interacts with NFAT in P815 cells. Cells were fractionated and proteins from the cytoplasmic and nuclear fractions were immunoprecipitated using JUN-agarose conjugated beads overnight. Samples were separated on a Western blot, and transferred to nitrocellulose membrane. The membrane was probed for NFAT2 and JUN. As expected, I saw no interaction between JUN and NFAT in the cytoplasm, despite the presence of both proteins. I did however,

see increased interaction between NFAT and JUN as the amount of nuclear lysate was increased (Figure 43A).

Next, I determined whether CSA and/or dasatinib interfered with this interaction. P815 cells were treated with 1uM CSA or 20nM dasatinib, fractionated, and immunoprecipitated using JUN-agarose conjugated beads. The membrane was probed for NFAT2 (Figure 43B). As expected, 1uM CSA shifts NFAT2 into the cytoplasm of the input sample (lane 2) and we did not see any interaction between NFAT and JUN in the cytoplasm of the IP samples (lanes 4-6). Also, treatment with dasatinib appears to decrease cytoplasmic JUN and to a lesser degree, nuclear JUN (lanes 3,12). In the nucleus, we see interaction between NFAT and JUN in untreated P815 cells (lane 7) which is decreased following CSA treatment (lane 8). NFAT:JUN interaction does not appear to be affected by dasatinib treatment, however the beads may have been saturated, and unable to reflect a decrease in JUN. Next, I repeated the experiment from Figure 43B and added a combination treatment lane so determine whether combination treatment was required to abolish JUN:NFAT interaction in the nucleus (Figure 43C). This experiment confirmed that treatment with dasatinib (or combination) decreased nuclear JUN protein levels. Again, this was not reflected in the lysates that underwent IP, and I suspect the beads were saturated so the changes in nuclear JUN protein levels were not detectable. This would also explain why treatment with dasatinib does not modulate NFAT:JUN interaction. I would need to repeat this experiment and titrate down the amount of JUN protein that I use until I can see appropriate response of nuclear JUN to dasatinib or combination treatment. Only then would I be able to determine whether NFAT:JUN interaction was disrupted by combination therapy.

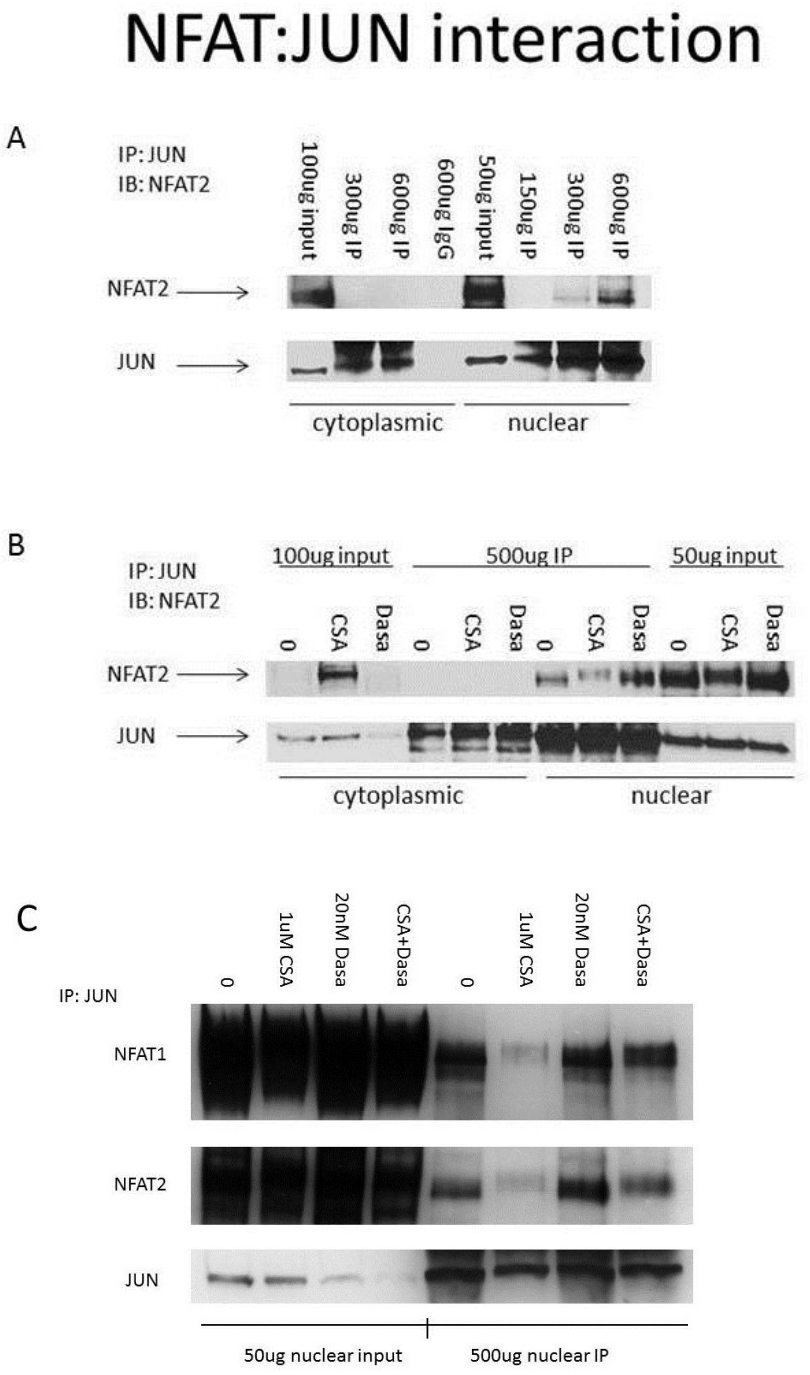

Figure 38 – NFAT and JUN interaction in P815 cells. Co-IP in P815 cells reveals interaction between NFAT and JUN in nuclear lysates. A) Blot shows that increasing JUN IP (ug) leads to increased NFAT2 detection via IB in nuclear lysates. B) Blot shows cytoplasmic and nuclear lysates following JUN IP. Treatment with CSA or dasatinib does not appear to affect NFAT:JUN interaction. C) P815 cells were treated with CSA, dasatinib, or a combination of the two. Nuclear lysates were IP'd for JUN. JUN IP appears to be saturated and may not reflect true changes in nuclear protein interactions.

I wanted to modulate JUN activity through pharmacologic inhibition, so we obtained a reported AP-1 inhibitor called SR11302. I have not been able to confirm its activity through immunoblotting, i.e. nuclear JUN levels and p-JUN levels are unaffected, but I did try SR11032 in combination with the NFAT inhibitor THPB. Briefly, P815 cells were treated with increasing doses of SR11302 alone or in combination with 5nM THPB. Cell viability was measured with Cell Titer-Glo and graphed on figure 44. There was a modest effect of combining THPB with SR11032, however these data represent a single experiment and confirmatory experiments were not able to be run. I repeated the same experiment with 1uM CSA and SR11302 and observed no combination effect (data not shown).

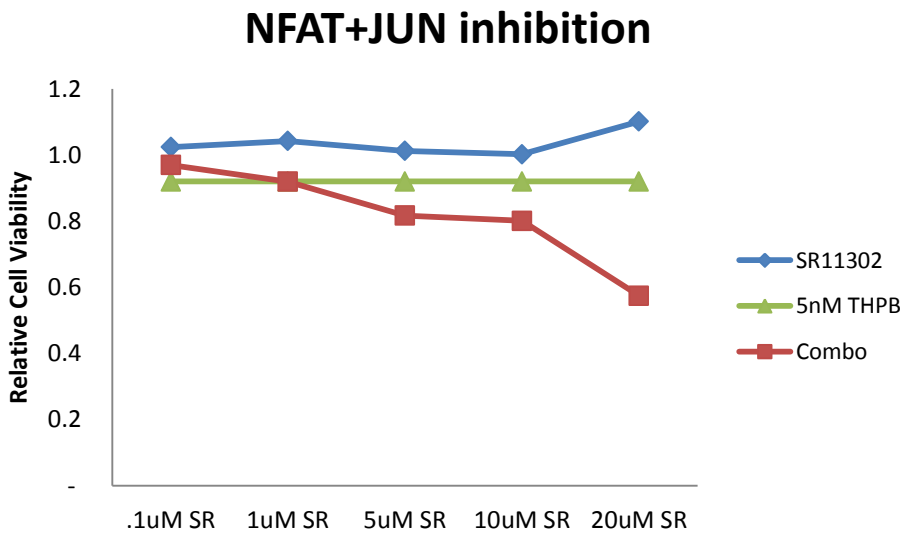

Figure 39 – Combining an NFAT inhibitor and an AP-1 inhibitor in P815 cells. P815 cells were treated with an NFAT specific inhibitor (THPB) and an AP-1 inhibitor (SR11302) for 48 hours and cell viability was measured. This combination only shows an effect at high concentrations of SR11302 (10-20uM).

To support our hypothesis that JUN may be mediating the observed synergy is the fact that dasatinib treatment led to a 50% decrease in JUN transcript levels as well as a similar decrease in nuclear protein levels (JUN is primarily localized to the nucleus in untreated P815 cells). Furthermore, combination treatment of 10nM dasatinib plus 1uM CSA led to a further decrease in nuclear JUN protein levels (data not shown).

Overall there appear to be both confirmatory and contradictory data on our hypothesis that JUN is playing a role in the observed synergy. Extensive further testing is needed to confirm or deny a role of JUN in the synergy between KIT and NFAT inhibitors in KIT-mutant mast cells.

Chapter 6: Discussion, Future Directions, Conclusions

6.1 Discussion

The goal of this thesis work was to establish whether a CNPI would combine with a KIT TKI to increase cell death in KIT-mutant mast cells. Once we confirmed that this combination treatment was effective in six different KIT-mutant mast cell lines, we used an RNA-Seq approach to identify novel combination therapies. This strategy revealed that the JAK-STAT pathway was significantly down-regulated following combination treatment with CSA and dasatinib in the P815 cell line. Further analysis revealed that combining a JAK inhibitor with a KIT inhibitor was as effective as CSA/dasatinib at decreasing long term cell viability and increasing apoptosis.

CSA and dasatinib synergistically inhibit Kit-mutant mast cells: Our first hypothesis was that a CNPI/KIT TKI combination would work in KIT-mutant cell lines based on the results of a similar combination in cell line models of BCR-ABL+ CML. We tested this hypothesis in six different KIT-mutant mast cell lines. In each cell line we found that combining a CNPI with a KIT TKI led to a synergistic decrease in cellular viability as measured by ATP. We further found that these combinations led to increases in caspase activity in the KIT-mutant cell lines. Finally, we found that long term treatment of the P815 cell line with CSA/dasatinib lead to a significant decrease in the replating efficiency of these cells. This finding laid the groundwork for the rest of my thesis research which further characterized this and other combination therapies in KIT-mutant cancer models.

NFAT is constitutively active in KIT-mutant mast cells: Following the discovery that CNPIs combined with KIT TKIs, we hypothesized that NFAT was mediating the

observed synergy. We fractionated KIT-mutant mast cells and determined that NFAT was constitutively active in P815, HMC1.1, HMC1.2, and RBL2H3 cells based on NFAT localization and phosphorylation in untreated cells. We also confirmed these results with IHC in HMC1.2 and P815 cell lines. This discovery was important because it explained why inhibiting calcineurin would have an impact on cellular viability. This also represents the first time that constitutive activation of NFAT has been reported in KIT-mutant cancer models.

NFAT-dependent transcriptional activity responds to both CNPIs and KIT inhibitors: To investigate whether constitutive NFAT activity was a mechanism of mutated NFAT or dyregulated upstream signaling, we established cell lines that stabley expressed an NFAT-dependent reporter with a luciferase read-out. We found the NFAT-P815 cell line exhibited significant basal signaling which we expected from constitutively active NFAT signaling. Next, we found that NFAT-dependent transcriptional activity decreased following treatment with CSA so we concluded that NFAT activity was not compromised in anyway, and that an upstream mechanism was responsible for the constitutive activation of NFAT rather than mutations within NFAT that were causing its activation. Finally, with this reporter system, we found that NFAT-dependent reporter activity was modulated following treatment with KIT inhibitors. This suggested a source of crosstalk between KIT and NFAT signaling pathways which could explain the efficacy of this combination in KIT-mutant cell lines.

KIT affects NFAT activity independent of calcineurin signaling pathway: In P815 cells we found that treatment with TPA plus ionomycin led to an increase in NFAT-dependent reporter activity. This increase was completely blocked by calcineurin, as we would expect. However, KIT inhibitors only partially inhibited this increase, suggesting that KIT affects NFAT activity through an additional mechanism. These results were

confirmed in an NFAT-DNA binding ELISA assay, where pretreatment with CSA blocked increases in DNA-NFAT binding, resulting from TPA+IonM but dasatinib did not. Finally we used immunoblotting to investigate whether KIT was affecting NFAT activity. We found that dasatinib had no effect on NFAT localization or phosphorylation. Together these results suggested that these two compounds were converging to affect NFAT signaling through two separate pathways, rather than hitting the same pathway at different points. We hypothesized that KIT was acting through an unknown DNA-binding partner such as AP-1 (see Chapter 5.3).

RNA-Seq study reveals downstream consequences of combination therapy in P815 cells: To identify the downstream consequences of combination therapy we used RNA-Seq. Comparing untreated P815 cells to cells treated with 1uM CSA, 20nM dasatinib, or a combination of the two we found that the JAK-STAT pathway was significantly down-modulated following combination therapy, more so than with either mono-therapy alone. To follow-up on this finding we tested novel combinations between KIT-inhibitors and JAK, MYC, and CCND inhibitors. We found that the JAK inhibitor CYT387, which is currently being developed to treat myelofibrosis, was just as effective in combination with dasatinib as CSA with respect to decreased cellular viability, increased apoptosis, and decreased long-term replating efficiency. This finding represents an alternative combination treatment to test *in vivo* should the CNPI+KIT TKI combination be found to cause significant adverse side-effects.

6.2 Future Directions

There are a number of areas for follow-up research on my thesis work. I am particularly hopeful that the novel combination therapies we have identified will be advanced to *in vivo* studies in mice to validate their potential efficacy in treating KIT-mutant mast diseases. In vivo studies will be an important first step in evaluating the pharmacodynamics and pharmacokinetics of this drug combination in a living organism. These studies will allow us to understand the toxicity of these drug combinations, as well as possible drug-drug interactions and drug metabolism. Experiments in mice will also enable us to study how the tumor microenvironment affects the efficacy of combination therapy due to the presence of stromal cells. This microenvironment contains immune cells, fibroblasts, and signaling molecules that may or may not be present in our *in vitro* models. Finally, studying these drugs *in vivo* will allow us to extend our disease persistence studies to determine whether combination therapy affects tumor stem cells.

In addition to *in vivo* studies with our combination therapies, it would be informative to validate the RNA-Seq results from the P815 cell line by expanding the original study to include other KIT-mutant mast cell lines such as the HMCs and RBL2H3s. There are also a number of other cancer cell line models that appear to respond to combination therapy of a CNPI plus a relevant kinase inhibitor. Expanding these preliminary studies to include NFAT immunoblotting and apoptosis studies would serve as a good starting point to establish whether this combination strategy will work in other cancer models. Finally, in an effort to identify the source of crosstalk between KIT and calcineurin/NFAT signaling pathways, more work is needed to characterize the interaction between NFAT and AP-1 in KIT-mutant mast cells.

My thesis work focused on the underlying molecular signaling mechanisms behind synergy and on how we can target unique characteristics of KIT-mutant cancer cells to

kill them. Although I was able to characterize the KIT TKI plus CNPI combination as well as KIT TKIs plus JAK, MYC, or CCND inhibitor combinations *in vitro*, I am unsure how these combinations will perform in animal models as it is universally acknowledged that what occurs in vitro is not always indicative of what will happen in a whole organism. The next step in this research is to test these treatment combinations in mice. Such studies would not only serve to validate or invalidate the efficacy of these combinations, but may also shed light on the potential deleterious effects of chronic CNPI administration, such as renal/kidney dysfunction or diabetogenesis. Fortunately the P815 cell line which I have used for a majority of my thesis work is syngeneic with DBA/2 mice and establishes aggressive systemic mastocytosis/mast cell leukemia following injection into the retro-orbital sinus. In this model, a rapid and fatal expansion of mastocytomas occurs within weeks [245, 246]. This mouse model would allow us to test each of the combinations of interest including dasatinib+CSA, dasatinib+CYT397, and dasatinib+palbociclib. These studies would allow for head-to-head comparison of our top novel combination candidates against the original dasatinib+CSA combination.

Another crucial step to advancing the RNA-Seq study would be to expand the study to include additional KIT-mutant cancer cell lines. We recognize that in using the P815 cell line as a representative of KIT-mutant mast cell disease we may find downstream targets that are unique to this particular cell line and not a true reflection of the phenomenon we see in all KIT-mutant mast cell lines. Additionally, there are a number of targets that we identified in the first RNA-Seq screen in the P815 cell line that we have not had a chance to validate yet. Expanding the studies to include the HMC1.2 and RBL2H3 cell line would allow us to compare the top hits across cell types and eliminate targets that were unique to an individual cell line. Not only would this focus our potential follow-up targets, but it would increase the likelihood of identifying novel combinations

that would work across an array of KIT-mutant mast cell diseases. I am hopeful that future funding will enable us to continue this type of targeted screening in KIT-mutant cancers.

Another application of the RNA-Seq screening method is to test other cell models that are found to have constitutively active NFAT and that respond to combination therapy. I have already identified a number of other cell lines that either contain constitutively active NFAT and/or respond to CNPI plus a kinase inhibitor *in vitro.* These promising leads are discussed in Chapter 5.1 and include the MC/9, MOLM-13/14, MV-4-11, and EOL-1 cell lines. It is possible that targeting NFAT may be a universal strategy against cancers with constitutively active NFAT. The first step in addressing this possibility is to establish whether NFAT is constitutively active in these cell lines. Next we would want to perform similar cell viability and apoptosis assays to characterize the response to combination therapy. Finally, an RNA-Seq method, similar to the one we used in the P815 cell line (Chapter 3) could be used to find novel combination therapy targets or crucial signaling pathways.

Aside from studying the downstream consequences of combination, there are a number of unanswered questions upstream of combination therapy, such as the point of crosstalk between the inhibitory targets. One question that I tried to address, unsuccessfully, was the upstream mechanism leading to constitutive NFAT signaling. We were unable to implicate Wnt/Fzd signaling in the activation of NFAT. Implication of an upstream target that leads to NFAT activation could be elucidated through the use of an RNAi type screen. However, unlike current RNAi screens, cell viability would not be the readout, but rather, NFAT phosphorylation. Successful RNAi of the upstream target(s) would result in increased NFAT phosphorylation. This could be read out with a cell-based ELISA assay. The P815 cell line would require a lentiviral transduction

platform to deliver the shRNA particles. Also, the RNAi assay would need to be compatible with the ELISA readout portion of the screen. This may mean that the P815 cells need to be lysed before being transferred to the ELISA plate since they are adherent cells. This type of study may require the advancement of RNAi and ELISA screening technologies before it could be used in this capacity.

The other upstream question surrounding the success of the NFAT/KIT combination treatment is the point of crosstalk between these two pathways. I began to investigate the interactions between AP-1 and NFAT through the use of co-immunoprecipitation. I was able to determine that these two transcription factors interact within the nucleus of P815 cells, and that this interaction can be modulated through treatment with CSA or dasatinib (Chapter 6). However, I was not able to determine whether this interaction was mediating the observed synergy. It was suggested during one of my thesis advisory committee meetings that I try using a constitutively active form of AP-1 to determine whether AP-1 inhibition was required for synergy. I was unable to locate a suitable clone for this purpose. Alternatively we could use a constitutively active form of JNK2 which has been shown to lead to increased phosphorylation of JUN [247]. There is a commercially available clone which contains two Thr/Tyr→ Ala/Phe mutations which renders JAK2 constitutively active. Transduction of this clone into KIT-mutant mast cells should lead to diminished synergy following combination treatment. JAK2 has alternate substrates such as ATF2 and ELK1, so addition testing would be required to implicate JUN involvement in the synergy. This could be accomplished through the use of transient lentiviral knockdown of JUN with an shRNA. This knockdown should sensitize cells to CSA treatment in the same way that calcineurin knockdown sensitized P815 cells to dasatinib treatment.

6.3 Conclusion

It is well recognized in the field of cancer biology that targeted kinase monotherapies are limited by cellular mechanisms that confer drug resistance and cellular persistence in the face of prolonged treatment. In an effort to overcome these limitations many scientists are searching for combination therapies to more effectively reduce or eliminate cancer cells before they can adopt alternative signaling mechanisms or mutate the original drug target (e.g. secondary KIT mutations). Development of these novel combination therapies relies heavily on unbiased screens such as shRNA or RNA-Seq screens.

I utilized both of these methods to design the combination therapies described in this thesis, which are now advancing to *in vivo* testing. Luckily I was able to utilize the results of a previously reported siRNA screen in BCR-ABL+ K562 cells to generate my initial hypothesis that, given parallels in BCR-ABL and KIT signaling, combining a KIT TKI and a CNPI would be effective in KIT-mutant cells. I quickly confirmed this hypothesis in six distinct KIT-mutant mast cell lines. I was less convinced of the efficacy of this combination in KIT-mutant GIST cell lines, and due to a lack of suitable antibodies, I was unable to determine NFAT activation status in the GIST cell lines. As a result, I focused the rest of my studies on KIT-mutant, NFAT active mast cells.

Further examination of these cell lines not only revealed constitutive NFAT signaling, but also enhanced sensitivity of cells to a KIT TKI when they were co-treated with a CNPI. Constitutive NFAT activation provided an explanation for the efficacy of the CNPI plus KIT TKI combination in KIT-mutant mast cells. Additionally, the sensitivity of NFAT-dependent transcriptional activity to KIT inhibition suggested a point of crosstalk between KIT and NFAT signaling pathways – again strengthening the mechanism behind the synergy. NFAT signaling is known to be critical to mast cell development and

survival, so perhaps co-targeting a mast cell specific pathway and an acquired (KIT) signaling pathway is enough to cripple these cells in culture.

Unfortunately the long-term use of CNPI's (CSA and FK506) in the context of organ transplantation has been associated with adverse side effects. It is unclear whether similar side-effects would be experienced in a mast cell leukemia context, or whether chronic therapy would be necessary. However, we chose to use an RNA-Seq approach to identify novel targets that could replace calcineurin in a KIT TKI-based combination therapy approach. Not only did this eliminate concerns over the use of a CNPI in cancer patients, but it generated additional novel combinations for testing *in vivo.*

We used the RNA-Seq screen as opposed to an siRNA screen for a number of reasons. First and foremost, siRNA screens rely on transfection of siRNAs into target cells. Our P815 cell line is not amenable to transfection. Also, the discovery that NFAT was mediating synergy pointed toward modulation of gene expression – which is measured directly by RNA-Seq. For these and other reasons we designed and optimized RNA-Seq experiments to identify downstream targets of KIT TKI and CNPI combination therapy.

As described in Chapter 3, the RNA-Seq studies identified the JAK-STAT pathway and its components as targets for combination therapy with a KIT TKI. Follow-up studies confirmed that knockdown of JAK1 or JAK2 sensitized KIT-mutant mast cells to the effects KIT TKIs. The next step is to test the original CNPI+KIT TKI head-to –head against the new JAK and CCND combinations *in vivo.*

We are also expanding our efforts to include other KIT-mutant mast cell lines as well as other KIT-mutant GIST cell lines. We believe this RNA-Seq approach could be used to generate hypotheses in any kinase-driven cancer model. This strategy could accelerate

the identification of novel targets, the design of novel combination therapies, and *in vivo* testing. Successful completion of *in vivo* studies would hopefully lead to the design and implementation of clinical studies.

Although the main focus of this work was to develop better treatment options for patients, I was also able to determine that constitutively active NFAT is not only a characteristic of KIT-mutant mast cells, but may be a vital target to go after in mast cell diseases. As the NFAT field evolves it will be interesting to see whether NFAT activation is a common feature of many or most kinase mutant human cancers.

Reference List

[1] Broudy VC. Stem cell factor and hematopoiesis. Blood 1997;90:1345-64.

[2] Heinrich MC, Blanke CD, Druker BJ, Corless CL. Inhibition of KIT tyrosine kinase activity: a novel molecular approach to the treatment of KIT-positive malignancies. J Clin Oncol 2002;20:1692-703.

[3] Lennartsson J, Ronnstrand L. The stem cell factor receptor/c-Kit as a drug target in cancer. Curr Cancer Drug Targets 2006;6:65-75.

[4] Dexter TM, Moore MAS. In vitro duplication and 'cure' of haemopoietic defects in genetically anaemic mice. Nature 1977;269:412-4.

[5] Lennartsson J, Jelacic T, Linnekin D, Shivakrupa R. Normal and oncogenic forms of the receptor tyrosine kinase kit. Stem Cells 2005;23:16-43.

[6] Craig FE, Foon KA. Flow cytometric immunophenotyping for hematologic neoplasms. Blood 2008;111:3941-67.

[7] Turner MS, Goldsmith JD. Best practices in diagnostic immunohistochemistry: spindle cell neoplasms of the gastrointestinal tract. Arch Pathol Lab Med 2009;133:1370-4.

[8] Miettinen M, Lasota J. KIT (CD117): a review on expression in normal and neoplastic tissues, and mutations and their clinicopathologic correlation. Appl Immunohistochem Mol Morphol 2005;13:205-20.

[9] Blay JY. A decade of tyrosine kinase inhibitor therapy: Historical and current perspectives on targeted therapy for GIST. Cancer Treat Rev 2010.

[10] Piccaluga PP, Rondoni M, Paolini S, Rosti G, Martinelli G, Baccarani M. Imatinib mesylate in the treatment of hematologic malignancies. Expert Opin Biol Ther 2007;7:1597-611.

[11] Andersson J, Bumming P, Meis-Kindblom JM, Sihto H, Nupponen N, Joensuu H, et al.. Gastrointestinal stromal tumors with KIT exon 11 deletions are associated with poor prognosis. Gastroenterology 2006;130:1573-81.

[12] Hou YY, Grabellus F, Weber F, Zhou Y, Tan YS, Li J, et al.. Impact of KIT and PDGFRA gene mutations on prognosis of patients with gastrointestinal stromal tumors after complete primary tumor resection. J Gastrointest Surg 2009;13:1583-92.

[13] Corless CL, Ballman KV, Antonescu C, et al.. Relation of tumor pathologic and molecular features to outcome after surgical resection of localized primary gastrointestinal stromal tumor (GIST): Results of the intergroup phase III trial ACOSOG Z9001. 28 ed. 2010. p. 15s.

[14] Heinrich MC, Corless CL, Demetri GD, Blanke CD, von Mehren M, Joensuu H, et al.. Kinase mutations and imatinib response in patients with metastatic gastrointestinal stromal tumor. J Clin Oncol 2003;21:4342-9.

[15] Debiec-Rychter M, Dumez H, Judson I, Wasag B, Verweij J, Brown M, et al.. Use of c-KIT/PDGFRA mutational analysis to predict the clinical response to imatinib in patients with advanced gastrointestinal stromal tumours entered on phase I and II studies of the EORTC Soft Tissue and Bone Sarcoma Group. Eur J Cancer 2004;40:689-95.

[16] Debiec-Rychter M, Sciot R, Le CA, Schlemmer M, Hohenberger P, Van Oosterom AT, et al.. KIT mutations and dose selection for imatinib in patients with advanced gastrointestinal stromal tumours. Eur J Cancer 2006;42:1093-103.

[17] Heinrich MC, Owzar K, Corless CL, Hollis D, Borden EC, Fletcher CD, et al.. Correlation of kinase genotype and clinical outcome in the North American Intergroup Phase III Trial of imatinib mesylate for treatment of advanced gastrointestinal stromal tumor: CALGB 150105 Study by Cancer and Leukemia Group B and Southwest Oncology Group. J Clin Oncol 2008;26:5360-7.

[18] Comparison of two doses of imatinib for the treatment of unresectable or metastatic gastrointestinal stromal tumors: a meta-analysis of 1,640 patients. J Clin Oncol 2010;28:1247-53.

[19] Ma Y, Carter E, Wang X, Shu C, McMahon G, Longley BJ. Indolinone derivatives inhibit constitutively activated KIT mutants and kill neoplastic mast cells. J Invest Dermatol 2000;114:392-4.

[20] Buchdunger E, Cioffi CL, Law N, Stover D, Ohno-Jones S, Druker BJ, et al.. Abl protein-tyrosine kinase inhibitor STI571 inhibits In vitro signal transduction mediated by c-Kit and platelet-derived growth factor receptors. J Pharmacol Exp Ther 2000 2000;295:139-45.

[21] Heinrich MC, Griffith DJ, Druker BJ, Wait CL, Ott KA, Zigler AJ. Inhibition of c-kit receptor tyrosine kinase activity by STI 571, a selective tyrosine kinase inhibitor. Blood 2000;96:925-32.

[22] Tuveson D, Willis N, Jacks T, Griffin J, Singer S, Fletcher C, et al.. STI571 inactivation of the gastrointestinal stromal tumor c-KIT oncoprotein: biological and clinical implications. Oncogene 2001;20:5054-8.

[23] Abrams TJ, Lee LB, Murray LJ, Pryer NK, Cherrington JM. SU11248 Inhibits KIT and Platelet-derived Growth Factor Receptor beta in Preclinical Models of Human Small Cell Lung Cancer. Mol Cancer Ther 2003;2:471-8.

[24] Gotlib J, Berube C, Growney JD, Chen CC, George TI, Williams C, et al.. Activity of the tyrosine kinase inhibitor PKC412 in a patient with mast cell leukemia with the D816V KIT mutation. Blood 2005;106:2865-70.

[25] Schittenhelm MM, Shiraga S, Schroeder A, Corbin AS, Griffith D, Lee FY, et al.. Dasatinib (BMS-354825), a Dual SRC/ABL Kinase Inhibitor, Inhibits the Kinase Activity of Wild-Type, Juxtamembrane, and Activation Loop Mutant KIT Isoforms Associated with Human Malignancies. Cancer Research 2006;66:473-81.

[26] Shah NP, Lee FY, Luo R, Jiang Y, Donker M, Akin C. Dasatinib (BMS-354825) inhibits KITD816V, an imatinib-resistant activating mutation that triggers neoplastic growth in most patients with systemic mastocytosis. Blood 2006;108:286-91.

[27] Beadling C, Jacobson-Dunlop E, Hodi FS, Le C, Warrick A, Patterson J, et al.. KIT gene mutations and copy number in melanoma subtypes. Clin Cancer Res 2008;14:6821-8.

[28] Jiang X, Zhou J, Yuen NK, Corless CL, Heinrich MC, Fletcher JA, et al.. Imatinib Targeting of KIT-Mutant Oncoprotein in Melanoma. Clinical Cancer Research 2008;14:7726-32.

[29] DeMatteo RP, Heinrich MC, el-Rifai W, Demetri GD. Clinical management of gastrointestinal stromal tumors: Before and after STI-571. Hum Pathol 2002;33:466-77.

[30] Heinrich MC, Corless CL, Blanke CD, Demetri GD, Joensuu H, Roberts PJ, et al.. Molecular Correlates of Imatinib Resistance in Gastrointestinal Stromal Tumors. Journal of Clinical Oncology 2006;24:4764-74.

[31] Heinrich MC, Maki RG, Corless CL, Antonescu CR, Harlow A, Griffith D, et al.. Primary and Secondary Kinase Genotypes Correlate With the Biological and Clinical Activity of Sunitinib in Imatinib-Resistant Gastrointestinal Stromal Tumor. Journal of Clinical Oncology 2008;26:5352-9.

[32] Verstovsek S, Tefferi A, Cortes J, O'Brien S, Garcia-Manero G, Pardanani A, et al.. Phase II study of dasatinib in Philadelphia chromosome-negative acute and chronic myeloid diseases, including systemic mastocytosis. Clin Cancer Res 2008;14:3906-15.

[33] Vega-Ruiz A, Cortes JE, Sever M, Manshouri T, Quintas-Cardama A, Luthra R, et al.. Phase II study of imatinib mesylate as therapy for patients with systemic mastocytosis. Leuk Res 2009;33:1481-4.

[34] Wyman K, Atkins MB, Prieto V, Eton O, McDermott DF, Hubbard F, et al.. Multicenter Phase II trial of high-dose imatinib mesylate in metastatic melanoma: significant toxicity with no clinical efficacy. Cancer 2006;106:2005-11.

[35] Carvajal R.D., Chapman PB, Wolchok JD, Cane L, Teitcher JB, Lutzky J, et al.. A phase II study of imatinib mesylate (IM) for patients with advanced melanoma harboring somatic alterations of KIT. J Clin Oncol 2009;27:abstr 9001.

[36] Hodi FS, Friedlander P, Corless CL, Heinrich MC, Mac RS, Kruse A, et al.. Major response to imatinib mesylate in KIT-mutated melanoma. J Clin Oncol 2008;26:2046-51.

[37] Flanagan JG, Leder P. The kit ligand: A cell surface molecule altered in steel mutant fibroblasts. Cell 1990;63:185-94.

[38] Zsebo KM, Wypych J, McNiece IK, Lu HS, Smith KA, Karkare SB, et al.. Identification, purification, and biological characterization of hematopoietic stem cell factor from buffalo rat liver-conditioned medium. Cell 1990;63:195-201.

[39] Martin FH, Suggs SV, Langley KE, Lu HS, Ting J, Okino KH, et al.. Primary structure and functional expression of rat and human stem cell factor DNAs. Cell 1990;63:203-11.

[40] Anderson DM, Lyman SD, Baird A, Wignall JM, Eisenman J, Rauch C, et al.. Molecular cloning of mast cell growth factor, a hematopoietin that is active in both membrane bound and soluble forms. Cell 1990;63:235-43.

[41] Zsebo KM, Williams DA, Geissler EN, Broudy VC, Martin FH, Atkins HL, et al.. Stem cell factor is encoded at the SI locus of the mouse and is the ligand for the c-kit tyrosine kinase receptor. Cell 1990;63:213-24.

[42] Huang E, Nocka K, Beier DR, Chu TY, Buck J, Lahm HW, et al.. The hematopoietic growth factor KL is encoded by the SI locus and is the ligand of the c-kit receptor, the gene product of the W locus. Cell 1990;63:225-33.

[43] Tsai M, Chen RH, Tam SY, Blenis J, Galli SJ. Activation of MAP kinases, pp90rsk and pp70-S6 kinases in mouse mast cells by signaling through the c-kit receptor tyrosine kinase or Fc-¦RI: rapamycin inhibits activation of pp70-S6 kinase and proliferation in mouse mast cells. Eur J Immunol 1993;23:3286-91.

[44] Deberry C, Mou S, Linnekin D. Stat1 associates with c-kit and is activated in response to stem cell factor. Biochem J 1997;327:73-80.

[45] Linnekin D. Early signaling pathways activated by c-Kit in hematopoietic cells. The International Journal of Biochemistry & Cell Biology 1999;31:1053-74.

[46] Sattler M, Salgia R, Shrikhande G, Verma S, Pisick E, Prasad KVS, et al.. Steel Factor Induces Tyrosine Phosphorylation of CRKL and Binding of CRKL to a Complex Containing c-Kit, Phosphatidylinositol 3-Kinase, and p120CBL. JBC 1997;272:10248-53.

[47] Serve H, Hsu YC, Besmer P. Tyrosine residue 719 of the c-kit receptor is essential for binding of the P85 subunit of phosphatidylinositol (PI) 3-kinase and for c-kit-associated PI 3-kinase activity in COS-1 cells. JBC 1994;269:6026-30.

[48] Berger SA. Signaling pathways influencing SLF and c-kit-mediated survival and proliferation. Immunol Res 2006;35:1-12.

[49] Seger R, Krebs EG. The MAPK signaling cascade. The FASEB Journal 1995;9:726-35.

[50] Chong H, Vikis HG, Guan KL. Mechanisms of regulating the Raf kinase family. Cellular Signalling 2003;15:463-9.

[51] Ferrell JE, Bhatt RR. Mechanistic Studies of the Dual Phosphorylation of Mitogen-activated Protein Kinase. JBC 1997;272:19008-16.

[52] Tang B, Mano H, Yi T, Ihle JN. Tec kinase associates with c-kit and is tyrosine phosphorylated and activated following stem cell factor binding. MCB 1994;14:8432-7.

[53] Joneja B, Chen HC, Seshasayee D, Wrentmore AL, Wojchowski DM. Mechanisms of Stem Cell Factor and Erythropoietin Proliferative Co-signaling in FDC2-ER Cells. Blood 1997;90:3533-45.

[54] Ryan J, Huang H, McReynolds L, Shelburne C, Hu-Li J, Huff T, et al.. Stem cell factor activates STAT-5 DNA binding in IL-3-derived bone marrow mast cells. Experimental Hematology 1997;25:357-62.

[55] Paner G, Silberman S, Hartman G, Micetich K, Aranha G, Alkan S. Analysis of signal transducer and activator of transcription 3 (STAT3) in gastrointestinal stromal tumors. Anticancer Research 2003;23:2253-60.

[56] Ferrag F, Pezet A, Chiarenza A, Buteau H+, Nelson BH, Goffin V, et al.. Homodimerization of IL-2 receptor +¦ chain is necessary and sufficient to activate Jak2 and dowstream signaling pathways. FEBS Letters 1998;421:32-6.

[57] Brizzi MF, Zini MG, Aronica MG, Blechman JM, Yarden Y, Pegoraro L. Convergence of signaling by interleukin-3, granulocyte-macrophage colony-stimulating factor, and mast cell growth factor on JAK2 tyrosine kinase. JBC 1994;269:31680-4.

[58] Weiler SR, Mou S, DeBerry CS, Keller JR, Ruscetti FW, Ferris DK, et al.. JAK2 is associated with the c-kit proto-oncogene product and is phosphorylated in response to stem cell factor. Blood 1996;87:3688-93.

[59] Radosevic N, Winterstein D, Keller JR, Neubauer H, Pfeffer K, Linnekin D. JAK2 contributes to the intrinsic capacity of primary hematopoietic cells to respond to stem cell factor. Experimental Hematology 2004;32:149-56.

[60] Gotoh A, Takahira H, Mantel C, Litz-Jackson S, Boswell HS, Broxmeyer HE. Steel factor induces serine phosphorylation of Stat3 in human growth factor-dependent myeloid cell lines. Blood 1996;88:138-45.

[61] McBride KM, Banninger G, McDonald C, Reich NC. Regulated nuclear import of the STAT1 transcription factor by direct binding of importin-[alpha]. EMBO J 2002;21:1754-63.

[62] Liu L, McBride KM, Reich NC. STAT3 nuclear import is independent of tyrosine phosphorylation and mediated by importin-+¦3. Proc Natl Acad Sci U S A 2005;102:8150-5.

[63] Shin HY, Reich NC. Dynamic trafficking of STAT5 depends on an unconventional nuclear localization signal. J Cell Sci 2013;126:3333-43.

[64] Liang J, Wu Y, Chen B, Zhang W, Tanaka Y, Sugiyama H. The C-Kit Receptor-Mediated Signal Transduction and Tumor-Related Disease. International Journal of Biological Sciences 2013;9:435-43.

[65] Taylor ML, Dastych J, Sehgal D, Sundstrom M, Nilsson G, Akin C, et al.. The Kit-activating mutation D816V enhances stem cell factor co-dependent chemotaxis. Blood 2001;98:1195-9.

[66] Nagata H, Worobec AS, Oh CK, Chowdhury BA, Tannenbaum S, Suzuki Y, et al.. Identification of a point mutation in the catalytic domain of the protooncogene c-kit in peripheral blood mononuclear cells of patients who have mastocytosis with an associated hematologic disorder. Proceedings of the National Academy of Sciences 1995;92:10560-4.

[67] Furitsu T, Tsujimura T, Tono T, Ikeda H, Kitayama H, Koshimizu U, et al.. Identification of mutations in the coding sequence of the proto-oncogene c-kit in a human mast cell leukemia cell line causing ligand-independent activation of c-kit product. J Clin Invest 1993;92:1736-44.

[68] Pardanani A. Systemic mastocytosis in adults: 2012 Update on diagnosis, risk stratification, and management. Am J Hematol 2012;87:401-11.

[69] Tsujimura T, Furitsu T, Morimoto M, Isozaki K, Nomura S, Matsuzawa Y, et al.. Ligand-independent activation of c-kit receptor tyrosine kinase in a murine mastocytoma cell line P-815 generated by a point mutation. Blood 1994;83:2619-26.

[70] Tsujimura T, Furitsu T, Morimoto M, Kanayama Y, Nomura S, Matsuzawa Y, et al.. Substitution of an Aspartic Acid Results in Constitutive Activation of c-kit Receptor Tyrosine Kinase in Rat Tumor Mast Cell Line RBL-2H3. International Archives of Allergy and Immunology 1995;106:377-85.

[71] London CA, Galli SJ, Yuuki T, Hu ZQ, Helfand SC, Geissler EN. Spontaneous canine mast cell tumors express tandem duplications in the proto-oncogene c-kit. Experimental Hematology 1999;27:689-97.

[72] Schwaab J, Schnittger S, Sotlar K, Walz C, Fabarius A, Pfirrmann M, et al.. Comprehensive mutational profiling in advanced systemic mastocytosis. Blood 2013.

[73] Orfao A, Garcia-Montero AsC, Sanchez L, Escribano L. Recent advances in the understanding of mastocytosis: the role of KIT mutations*. Br J Haematol 2007;138:12-30.

[74] von Bubnoff N, Gorantla SHP, Kancha R, Lordick F, Peschel C, Duyster J. The systemic mastocytosis-specific activating mutation D816V can be inhibited by the tyrosine kinase inhibitor AMN107. Leukemia 2005;19:1670-1.

[75] Gleixner KV, Mayerhofer M, Aichberger KJ, Derdak S, Sonneck K, B+¦hm A, et al.. PKC412 inhibits in vitro growth of neoplastic human mast cells expressing the D816V-mutated variant of KIT: comparison with AMN107, imatinib, and cladribine (2CdA) and evaluation of cooperative drug effects. Blood 2006;107:752-9.

[76] Gotlib J, Berub C, Growney JD, Chen CC, George TI, Williams C, et al.. Activity of the tyrosine kinase inhibitor PKC412 in a patient with mast cell leukemia with the D816V KIT mutation. Blood 2005;106:2865-70.

[77] Ustun C, Corless CL, Savage N, Fiskus W, Manaloor E, Heinrich MC, et al.. Chemotherapy and dasatinib induce long-term hematologic and molecular remission in systemic mastocytosis with acute myeloid leukemia with KITD816V. Leukemia Research 2009;33:735-41.

[78] Letard S+, Yang Y, Hanssens K, Palm+¬rini F, Leventhal PS, Gu+¬ry Sp, et al.. Gain-of-Function Mutations in the Extracellular Domain of KIT Are Common in Canine Mast Cell Tumors. Molecular Cancer Research 2008;6:1137-45.

[79] Sabattini S, Frizzon MG, Gentilini F, Turba ME, Capitani O, Bettini G. Prognostic Significance of Kit Receptor Tyrosine Kinase Dysregulations in Feline Cutaneous Mast Cell Tumors. Veterinary Pathology Online 2013.

[80] Longley BJ, Tyrrell L, Lu SZ, Ma YS, Langley K, Ding TG, et al.. Somatic c-KIT activating mutation in urticaria pigmentosa and aggressive mastocytosis: establishment of clonality in a human mast cell neoplasm. Nat Genet 1996;12:312-4.

[81] Piao X, Bernstein A. A point mutation in the catalytic domain of c-kit induces growth factor independence, tumorigenicity, and differentiation of mast cells. Blood 1996;87:3117-23.

[82] Gerbaulet A, Wickenhauser C, Scholten J, Peschke K, Drube S, Horny HP, et al.. Mast cell hyperplasia, B-cell malignancy, and intestinal inflammation in mice with conditional expression of a constitutively active kit. Blood 2011;117:2012-21.

[83] Zappulla JP, Dubreuil P, Desbois S, Letard S, Hamouda NB, Daeron M, et al.. Mastocytosis in mice expressing human Kit receptor with the activating Asp816Val mutation. J Exp Med 2005;202:1635-41.

[84] Valent P. Mastocytosis: a paradigmatic example of a rare disease with complex biology and pathology. Am J Cancer Res 2013;3:159-72.

[85] Klee C, Crouch T, Krinks M. Calcineurin: a calcium- and calmodulin-binding protein of the nervous system. Proc Natl Acad Sci U S A 1979;76:6270-3.

[86] Guerini D. Calcineurin: not just a simple protein phosphatase. Biochem Biophys Res Commun 1997;235:271-5.

[87] Rusnak F, Mertz P. Calcineurin: form and function. Physiol Rev 2000;80:1483-521.

[88] Li H, Rao A, Hogan PG. Interaction of calcineurin with substrates and targeting proteins. Trends in Cell Biology 2011;21:91-103.

[89] Liu J, Farmer JD, Lane WS, Friedman J, Weissman I, Schreiber SL. Calcineurin is a common target of cyclophilin-cyclosporin A and FKBP-FK506 complexes. 66 ed. 1991. p. 807-15.

[90] Jain J, McCafffrey PG, Miner Z, Kerppola TK, Lambert JN, Verdine GL, et al.. The T-cell transcription factor NFATp is a substrate for calcineurin and interacts with Fos and Jun. Nature 1993;365:352-5.

[91] Clipstone NA, Crabtree GR. Identification of calcineurin as a key signalling enzyme in T-lymphocyte activation. Nature 1992;357:695-7.

[92] Shibasaki F, Price ER, Milan D, McKeon F. Role of kinases and the phosphatase calcineurin in the nuclear shuttling of transcription factor NF-AT4. Nature 1996;382:370-3.

[93] Fruman DA, Mather PE, Burakoff SJ, Bierer BE. Correlation of calcineurin phosphatase activity and programmed cell death in murine T cell hybridomas. Eur J Immunol 1992;22:2513-7.

[94] Genestier L, Dearden-Badet MT, Bonnefoy-Berard N, Lizard G, Revillard JP. Cyclosporin A and FK506 Inhibit Activation-Induced Cell Death in the Murine WEHI-231 B Cell Line. Cellular Immunology 1994;155:283-91.

[95] Bonnefoy-Berard N, Genestier L, Flacher M, Revillard JP. The phosphoprotein phosphatase calcineurin controls calcium-dependent apoptosis in B cell lines. Eur J Immunol 1994;24:325-9.

[96] Holtz-Heppelmann CJ, Algeciras A, Badley AD, Paya CV. Transcriptional Regulation of the Human FasL Promoter-Enhancer Region. JBC 1998;273:4416-23.

[97] Rothermel B, Vega RB, Yang J, Wu H, Bassel-Duby R, Williams RS. A Protein Encoded within the Down Syndrome Critical Region Is Enriched in Striated Muscles and Inhibits Calcineurin Signaling. JBC 2000;275:8719-25.

[98] Yang J, Rothermel B, Vega RB, Frey N, McKinsey TA, Olson EN, et al.. Independent Signals Control Expression of the Calcineurin Inhibitory Proteins MCIP1 and MCIP2 in Striated Muscles. Circulation Research 2000;87:e61-e68.

[99] Gold B. FK506 and the role of immunophilins in nerve regeneration. Mol Neurobiol 1997;15:285-306.

[100] Jain A, Reyes J, Kashyap R, Rohal S, Abu-Elmagd K, Starzl T, et al.. What Have We Learned About Primary Liver Transplantation Under Tacrolimus Immunosuppression?: Long-Term Follow-up of the First 1000 Patients. Annals of Surgery 1999;230.

[101] Kunz J, Hall MN. Cyclosporin A, FK506 and rapamycin: more than just immunosuppression. Trends in Biochemical Sciences 1993;18:334-8.

[102] Fung J, Alessiani M, Abu-Elmagd K, Todo S, Shapiro R, Tzakis A, et al.. Adverse Effects Associated With the Use of FK506. Transplant Proc 1991;23:3105-8.

[103] Bennett WM. Mechanisms of acute and chronic nephrotoxicity from immunosuppressive drugs. Ren Fail 1996;18:453-60.

[104] Vajdic C, McDonald S, McCredie M, van Leeuwen M, Stewart J, Law M, et al.. Cancer incidence before and after kidney transplantation. Journal of the American Medical Association 2006;296:2823-31.

[105] Birkeland S, Storm H, Lamm L, Barlow L, Blohme I, Forsberg B, et al.. Cancer risk after renal transplantation in the Nordic countries. Int J Cancer 1995;60:183-9.

[106] Yang X, Zhang F, Kudlow JE. Recruitment of O-GlcNAc Transferase to Promoters by Corepressor mSin3A: Coupling Protein O-GlcNAcylation to Transcriptional Repression. Cell 2002;110:69-80.

[107] Chan CP, Mak T-Y, Chin KT, Ng IO-L, Jin DY. N-linked glycosylation is required for optimal proteolytic activation of membrane-bound transcription factor CREB-H. J Cell Sci 2010;123:1438-48.

[108] Tootle TL, Rebay I. Post-translational modifications influence transcription factor activity: A view from the ETS superfamily. BioEssays 2005;27:285-98.

[109] Cao Z, Fan-Minogue H, Bellovin DI, Yevtodiyenko A, Arzeno J, Yang Q, et al.. MYC Phosphorylation, Activation, and Tumorigenic Potential in Hepatocellular Carcinoma Are Regulated by HMG-CoA Reductase. Cancer Research 2011;71:2286-97.

[110] Muller MR, Rao A. NFAT, immunity and cancer: a transcription factor comes of age. Nat Rev Immunol 2010;10:645-56.

[111] Viola JP, Carvalho LD, Fonseca BP, Teixeira LK. NFAT transcription factors: from cell cycle to tumor development. Braz J Med Biol Res 2005;38:335-44.

[112] Hogan PG, Chen L, Nardone J, Rao A. Transcriptional regulation by calcium, calcineurin, and NFAT. Genes Dev 2003;17:2205-32.

[113] Muller MR, Rao A. NFAT, immunity and cancer: a transcription factor comes of age. Nat Rev Immunol 2010;10:645-56.

[114] Macian F, Lopez-Rodriguez C, Rao A. Partners in transcription: NFAT and AP-1. Oncogene 2001;20:2476-89.

[115] Sharma S, Findlay GM, Bandukwala HS, Oberdoerffer S, Baust B, Li Z, et al.. Dephosphorylation of the nuclear factor of activated T cells (NFAT) transcription factor is regulated by an RNA-protein scaffold complex. Proc Natl Acad Sci U S A 2011;108:11381-6.

[116] Terui Y, Saad N, Jia S, McKeon F, Yuan J. Dual role of sumoylation in the nuclear localization and transcriptional activation of NFAT1. J Biol Chem 2004;279:28257-65.

[117] Arron JR, Winslow MM, Polleri A, Chang CP, Wu H, Gao X, et al.. NFAT dysregulation by increased dosage of DSCR1 and DYRK1A on chromosome 21. Nature 2006;441:595-600.

[118] Mancini M, Toker A. NFAT proteins: emerging roles in cancer progression. Nat Rev Cancer 2009;9:810-20.

[119] Mognol GP, de Araujo-Souza PS, Robbs BK, Teixeira LK, Viola JP. Transcriptional regulation of the c-Myc promoter by NFAT1 involves negative and positive NFAT-responsive elements. Cell Cycle 2012;11.

[120] Konig A, Fernandez-Zapico ME, Ellenrieder V. Primers on molecular pathways--the NFAT transcription pathway in pancreatic cancer. Pancreatology 2010;10:416-22.

[121] Robbs BK, Cruz AL, Werneck MB, Mognol GP, Viola JP. Dual roles for NFAT transcription factor genes as oncogenes and tumor suppressors. Mol Cell Biol 2008;28:7168-81.

[122] Tsukamoto H, Irie A, Nishimura Y. B-Raf contributes to sustained extracellular signal-regulated kinase activation associated with interleukin-2 production stimulated through the T cell receptor. J Biol Chem 2004;279:48457-65.

[123] Flockhart RJ, Armstrong JL, Reynolds NJ, Lovat PE. NFAT signalling is a novel target of oncogenic BRAF in metastatic melanoma. Br J Cancer 2009;101:1448-55.

[124] Gregory MA, Phang TL, Neviani P, Alvarez-Calderon F, Eide CA, O'Hare T, et al.. Wnt/Ca2+/NFAT signaling maintains survival of Ph+ leukemia cells upon inhibition of Bcr-Abl. Cancer Cell 2010;18:74-87.

[125] Perotti V, Baldassari P, Bersani I, Molla A, Vegetti C, Tassi E, et al.. NFATc2 Is a Potential Therapeutic Target in Human Melanoma. J Invest Dermatol 2012.

[126] Ryeom S, Baek KH, Zaslavsky A. Down's syndrome: protection against cancer and the therapeutic potential of DSCR1. Future Oncol 2009;5:1185-8.

[127] Baek KH, Zaslavsky A, Lynch RC, Britt C, Okada Y, Siarey RJ, et al.. Down's syndrome suppression of tumour growth and the role of the calcineurin inhibitor DSCR1. Nature 2009;459:1126-30.

[128] Pham LV, Tamayo AT, Yoshimura LC, Lin-Lee YC, Ford RJ. Constitutive NF-+¦B and NFAT activation in aggressive B-cell lymphomas synergistically activates the CD154 gene and maintains lymphoma cell survival. Blood 2005;106:3940-7.

[129] Fu L, Lin-Lee YC, Pham LV, Tamayo A, Yoshimura L, Ford RJ. Constitutive NF-+¦B and NFAT activation leads to stimulation of the BLyS survival pathway in aggressive B-cell lymphomas. Blood 2006;107:4540-8.

[130] Glud SZ, S++rensen AB, Andrulis M, Wang B, Kondo E, Jessen R, et al.. A tumor-suppressor function for NFATc3 in T-cell lymphomagenesis by murine leukemia virus. Blood 2005;106:3546-52.

[131] Medyouf H, Alcalde H, Berthier C, Guillemin MC, dos Santos NR, Janin A, et al.. Targeting calcineurin activation as a therapeutic strategy for T-cell acute lymphoblastic leukemia. Nat Med 2007;13:736-41.

[132] Gregory MA, Phang TL, Neviani P, Alvarez-Calderon F, Eide CA, O'Hare T, et al.. Wnt/Ca2+/NFAT signaling maintains survival of Ph+ leukemia cells upon inhibition of Bcr-Abl. Cancer Cell 2010;18:74-87.

[133] Yoeli-Lerner M, Yiu GK, Rabinovitz I, Erhardt P, Jauliac S, Toker A. Akt Blocks Breast Cancer Cell Motility and Invasion through the Transcription Factor NFAT. Molecular Cell 2005;20:539-50.

[134] Yoeli-Lerner M, Chin YR, Hansen CK, Toker A. Akt/Protein Kinase B and Glycogen Synthase Kinase-3+¦ Signaling Pathway Regulates Cell Migration through the NFAT1 Transcription Factor. Molecular Cancer Research 2009;7:425-32.

[135] Buchholz M, Schatz A, Wagner M, Michl P, Linhart T, Adler G, et al.. Overexpression of c-myc in pancreatic cancer caused by ectopic activation of NFATc1 and the Ca2+/calcineurin signaling pathway. EMBO J 2006;25:3714-24.

[136] K+¦enig A, Linhart T, Schlengemann K, Reutlinger K, Wegele J, Adler G, et al.. NFAT-Induced Histone Acetylation Relay Switch Promotes c-Myc-Dependent Growth in Pancreatic Cancer Cells. Gastroenterology 2010;138:1189-99.

[137] Lehen'Kyi V, Flourakis M, Skryma R, Prevarskaya N. TRPV6 channel controls prostate cancer cell proliferation via Ca2+//NFAT-dependent pathways. Oncogene 2007;26:7380-5.

[138] Flockhart RJ, Armstrong JL, Reynolds NJ, Lovat PE. NFAT signalling is a novel target of oncogenic BRAF in metastatic melanoma. Br J Cancer 2009;101:1448-55.

[139] Sales KJ, Maldonado-P+¬rez D, Grant V, Catalano RD, Wilson MR, Brown P, et al.. Prostaglandin F2+¦-F-prostanoid receptor regulates CXCL8 expression in endometrial adenocarcinoma cells via the calciumΓÇôcalcineurinΓÇôNFAT pathway. Biochimica et Biophysica Acta (BBA) - Molecular Cell Research 2009;1793:1917-28.

[140] Sales KJ, Grant V, Cook IH, Maldonado-P+¬rez D, Anderson RA, Williams ARW, et al.. Interleukin-11 in Endometrial Adenocarcinoma Is Regulated by Prostaglandin F2+¦-F-Prostanoid Receptor Interaction via the Calcium-Calcineurin-Nuclear Factor of Activated T Cells Pathway and Negatively Regulated by the Regulator of Calcineurin-1. The American Journal of Pathology 2010;176:435-45.

[141] Rubinstein JC, Sznol M, Pavlick AC, Ariyan S, Cheng E, Bacchiocchi A, et al.. Incidence of the V600K mutation among melanoma patients with BRAF mutations, and potential therapeutic response to the specific BRAF inhibitor PLX4032. J Transl Med 2010;8:67.

[142] Li X, Zhu L, Yang A, Lin J, Tang F, Jin S, et al.. Calcineurin-NFAT signaling critically regulates early lineage specification in mouse embryonic stem cells and embryos. Cell Stem Cell 2011;8:46-58.

[143] Guha M, Srinivasan S, Biswas G, Avadhani NG. Activation of a novel calcineurin-mediated insulin-like growth factor-1 receptor pathway, altered metabolism, and tumor cell invasion in cells subjected to mitochondrial respiratory stress. J Biol Chem 2007;282:14536-46.

[144] Chou A, Chen J, Clarkson A, Samra JS, Clifton-Bligh RJ, Hugh TJ, et al.. Succinate dehydrogenase-deficient GISTs are characterized by IGF1R overexpression. Mod Pathol 2012.

[145] Taylor ML, Dastych J, Sehgal D, Sundstrom M, Nilsson G, Akin C, et al.. The Kit-activating mutation D816V enhances stem cell factor co-dependent factor. Blood 2001;98:1195-9.

[146] Nagata H, Worobec AS, Semere T, Metcalfe DD. Elevated expression of the proto-oncogene c-kit in patients with mastocytosis. Leukemia 1998;12:175-81.

[147] Kitayama H, Kanakura Y, Furitsu T, Tsujimura T, Oritani K, Ikeda H, et al.. Constitutively activating mutations of c-kit receptor tyrosine kinase confer factor-independent growth and tumorigenicity of factor-dependent hematopoietic cell lines. Blood 1995;85:790-8.

[148] Piao X, Paulson R, van der Geer P, Pawson T, Bernstein A. Oncogenic mutation in the Kit receptor tyrosine kinase alters substrate specificity and induces degradation of the protein tyrosine phosphatase SHP-1. Proceedings of the National Academy of Sciences 1996;93:14665-9.

[149] Peter B, Hadzijusufovic E, Blatt K, Gleixner KV, Pickl WF, Thaiwong T, et al.. KIT polymorphisms and mutations determine responses of neoplastic mast-ácells to bafetinib (INNO-406). Experimental Hematology 2010;38:782-91.

[150] Pardanani A, Elliott M, Reeder T, Li CY, Baxter EJ, Cross NCP, et al.. Imatinib for systemic mast-cell disease. The Lancet 2003;362:535-6.

[151] Le Cesne A, Ray-Coquard I, Bui BN, Adenis A, Rios M, Bertucci F, et al.. Discontinuation of imatinib in patients with advanced gastrointestinal stromal tumours after 3 years of treatment: an open-label multicentre randomised phase 3 trial. The Lancet Oncology 2010;11:942-9.

[152] Hanks SK, Quinn AM, Hunter T. The protein kinase family: conserved features and deduced phylogeny of the catalytic domains. Science 1988;241:42-52.

[153] Anette D, Fabiola M, Bryna M, Nora E Joseph, Dipak P, Samuel S, et al.. Mechanisms of oncogenic KIT signal transduction in primary gastrointestinal stromal tumors (GISTs). Oncogene 2004;23:3999-4006.

[154] Matsui J, Wakabayashi T, Asada M, Yoshimatsu K, Okada M. Stem Cell Factor/c-kit Signaling Promotes the Survival, Migration, and Capillary Tube Formation of Human Umbilical Vein Endothelial Cells. JBC 2004;279:18600-7.

[155] Lux ML, Rubin BP, Biase TL, Chen CJ, Maclure T, Demetri G, et al.. KIT Extracellular and Kinase Domain Mutations in Gastrointestinal Stromal Tumors. The American Journal of Pathology 2000;156:791-5.

[156] Broudy VC, Smith FO, Lin N, Zsebo KM, Egrie J, Bernstein ID. Blasts from patients with acute myelogenous leukemia express functional receptors for stem cell factor. Blood 1992;80:60-7.

[157] Ohashi A, Funasaka Y, Ueda M, Ichihashi M. c-KIT receptor expression in cutaneous malignant melanoma and benign melanotic naevi. Melanoma Res 1996;6:25-30.

[158] Meyts ER-D, Skakkebkk N. Expression of the c-kit protein product in carcinoma-in-situ and invasive testicular germ cell tumours. International Journal of Andrology 1994;17:85-92.

[159] Spreafico A, Tentler JJ, Pitts TM, Tan AC, Gregory MA, Arcaroli JJ, et al.. Rational Combination of a MEK Inhibitor, Selumetinib, and the Wnt/Calcium Pathway Modulator, Cyclosporin A, in Preclinical Models of Colorectal Cancer. Clin Cancer Res 2013;19:4149-62.

[160] Dissanayake SK, Olkhanud PB, O'Connell MP, Carter A, French AD, Camilli TC, et al.. Wnt5A regulates expression of tumor-associated antigens in melanoma via changes in signal transducers and activators of transcription 3 phosphorylation. Cancer Res 2008;68:10205-14.

[161] Perotti V, Baldassari P, Bersani I, Molla A, Vegetti C, Tassi E, et al.. NFATc2 Is a Potential Therapeutic Target in Human Melanoma. J Invest Dermatol 2012.

[162] Robbs BK, Cruz AL, Werneck MB, Mognol GP, Viola JP. Dual roles for NFAT transcription factor genes as oncogenes and tumor suppressors. Mol Cell Biol 2008;28:7168-81.

[163] Viola JP, Carvalho LD, Fonseca BP, Teixeira LK. NFAT transcription factors: from cell cycle to tumor development. Braz J Med Biol Res 2005;38:335-44.

[164] Macian F, Lopez-Rodriguez C, Rao A. Partners in transcription: NFAT and AP-1. Oncogene 2001;20:2476-89.

[165] Hogan PG, Chen L, Nardone J, Rao A. Transcriptional regulation by calcium, calcineurin, and NFAT. Genes Dev 2003;17:2205-32.

[166] Ralph P, Moore MA, Nilsson K. Lysozyme synthesis by established human and murine histiocytic lymphoma cell lines. The Journal of Experimental Medicine 1976;143:1528-33.

[167] Butterfield JH, Weiler D, Dewald G, Gleich G. Establishment of an immature mast cell line from a patient with mast cell leukemia. Leuk Res 1988;12:345-55.

[168] Seldin D, Adelman S, Austen K, Stevens R, Hein A, Caulfield J, et al.. Homology of the rat basophilic leukemia cell and the rat mucosal mast cell. Proc Natl Acad Sci U S A 1985;82:3871-5.

[169] DeVinney R, Gold WM. Establishment of Two Dog Mastocytoma Cell Lines in Continuous Culture. Am J Respir Cell Mol Biol 1990;3:413-20.

[170] Schmittgen TD, Livak KJ. Analyzing real-time PCR data by the comparative CT method. Nat Protocols 2008;3:1101-8.

[171] Chou TC, Talalay P. Quantitative analysis of dose-effect relationships: the combined effects of multiple drugs or enzyme inhibitors. Adv Enzyme Regul 1984;22:27-55.

[172] Coley HM, Twentyman PR, Workman P. Identification of anthracyclines and related agents that retain preferential activity over adriamycin in multidrug-resistant cell lines, and further resistance modification by verapamil and cyclosporin A. Cancer Chemother Pharmacol 1989;24:284-90.

[173] Gaveriaux C, Boesch D, Boelsterli JJ, Bollinger P, Eberle MK, Hiestand P, et al.. Overcoming multidrug resistance in Chinese hamster ovary cells in vitro by cyclosporin A (Sandimmune) and non-immunosuppressive derivatives. Br J Cancer 1989;60:867-71.

[174] Nooter K, Sonneveld P, Janssen A, Oostrum R, Boersma T, Herweijer H, et al.. Expression of the mdr3 gene in prolymphocytic leukemia: association with cyclosporin-A-induced increase in drug accumulation. Int J Cancer 1990;45:626-31.

[175] Sivalenka RR, Jessberger R. SWAP-70 regulates c-kit-induced mast cell activation, cell-cell adhesion, and migration. Mol Cell Biol 2004;24:10277-88.

[176] Ueda S, Mizuki M, Ikeda H, Tsujimura T, Matsumura I, Nakano K, et al.. Critical roles of c-Kit tyrosine residues 567 and 719 in stem cell factor-induced

chemotaxis: contribution of src family kinase and PI3-kinase on calcium mobilization and cell migration. Blood 2002;99:3342-9.

[177] Ishikawa J, Ohga K, Yoshino T, Takezawa R, Ichikawa A, Kubota H, et al.. A Pyrazole Derivative, YM-58483, Potently Inhibits Store-Operated Sustained Ca2+ Influx and IL-2 Production in T Lymphocytes. The Journal of Immunology 2003;170:4441-9.

[178] Kiyonaka S, Kato K, Nishida M, Mio K, Numaga T, Sawaguchi Y, et al.. Selective and direct inhibition of TRPC3 channels underlies biological activities of a pyrazole compound. Proceedings of the National Academy of Sciences 2009;106:5400-5.

[179] Proksch P, Giaisi M, Treiber MK, Palfi K, Merling A, Spring H, et al.. Rocaglamide Derivatives Are Immunosuppressive Phytochemicals That Target NF-AT Activity in T Cells. The Journal of Immunology 2005;174:7075-84.

[180] Umehara H, Asai A. Tributylhexadecylphosphonium Bromide, a Novel Nuclear Factor of Activated T Cells Signaling Inhibitor, Blocks Interleukin-2 Induction Associated with Inhibition of p70 Ribosomal Protein S6 Kinase Phosphorylation. Biological and Pharmaceutical Bulletin 2012;35:805-9.

[181] Ueda S, Mizuki M, Ikeda H, Tsujimura T, Matsumura I, Nakano K, et al.. Critical roles of c-Kit tyrosine residues 567 and 719 in stem cell factorΓÇôinduced chemotaxis: contribution of src family kinase and PI3-kinase on calcium mobilization and cell migration. Blood 2002;99:3342-9.

[182] Druker BJ, Talpaz M, Resta DJ, Peng B, Buchdunger E, Ford JM, et al.. Efficacy and safety of a specific inhibitor of the bcr-abl tyrosine kinase in chronic myeloid leukemia. N Engl J Med 2001;344:1031-7.

[183] Taylor ML, Dastych J, Sehgal D, Sundstrom M, Nilsson G, Akin C, et al.. The Kit-activating mutation D816V enhances stem cell factorΓÇôdependent chemotaxis. Blood 2001;98:1195-9.

[184] Azorsa D, Gonzales I, Basu G, Choudhary A, Arora S, Bisanz K, et al.. Synthetic lethal RNAi screening identifies sensitizing targets for gemcitabine therapy in pancreatic cancer. Journal of Translational Medicine 2009;7:43.

[185] Whitehurst AW, Bodemann BO, Cardenas J, Ferguson D, Girard L, Peyton M, et al.. Synthetic lethal screen identification of chemosensitizer loci in cancer cells. Nature 2007;446:815-9.

[186] Luo J, Emanuele MJ, Li D, Creighton CJ, Schlabach MR, Westbrook TF, et al.. A Genome-wide RNAi Screen Identifies Multiple Synthetic Lethal Interactions with the Ras Oncogene. Cell 2009;137:835-48.

[187] Corless CL, Heinrich MC. Molecular Pathobiology of Gastrointestinal Stromal Sarcomas. Annual Reviews of Pathology: Mechanisms of Disease 2008;3:557-86.

[188] Wells G, Haguenauer D, Shea B, Suarez-Almazor M, Wlech V, Tugwell P, et al.. Cyclosporine for treating rheumatoid arthritis. Cochrane Database Of Systematic Reviews 1998.

[189] Ellis C, Gorsulowsky D, Hamilton T. Cyclosporine improves psoriasis in a double-blind study. Journal of the American Medical Association 1986;256:3110-6.

[190] Sall K, Stevenson OD, Mundorf TK, Reis BL. Two multicenter, randomized studies of the efficacy and safety of cyclosporine ophthalmic emulsion in moderate to severe dry eye disease. Ophthalmology 2000;107:631-9.

[191] Marioni JC, Mason CE, Mane SM, Stephens M, Gilad Y. RNA-seq: An assessment of technical reproducibility and comparison with gene expression arrays. Genome Research 2008;18:1509-17.

[192] Wang Z, Gerstein M, Snyder M. RNA-Seq: a revolutionary tool for transcriptomics. Nature Reviews Genetics 2009;10:57-63.

[193] Livak KJ, Schmittgen TD. Analysis of relative gene expression data using real-time quantitative PCR and the 2(-Delta Delta C(T)) Method. Methods 2001;25:402-8.

[194] Franceschini A, Szklarczyk D, Frankild S, Kuhn M, Simonovic M, Roth A, et al.. STRING v9.1: protein-protein interaction networks, with increased coverage and integration. Nucl Acids Res 2013;41:D808-D815.

[195] Pardanani A, Lasho T, Smith G, Burns CJ, Fantino E, Tefferi A. CYT387, a selective JAK1/JAK2 inhibitor: in vitro assessment of kinase selectivity and preclinical studies using cell lines and primary cells from polycythemia vera patients. Leukemia 2009;23:1441-5.

[196] Dawson MA, Prinjha RK, Dittmann A, Giotopoulos G, Bantscheff M, Chan W-I, et al.. Inhibition of BET recruitment to chromatin as an effective treatment for MLL-fusion leukemia. Nature 2011;478:529-33.

[197] Fry DW, Harvey PJ, Keller PR, Elliott WL, Meade M, Trachet E, et al.. Specific inhibition of cyclin-dependent kinase 4/6 by PD 0332991 and associated antitumor activity in human tumor xenografts. Molecular Cancer Therapeutics 2004;3:1427-38.

[198] Tolani B, Gopalakrishnan R, Punj V, Matta H, Chaudhary PM. Targeting Myc in KSHV-associated primary effusion lymphoma with BET bromodomain inhibitors. Oncogene 2013.

[199] Delmore J, Issa G, Lemieux M, Rahl P, Shi J, Jacobs H, et al.. BET Bromodomain Inhibition as-áa Therapeutic Strategy to Target c-Myc. Cell 2011;146:904-17.

[200] Mertz JA, Conery AR, Bryant BM, Sandy P, Balasubramanian S, Mele DA, et al.. Targeting MYC dependence in cancer by inhibiting BET bromodomains. Proceedings of the National Academy of Sciences 2011;108:16669-74.

[201] Ning H, Mitsui H, Wang CQF, Su+írez-Fari+¦as M, Gonzalez J, Shah KR, et al.. Identification of anaplastic lymphoma kinase as a potential therapeutic target in Basal Cell Carcinoma. Oncotarget; Vol 4: Advance Online Publications 2013.

[202] Wang Y, Chen J, Wang L, Huang Y, Leng Y, Wang G. Fangchinoline induces G0/G1 arrest by modulating the expression of CDKN1A and CCND2 in K562 human chronic myelogenous leukemia cells. Experimental and Therapeutic Medicine 2013;5:1105-12.

[203] Bennett WM, DeMattos A, Meyer MM, Andoh T, Barry JM. Chronic cyclosporine nephropathy: the Achilles' heel of immunosuppressive therapy. Kidney Int 1996;50:1089-100.

[204] Bennett WM, DeMattos A, Meyer MM, Andoh T, Barry JM. Chronic cyclosporine nephropathy in renal transplantation. Transplant Proc 1996;28:2100-3.

[205] Mihatsch MJ, Thiel G, Ryffel B. Cyclosporin A: action and side-effects. Toxicol Lett 1989;46:125-39.

[206] Nankivell BJ, Borrows RJ, Fung CL, O'Connell PJ, Allen RD, Chapman JR. The natural history of chronic allograft nephropathy. N Engl J Med 2003;349:2326-33.

[207] Kinlen LJ, Sheil AG, Peto J, Doll R. Collaborative United Kingdom-Australasian study of cancer in patients treated with immunosuppressive drugs. Br Med J 1979;2:1461-6.

[208] Penn I. Depressed immunity and the development of cancer. Cancer Detect Prev 1994;18:241-52.

[209] Wessendorf S, Schwaenen C, Kohlhammer H, Kienle D, Wrobel G, Barth TF, et al.. Hidden gene amplifications in aggressive B-cell non-Hodgkin lymphomas detected by microarray-based comparative genomic hybridization. Oncogene 0 AD;22:1425-9.

[210] Walz C, Crowley BJ, Hudon HE, Gramlich JL, Neuberg DS, Podar K, et al.. Activated Jak2 with the V617F Point Mutation Promotes G1/S Phase Transition. JBC 2006;281:18177-83.

[211] Martino A, Holmes JH, Lord JD, Moon JJ, Nelson BH. Stat5 and Sp1 Regulate Transcription of the Cyclin D2 Gene in Response to IL-2. The Journal of Immunology 2001;166:1723-9.

[212] Mroz P, Vatansever F, Muchowicz A, Hamblin MR. Photodynamic Therapy of Murine Mastocytoma Induces Specific Immune Responses against the Cancer/Testis Antigen P1A. Cancer Research 2013;73:6462-70.

[213] Gajewski TF, Markiewicz MA, Uyttenhove C. The P815 Mastocytoma Tumor Model. Current Protocols in Immunology. John Wiley & Sons, Inc.; 2001.

[214] Yang H, Wei J, Zhang H, Lin L, Zhang W, He S. Upregulation of Toll-like receptor (TLR) expression and release of cytokines from P815 mast cells by GM-CSF. BMC Cell Biology 2009;10:37.

[215] Pel A, Plaen E, Boon T. Selection of highly transfectable variant from mouse mastocytoma P815. Somat Cell Mol Genet 1985;11:467-75.

[216] W+¦lfel T, Pel A, Plaen E, Lurquin C, Maryanski J, Boon T. Immunogenic (tumΓêÆ) variants obtained by mutagenesis of mouse mastocytoma P815. Immunogenetics 1987;26:178-87.

[217] Leonard B, Eccleston E, Jones D, Lowe J, Turner E. Basophilic leukemia in the rat induced by a -chlorethylamine--ICI 42464. The Journal of Pathology 1971;103.

[218] Passante E, Frankish N. The RBL-2H3 cell line: its provenance and suitability as a model for the mast cell. Inflamm Res 2009;58:737-45.

[219] Lazarus S, DeVinney R, McCabe L, Finkbeiner W, Elias D, Gold W, et al.. Isolated canine mastocytoma cells: propagation and characterization of two cell lines. Am J Physiol 1986;251:935-44.

[220] Andre C, d'Auriol L, Lacombe C, Gisselbrecht S, Galibert F. c-kit mRNA expression in human and murine hematopoietic cell lines. Oncogene 1989;4:1047-9.

[221] Sundstrom M, Vliagoftis H, Karlberg P, Butterfield J, Nilsson K, Metcalfe D, et al.. Functional and phenotypic studies o two variants of a human mast cell line with a distinct set of mutations in the c-kit proto-oncogene. Immunology 2003;108:89-97.

[222] Nabel G, Galli SJ, Dvorak AM, Dvorak HF, Cantor H. Inducer T lymphocytes synthesize a factor that stimulates proliferation of cloned mast cells. Nature 1981;291:332-4.

[223] Galli SJ, Dvorak AM, Marcum JA, Ishizaka T, Nabel G, Der Simonian H, et al.. Mast cell clones: a model for the analysis of cellular maturation. The Journal of Cell Biology 1982;95:435-44.

[224] Ito F, Toyota N, Sakai H, Takahashi H, Iizuka H. FK506 and cyclosporin A inhibit stem cell factor-dependent cell proliferation/survival, while inducing upregulation of c-kit expression in cells of the mast cell line MC/9. Arch Dermatol Res 1999;291:275-83.

[225] Salvato G. Mast Cells in Bronchial Connective Tissue of Man: Their Modifications in Asthma and after Treatment with the Histamine Liberator 48/80. International Archives of Allergy and Immunology 1961;18:348-58.

[226] Klein E, Ben-Bassat H, Neumann H, Ralph P, Zeuthen J, Polliack A, et al.. Properties of the K562 cell line, derived froma patient with chronic myeloid leukemia. Int J Cancer 1976;18:421-31.

[227] Gambacorti-Passerini C, le Coutre P, Mologni L, Fanelli M, Bertazzoli C, Marchesi E, et al.. Inhibition of the ABL Kinase Activity Blocks the Proliferation of BCR/ABL+Leukemic Cells and Induces Apoptosis. Blood Cells, Molecules, and Diseases 1997;23:380-94.

[228] LaMontagne KR, Hannon G, Tonks NK. Protein tyrosine phosphatase PTP1B suppresses p210 bcr-abl-induced transformation of Rat-1 fibroblasts and promotes differentiation of K562 cells. Proceedings of the National Academy of Sciences 1998;95:14094-9.

[229] Bauer S, Yu LK, Demetri GD, Fletcher JA. Heat Shock Protein 90 Inhibition in Imatinib-Resistant Gastrointestinal Stromal Tumor. Cancer Research 2006;66:9153-61.

[230] Taguchi T, Sonobe H, Toyonaga Si, Yamasaki I, Shuin T, Takano A, et al.. Conventional and Molecular Cytogenetic Characterization of a New Human Cell Line, GIST-T1, Established from Gastrointestinal Stromal Tumor. Lab Invest 2002;82:663-5.

[231] Abbas S, Rotmans Gl, L+¦wenberg B, Valk PJM. Exon 8 splice site mutations in the gene encoding the E3-ligase CBL are associated with core binding factor acute myeloid leukemias. Haematologica 2008;93:1595-7.

[232] Matsuo Y, MacLeod RA, Uphoff CC, Drexler HG, Nishizaki C, Katayama Y, et al.. Two acute monocytic leukemia (AML-M5a) cell lines (MOLM-13 and MOLM-14) with interclonal phenotypic heterogeneity showing MLL-AF9 fusion resulting from an occult chromosome insertion, ins(11;9)(q23;p22p23). Leukemia 1997;11:1469-77.

[233] Quentmeier H, Reinhardt J, Zaborski M, Drexler HG. FLT3 mutations in acute myeloid leukemia cell lines. Leukemia 2003;17:120-4.

[234] Saito H, Bourinbaiar A, Ginsburg M, Minato K, Ceresi E, Yamada K, et al.. Establishment and characterization of a new human eosinophilic leukemia cell line. Blood 1985;66:1233-40.

[235] Cools J, DeAngelo DJ, Gotlib J, Stover EH, Legare RD, Cortes J, et al.. A Tyrosine Kinase Created by Fusion of the PDGFRA and FIP1L1 Genes as a Therapeutic Target of Imatinib in Idiopathic Hypereosinophilic Syndrome. N Engl J Med 2003;348:1201-14.

[236] Cools J, Quentmeier H, Huntly BJP, Marynen P, Griffin JD, Drexler HG, et al.. The EOL-1 cell line as an in vitro model for the study of FIP1L1-PDGFRAΓÇôpositive chronic eosinophilic leukemia. Blood 2004;103:2802-5.

[237] Dewaele B, Wasag B, Cools J, Sciot R, Prenen H, Vandenberghe P, et al.. Activity of Dasatinib, a Dual SRC/ABL Kinase Inhibitor, and IPI-504, a Heat

Shock Protein 90 Inhibitor, against Gastrointestinal Stromal TumorΓÇôAssociated PDGFRAD842V Mutation. Clinical Cancer Research 2008;14:5749-58.

[238] Carey T, Takahashi T, Resnick L, Oettgen H, Old L. Cell surface antigens of human malignant melanoma: mixed hemadsorption assays for humoral immunity to cultured autologous melanoma cells. Proceedings of the National Academy of Sciences 1976;73:3278-82.

[239] Smalley KSM, Lioni M, Palma MD, Xiao M, Desai B, Egyhazi S, et al.. Increased cyclin D1 expression can mediate BRAF inhibitor resistance in BRAF V600EΓÇômutated melanomas. Molecular Cancer Therapeutics 2008;7:2876-83.

[240] Tjio J, Puck T. Genetics of somatic Mammalian Cells. J Exp Med 1958;108:259-68.

[241] Graham FL, Smiley J, Russell WC, Nairn R. Characteristics of a Human Cell Line Transformed by DNA from Human Adenovirus Type 5. J Gen Virol 1977;36:59-72.

[242] Shan J, Shi DL, Wang J, Zheng J. Identification of a Specific Inhibitor of the Dishevelled PDZ DomainΓÇá. Biochemistry 2005;44:15495-503.

[243] Hess J, Angel P, Schorpp-Kistner M. AP-1 subunits: quarrel and harmony among siblings. J Cell Sci 2004;117:5965-73.

[244] Meng Q, Xia Y. c-Jun, at the crossroad of the signaling network. Protein Cell 2011;2:889-98.

[245] Dunn TB, Potter M. A Transplantable Mast-Cell Neoplasm in the Mouse. J Natl Cancer Inst 1957;18:587-601.

[246] Demehri S, Corbin A, Loriaux M, Druker BJ, Deininger MW. Establishment of a murine model of aggressive systemic mastocytosis/mast cell leukemia. Experimental Hematology 2006;34:284-8.

[247] Tsuiki H, Tnani M, Okamoto I, Kenyon LC, Emlet DR, Holgado-Madruga M, et al.. Constitutively Active Forms of c-Jun NH2-terminal Kinase Are Expressed in Primary Glial Tumors. Cancer Research 2003;63:250-5.